Fall 1985

THE ANALYSIS AND SIMULATION OF HYBRID STEPPING MOTORS USING THE PHASE PLANE APPROACH

TIMOTHY JAMES HARNED
University of New Hampshire, Durham

8527884

Harned, Timothy James

THE ANALYSIS AND SIMULATION OF HYBRID STEPPING MOTORS USING THE PHASE PLANE APPROACH

University of New Hampshire PH.D. 1985

University Microfilms International 300 N. Zeeb Road, Ann Arbor, MI 48106

PLEASE NOTE:

In all cases this material has been filmed in the best possible way from the available copy. Problems encountered with this document have been identified here with a check mark __√__.

1. Glossy photographs or pages _____
2. Colored illustrations, paper or print _____
3. Photographs with dark background _____
4. Illustrations are poor copy _____
5. Pages with black marks, not original copy _____
6. Print shows through as there is text on both sides of page _____
7. Indistinct, broken or small print on several pages __✓__
8. Print exceeds margin requirements _____
9. Tightly bound copy with print lost in spine _____
10. Computer printout pages with indistinct print _____
11. Page(s) _____ lacking when material received, and not available from school or author.
12. Page(s) _____ seem to be missing in numbering only as text follows.
13. Two pages numbered _____. Text follows.
14. Curling and wrinkled pages _____
15. Other _____

University
Microfilms
International

THE ANALYSIS AND SIMULATION OF HYBRID STEPPING MOTORS USING THE PHASE PLANE APPROACH

by

TIMOTHY JAMES HARNED

B.S., UNIVERSITY of NEW HAMPSHIRE, 1977
M.S., UNIVERSITY of NEW HAMPSHIRE, 1979

A DISSERTATION

Submitted to the University of New Hampshire
in partial fulfillment of
the Requirements for the Degree of

Doctor of Philosophy
in
Engineering

September, 1985

This dissertation has been examined and approved.

Dissertation Director, Charles K. Taft
Professor of Mechanical Engineering

David E. Limbert
Professor of Mechanical Engineering

Russell L. Valentine
Professor and Chairman of Mechanical Engineering

Ronald R. Clark
Professor and Chairman of Electrical Engineering

L. David Meeker
Professor of Mathematics

Date: July 15, 1985

ACKNOWLEDGMENTS

I would like to express my appreciation to the many people who contributed to my research efforts at the University of New Hampshire. In particular my committee members who provided many insightful suggestions and criticisms.

In addition, I thank Daryle Cooper and Eastern Air Devices for their long standing support.

I would also like to thank my wife Kathy, for her support and the many hours she contributed to making this a respectable "english" document as well as my parents for their continued encouragement.

Lastly, a very special thank you to Dr. Charles Taft for the many opportunities and experiences he provided during my education.

TABLE OF CONTENTS

LIST OF TABLES

LIST OF FIGURES

LIST OF SYMBOLS

A	=	The number of cycles of the torque angle curve per revolution
a_2	=	The coefficient for the I^2 term in the saturation polynomial
a_1	=	The coefficient for the I^1 term in the saturation polynomial
a_0	=	The coefficient for the I^0 term in the saturation polynomial
B	=	The total damping of the motor and load
$\bar{B}$	=	The damping coefficient of a linear system
B_e	=	The velocity dependent eddy current loss term
B_u	=	The mechanical damping of the motor and load
D_t	=	The magnitude of the detent torque of a hybrid motor
D_m	=	The number of cycles of the detent torque angle curve per cycle of the stator torque angle curve
EQTQ	=	The equal torques when half stepping, a flag for the simulation package (Y or N)
FD	=	The flyback diodes during all steps, a flag for the simulation package (Y or N)
FDL	=	The flyback diodes during the last step, a flag for the simulation package (Y or N)
I	=	The instantaneous stator winding current
I_{1ac}	=	The instantaneous AC stator winding current in winding 1
I_{2ac}	=	The instantaneous AC stator winding current in winding 2
I_{1n}	=	The instantaneous modulation stator winding current, term n in winding 1

I_{2n} = The instantaneous modulation stator winding current, term n in winding 2

I_n = The instantaneous stator winding current in winding n

dI_n/dt = The first derivative of the stator winding current in winding n

I_r = The rated stator winding current

J_m = The total inertia of the motor and load

J_n = The Bessel funtion, term n

$\overline{J}$ = The inertia of a linear system

$\overline{K}$ = The spring constant of a linear system

K_b = The motor back EMF constant

K_{bs} = The motor back EMF constant reduced by magnetic saturation

K_t = The motor torque constant

K_{ts} = The motor torque constant reduced by magnetic saturation

K_{tt} = The torque transducer spring constant

L = Inductance

L_m = The stator winding inductance

L_{ms} = The stator winding inductance reduced by magnetic saturation

M_{mk} = The stator winding mutual inductance due to the magnetic coupling to stator winding k

p = The number of stator phases

PHO = The number of phases on at the start of a simulation (1 or 2)

R = Resistance

R_f = The current drive feedback resistor

R_m = The stator winding resistance

R_s = The L/R drive series resistor

S_f = The magnetic saturatic factor

S_s = The derivative of the magnetic saturation factor (dS_f/dI)

S_t = The total stiction of the motor and load

STPR = The number of steps per revolution of the motor

STS = The step size (.5 = half and 1 = full)

t = Time

$\overline{T}$ = The input torque to a linear system

T_f = The total friction of the motor and load

T_{fe} = The position dependent magnetic hysteresis losses

T_{fu} = The mechanical friction of the motor and load

$T(\theta)$ = The torque produced by the motor at some angle (θ)

T_0 = The DC torque component of a forced oscillation

T_1 = The AC torque component of a forced oscillation

V_r = The rated voltage of the motor

V_s = The drive supply voltage

W_l = The frequency of a limit cycle oscillation

W_n = The natural frequency of the system

W_o = The frequency of a forced oscillation

WRW = Simulation control flag, controls the location of the resistor in the flyback diode circuit

ζ_j = The damping ratio of a second order linear system

θ = The rotor angle

$\dot{\theta}$ = The rotor velocity

$\dot{\theta}_d$ = The rotor velocity DC component

$\dot{\theta}_l$ = The rotor limit cycle velocity ripple

$\dot{\theta}_o$ = The rotor forced oscillation velocity ripple

$\ddot{\theta}$ = The rotor acceleration

θ_e = The stepping rotor angle error

$\dot{\theta}_e$ = The stepping rotor velocity error

$\dot{\theta}_s$ = The AC synchronous drive frequency

θ_t = The torque transducer input position

$\dot{\theta}_t$ = The torque transducer input velocity

ϕ = Magnetic flux

Ψ = The synchronous motor angle error

$\dot{\Psi}$ = The synchronous motor velocity error

Ψ = The synchronous motor steady state power angle

Ψ_{ac} = The phase shift in the AC drive term

Ψ_n = The phase shift in modulation term n

Ψ_o = The forced oscillation phase margin

ABSTRACT

THE ANALYSIS AND SIMULATION OF
HYBRID STEPPING MOTORS USING THE
PHASE PLANE APPROACH

by

TIMOTHY JAMES HARNED

University of New Hampshire, September, 1985

Stepping motors have become very popular electromechanical interface devices because they are easy to interface to digital control logic. The most popular stepping motor currently used is the hybrid design stepping motor. It incorporates an efficient magnetic structure to obtain a high output torque, while maintaining a position resolution of fifty parts per million.

All stepping motors are nonlinear devices and, therefore, control strategies have been difficult to develop and implement. A second order, nonlinear model was developed by Gauthier to describe the permanent magnet stepping motor. The results of this model are displayed using the phase plane and considerable insight into the motor's performance and operating characteristics are obtained. In this work the

model is modified to describe the hybrid stepping motor by including inductance, magnetic saturation, hysteresis and eddy current losses. This yields a sixth order, nonlinear model, the solution of which requires a six dimension space to display the results.

The six dimension solution can be projected back into the two dimension phase plane. A strong understanding of the implications of this projection is necessary to properly interpret the results. Once this understanding is obtained, many of the operating and dynamic characteristics of the hybrid stepping motor can be understood and explained. In addition, the techniques that were developed for designing sequences or control strategies for the permanent magnet stepping motor can now be applied to the hybrid stepping motor.

The hybrid motor can also be operated as a synchronous device. The model that was developed to describe its performance when being stepped can be used to predict the operating modes when the motor is driven by a synchronous AC source. The solution of the equations is again projected back into a two dimension space where many of the dynamic characteristics are easily seen.

Both the stepping and synchronously driven models are then used to investigate the characteristics and cause of mid-frequency resonance in the hybrid motor. This

instability phenomenon is shown to be caused by amplitude and frequency modulation effects in the stepping motor.

CHAPTER I

INTRODUCTION

During the past ten years there has been an explosive growth in semiconducter technology. This has put tremendous pressure on related fields to make similar advancements. In particular, the area of mechanical actuators has felt a substantial push, both by those trying to make "smaller and better" computer peripherals and by those who are using the micro/mini processor as a controller for some other process. At the same time these mechanical devices have been asked to surpass yesterday's performance, they have also been asked to do it more economically.

One device that has seen extensive use is the stepping motor. The stepping motor is an ideal actuator for digital logic because the only information it needs is the on or off status of its windings. The trick is when to turn on and when to turn off these phases. As discussed by Gauthier[1], a stepping motor will usually, easily and accurately perform the simple tasks. Unfortunately, it is not difficult to devise step sequences that will cause the motor to fail to execute correctly. These failures seem to occur either at random or when previous experience indicates that the motor should perform satisfactorily.

Gauthier performed extensive work in developing a mathematical model to describe the performance of stepping motors using the phase plane. The major emphasis was in developing a second order model to describe the 90' permanent magnet stepping motor. As the stepping motor industry has progressed, the motor most widely used is the hybrid stepping motor. The most popular hybrid stepping motor is the 1.8' design. Because of its more efficient magnetic structure, the 1.8' stepper produces significantly higher torques than the 90' motor for the same frame size and power consumption. Its small step size is also better suited for applications that require small incremental motions and high position resolution.

As its name implies, the hybrid motor is a combination of two motor designs, the permanent magnet motor (PM) and the variable reluctance motor (VR). The simplest PM motor consists of a permanent magnet rotor which is magnetized radially and a stator field structure which establishes a radial flux density distribution in the air gap of the motor. See Figure I-1. The stator has a series of poles. For the motor shown in Figure I-1, each pole has a winding around it. The four windings become the four stator phases. Energizing a phase establishes a magnetic field in the motor. The rotor, like a compass, tries to align itself with the magnetic field. When the two are lined up, the motor is said to be at its desired step location. When a

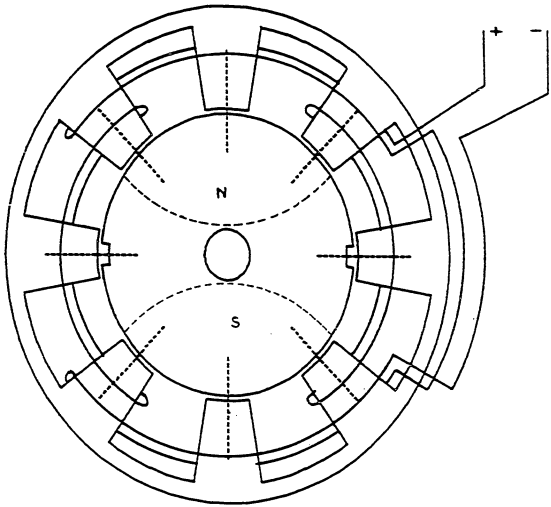

A FOUR PHASE PERMANENT MAGNET MOTOR

FIGURE I-1

different stator phase is energized, the orientation of the magnetic field is changed and the rotor moves to the new maximum flux density direction. In this way the motor executes a step. The configuration used to accomplish this can be rather simple. Shown in Figure I-1 is a four phase 90' stepping motor, which would make four steps per revolution. One of the major advantages of the PM motor design is that even after the motor is deenergized it still produces a holding torque. This torque is due to the flux produced by the permanent magnet rotor. The rotor attempts to minimize the reluctance of its magnetic flux path by aligning with the nearest stator pole.

The VR motor has no magnetic material in the rotor. Instead, its rotor is made of a material with low magnetic reluctance and is shaped like a gear. In principle it operates like a solenoid. The stator is similar to the PM motor's stator, consisting of a series of poles and winding phases. When a stator phase is energized, the rotor moves to minimize the reluctance of the flux path for the energized winding. Figure I-2 shows the configuration of a four phase, 24 step per revolution motor. Each phase consists of two windings around opposite poles connected in series. As different phases are energized, the motor will step to each new point of minimum reluctance.

The VR motor can be manufactured to have smaller step sizes than the PM motor for applications requiring

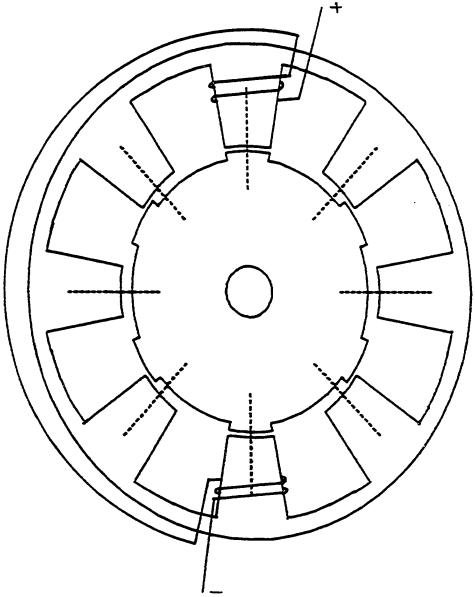

A FOUR PHASE VARIABLE RELUCTANCE MOTOR

FIGURE I-2

higher resolution. However, when the windings are deenergized the VR has no residual magnetism and, therefore, no holding torque.

The hybrid motor incorporates some of the benefits of both the PM and VR designs. It produces high torque, has a small step angle and generates a residual torque when deenergized. This motor is shown in Figure I-3.

A permanent magnet is used in the rotor which is now magnetized axially with respect to the rotor axis. At each end of the magnet is a pole piece much like a gear with several teeth on it. The teeth of the pole pieces on either end are staggered one-half tooth so that, looking down the axis of the rotor, the tooth on one pole piece falls in the valley of the teeth on the other pole piece. As before, the stator phases are now excited to produce a flux density direction. One of the rotor north pole pieces tries to line up with the direction of maximum flux density, while the south pole piece does the same. See Figure I-3. With this structure it is possible to obtain permanent magnet stepping motors with as many as 100 steps per revolution using a hundred-tooth rotor and four stator phases. Figure I-4 shows the actual stator and rotor pieces that are used in Eastern Air Devices 1.8', size 34, hybrid stepping motor.

In attempting to apply the work of Gauthier to the hybrid motor, it was necessary to include in the hybrid

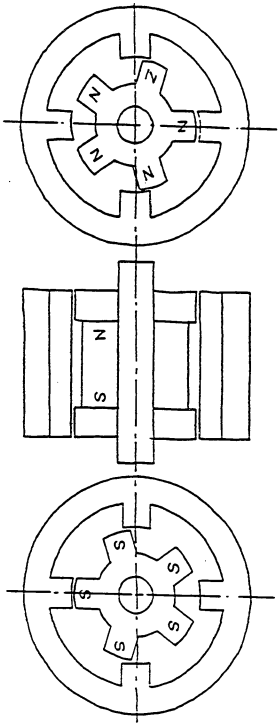

A FOUR PHASE HYBRID MOTOR

FIGURE I-3

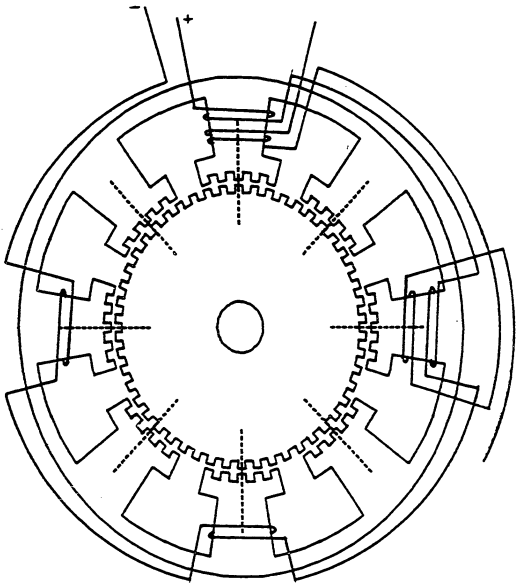

AN EAD 1.8′ FOUR PHASE HYBRID MOTOR

FIGURE I-4

model some of the phenomena that had a negligible effect on the permanent magnet stepping motor. In particular, the L/R current rise time must be included in all applications, not just the high speed ones, as is the case with the permanent magnet stepper. Also, magnetic saturation of the stator iron, magnetic hysteresis and eddy current losses in the stator iron must be considered.

The main purpose of this work is to extend the model developed by Gauthier to describe the hybrid stepping motor. Once that is accomplished it will be seen that many of the failure modes and dynamic characteristics discussed by Gauthier also occur in the hybrid motor. In addition, the model will then be used to investigate other dynamic characteristics of the motor.

When the hybrid stepper motor was first developed by General Electric Company, it was intended to be a low speed AC synchronous device. It was only later that the hybrid motor was used as a stepper. The model that will be developed to describe the stepping behavior of the hybrid motor, can also be used to describe the behavior of the motor when it is being driven synchronously. By plotting the trajectories of the synchronous model in the phase plane, it is also possible to describe many of the start/stop and failure mechanisms that pertain to permanent magnet synchronous motors. Synchronous startup and reversal, as well as stable and unstable operating regions, maximum speed

and the system's response to external disturbances will be discussed.

The final topics to be discussed will be angle accuracy and mid-frequency resonance. Angle accuracy is a motor's ability to make uniform, repeatable, constant angle steps. Mid-frequency resonance is an instability that affects most stepping motors when operating at speeds between 40% and 70% of their maximum speed. Both problems are of considerable interest to the users of stepping motors. Confusion and misconceptions still exist concerning these topics and it is hoped that light will be shed on both.

Finally, two comments that will aid the reader of this manuscript: First, this work is intended to be a continuation of the work performed by Gauthier. To understand many of the concepts used or developed here, a strong understanding of his work will be necessary. And, second the stepping motor system consists of three basic parts. The stepping motor itself, the load the stepping motor must move in an application, and the drive amplifier or power amplifier which is used to apply the voltages to the stator phases. In this research, the stepping motor and drive amplifier are the components of interest. It is assumed that the load is rigidly coupled to the motor. Therefore, when mechanical terms like inertia are used it implies the inertia is the total inertia of the motor and

the load inertia reflected to the motor. In general the term "motor" will imply motor and load where applicable unless otherwise stated.

CHAPTER II

THE HIGHER ORDER MODEL

Introduction

Early in his work, Gauthier developed Equation II-1

$$\frac{V_s}{(R_s+R_m)} = I + \frac{L_m}{(R_s+R_m)}\frac{dI}{dt} - \frac{K_b\dot{\theta}}{(R_s+R_m)}\,\mathrm{Sin}(A\theta) \qquad \text{(II-1)}$$

Where: θ = Angular position
$\dot{\theta}$ = Angular velocity
I = Stator winding current
K_b = Back EMF constant
R_m = Stator winding resistance
L_m = Stator winding inductance
V_s = Drive supply voltage
R_s = Drive series resistance
A = Number of north poles on the rotor

which describes the current in a stator phase. In most applications involving the 90' permanent magnet stepping motor, the inductive rise time is small compared to the phase on time. This makes it possible to neglect the $L_m/(R_s+R_m)\ dI/dt$ term. Equation II-1 is then reduced to an algebraic expression, Equation II-2, that can be solved for I, the stator phase current. Equation II-2, when used in conjunction with the second order differential equation

$$I = \frac{V_s}{(R_s+R_m)} + \frac{K_b\dot{\theta}}{(R_s+R_m)} \sin(A\theta) \qquad \text{(II-2)}$$

describing the rotor's motion, Equation II-3[1], results in a

$$\ddot{\theta} = -\frac{B\dot{\theta}}{J} - \frac{T_f}{J}\frac{\dot{\theta}}{|\dot{\theta}|} - \frac{K_t I}{J}\sin(A\theta) - \frac{D_t}{J}\sin(D_m A\theta) \qquad \text{(II-3)}$$

Where: θ = Angular position
$\dot{\theta}$ = Angular velocity
$\ddot{\theta}$ = Angular acceleration
I = Stator phase current
J = Rotor and load inertia
B = Rotor and load damping
T_f = Rotor and load friction
K_t = Torque constant
D_t = Detent torque
D_m = Number of cycles of the detent torque per cycle of stator torque
A = Number of north poles on the rotor

second order, nonlinear differential equation that represents the stepping motor and electronic drive. In a more generalized form they can be rewritten as Equation II-4.

$$\ddot{\theta} = -\frac{B\dot{\theta}}{J} - \frac{T_f}{J}\frac{\dot{\theta}}{|\dot{\theta}|} - \frac{K_t}{J}\sum_{n=1}^{p} I_n \sin\left(A\theta-(n-1)\frac{2\pi}{p}\right) - \frac{D_t}{J}\sin(D_m A\theta) \qquad \text{(II-4a)}$$

and

$$I_n = \frac{V_s}{(R_s+R_m)} + \frac{K_b\dot{\theta}}{(R_s+R_m)} \sin(A\theta-(n-1)\frac{2\pi}{p}) \qquad \text{(II-4b)}$$

Where: p = Number of electrical phases

The solution of Equation II-4 can be obtained by using one of several numerical integration techniques. The solution can be plotted in the phase plane. The phase plane is the particular case of a nonlinear second order state space having position and velocity as the state variables.

As stated earlier, Equation II-4 is valid as long as the L/R rise time remains small compared to the total stator on time. Experience has shown that a ratio of 1:10, rise time to on time, is the upper limit for the second order model to yield accurate results.

For a typical 90' permanent magnet stepping motor with a stator resistance of 12 ohms, a stator inductance of 15 millihenries and a L/R drive with a 20 ohm series resistor, the current rise time equals 4.69×10^{-4} seconds. Assuming of rise time of ten percent of the phase on time yields a step rate of 213 steps/second. This corresponds to 3195 revolutions/minute. Below this speed the inductive effects are neglible, above this speed the model will no longer describe the motor and drive system accurately enough for analysis and design purposes. The start-stop rate for this 90' stepping motor is approximately 200 steps per second. Therefore, the second order model is valid up to the

start-stop rate for the 90' stepper. However, for a 1.8' hybrid stepping motor with a stator resistance of 3.5 ohms, an inductance of 12 millihenries and the same 20 ohms series resistor, the step rate equals 196 steps/second or 58 revolutions/minute. The start-stop rate of the 1.8' step motor is approximately 450 steps/second.

This comparison demonstrates that while the second order model was adequate for the 90' stepper at speeds up to and beyond the start-stop rate, it is necessary to include inductance in the model of the hybrid motor for speeds well below the start-stop rate. Because the majority of hybrid motor applications concern systems operating at or above the start-stop rate, a model that does not include inductance has little value in investigating the performance of the hybrid motor.

Dietz[2] conducted a substantial research effort in modeling the various types of stepping motor drives. In his work he did include the inductive current rise time. However, the resulting equations were used to investigate the drive's effect on the single step response and steady state, constant velocity modes of operation. The effects of the inductive rise time and of using a higher order model in the phase plane were not discussed in detail.

The Effects of Including Inductance In the Stator Winding Model

Referring to the circuit diagram for one phase of a stator (Figure II-1), the following equation can be developed:

$$V_s = I_n R_m + L_m \frac{dI_n}{dt} + M_{mk} \frac{dI_k}{dt} - K_b \dot{\theta} \mathrm{Sin}(A\theta - (n-1)\frac{2\pi}{p}) \quad \text{(II-5)}$$

Where: M_{mk} = Mutual inductive terms (k=1 to p, k≠n)

$L_m \, dI_n/dt$ is the self-inductive term which accounts for the rate of change of current within the winding. $M_{mk} \, dI_k/dt$ is the mutual inductive term which will account for the rate of change of the current within any other magnetically coupled stator winding. It should be noted that there may not be any or there may be several mutual inductive terms depending upon the magnetic configuration of the motor.

A generalized differential equation describing the current in a phase can be found by solving for dI_n/dt:

$$\frac{dI_n}{dt} = \frac{V_s}{L_m} - I_n \frac{(R_s+R_m)}{L_m} - \left(\sum_{k=1,(k\neq n)}^{p} \frac{M_{mk}}{L_m} \frac{dI_k}{dt} \right) + \frac{K_b \dot{\theta}}{L_m} \mathrm{Sin}(A\theta-(n-1)\frac{2\pi}{p}) \quad \text{(II-6)}$$

Where n can equal from 1 to p for a p-phase motor. k can also equal 1 to p for a p-phase motor. However, k cannot

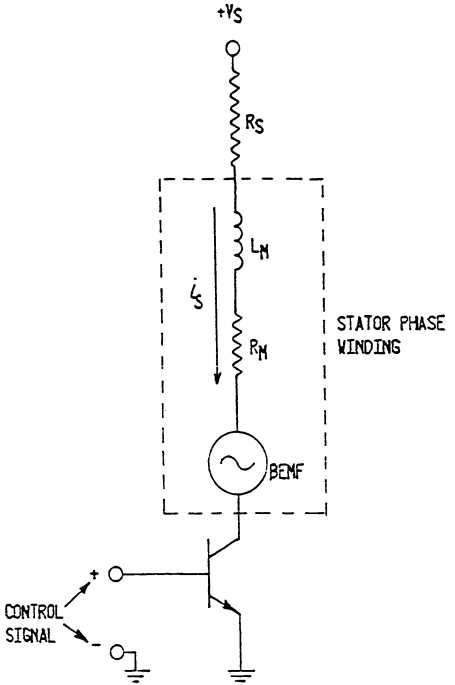

A STATOR WINDING CIRCUIT DIAGRAM

FIGURE II-1

equal n as that would be the self-inductive term. This expression, along with the second order mechanical model, Equation II-7, now more accurately describes the stepping

$$\ddot{\theta} = -\frac{B\dot{\theta}}{J} - \frac{T_f}{J}\frac{\dot{\theta}}{|\dot{\theta}|} - \frac{K_t}{J}\sum_{n=1}^{\frac{p}{2}} I_n \sin\left(A\theta-(n-1)\frac{2\pi}{p}\right) - \frac{D_t}{J}\sin(D_m A\theta) \qquad \text{(II-7)}$$

motor and drive system. Because of the dynamics incorporated into the current model, the system model is no longer second order. The order of the new model is two more than the number of phases. For a four phase motor, the model is sixth order. Obviously this model can no longer be represented in the velocity-error phase plane; a six dimensional state space is now required.

The differential equations are coupled through position, velocity and current. In order to find the system response using the model, initial conditions are selected for the position, velocity and currents. Equation II-6 is then evaluated with those initial conditions and the stator phase currents can be calculated using any of the numerical integration techniques. Equation II-7 is now evaluated with the original position, velocity and current values. Numerical integration is again used to calculate new values for position and velocity. The new values of position, velocity and current are returned to Equation II-6, time is

increased by the integration interval and the process is repeated.

The addition of the L/R current rise time has made the system model more complex. In addition to numerically solving the differential equation describing mechanical motion, the differential equation representing the currents must also be solved. However, the current equation is solved by exactly the same method used with the mechanical equations. Therefore, no new techniques are required by the higher order model, merely an increase in computation time.

The current waveform is now dependent upon both the back EMF and the L/R rise time. To better understand the effect of these two parameters, it would be helpful to look at each one individually. In Figure II-2 the L/R current rise time equals zero. The oscillation is entirely due to the back EMF as the rotor oscillates around the stable equilibrium point. The back EMF constant has been set equal to zero in Figure II-3 and the L/R current rise time is clearly shown. The effect on the current waveform of both the back EMF and the L/R rise time is shown in Figure II-4. It is obvious that the back EMF and the inductance both have a significant effect on the current.

JM=	3.25m	TF=	1.61	ST=	0.00	B=	11.60m	KT=	78.00
DTR=	5.50	DTRM=	4.00	KB=	448.60m	VR=	5.40	IR=	1.50
RM=	3.60	LM=	20.00m	PHZE=	4.00	STPR=	200.00		
VS=	35.40	RS=	20.00	RF=	0.00	STS=	1.00	PHO=	2.00
EQTB=N		FD=N		FDL=N		WRW=N		DRTP=0	

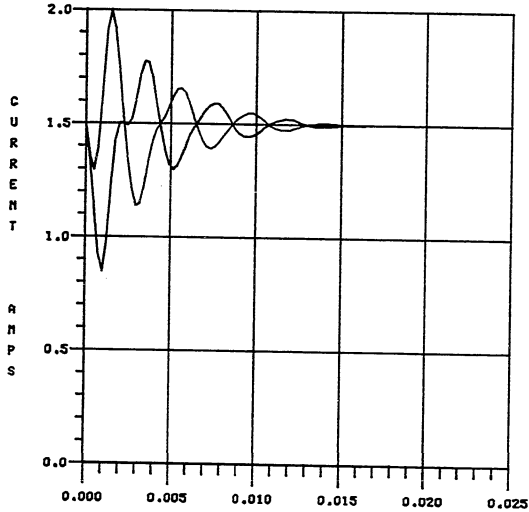

WINDING CURRENT TRANSIENT L_m = 0.0

FIGURE II-2

JM=	3.25m	TF=	1.61	ST=	0.00	B=	11.80m	KT=	78.00
DTR=	5.50	DTRM=	4.00	KB=	0.00	VR=	5.40	IR=	1.50
RM=	3.60	LM=	20.00m	PHZE=	4.00	STPR=	200.00		
VS=	35.40	RS=	20.00	RF=	0.00	STS=	1.00	PHO=	2.00
EQTB=N		FD=M		FDL=N		WRW=M		DRTP=1	

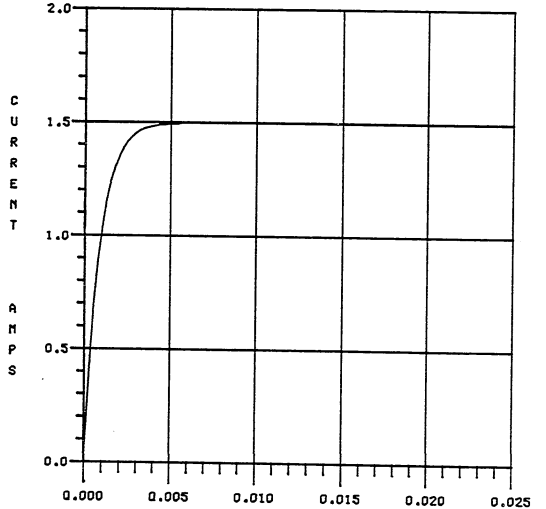

WINDING CURRENT TRANSIENT K_b = 0.0

FIGURE II-3

JM=	3.25m	TF=	1.01	ST=	0.00	B=	11.80m	KT=	78.00
DTR=	5.50	DTRM=	4.00	KB=	448.80m	VR=	5.40	IR=	1.50
RM=	3.60	LM=	20.00m	PHZE=	4.00	STPR=	200.00		
VS=	35.40	RS=	20.00	RF=	0.00	STS=	1.00	PHO=	2.00
EQTQ=N		FD=N		FDL=N		WRW=N		DRTP=1	

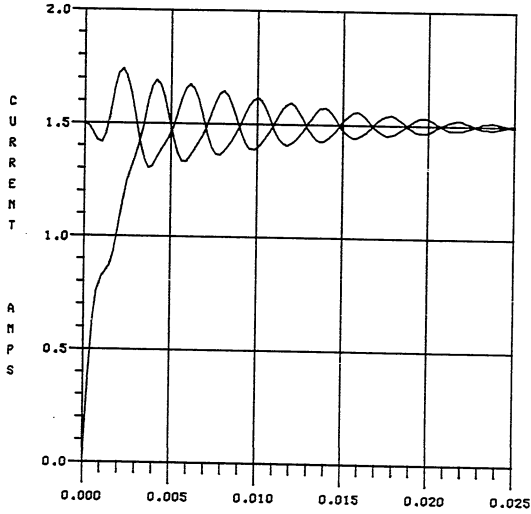

WINDING CURRENT TRANSIENT $L_m, K_b > 0.0$

FIGURE II-4

The Higher Order Model in the Phase Plane

It was stated earlier that, because of the inductive dyamics added to the model, the system response can no longer be completely described in the two dimensional phase plane. Rather the system response is now represented by a trajectory that travels through the state space of coordinates θ, $\dot{\theta}$, I_1, $I_2 \ldots I_p$.

Trying to visualize a trajectory traveling through a four or greater dimension state space is difficult at best. However, for the case where the motor operates with only one phase energized at a time, the response can be shown in a three dimensional space. In this mode of operation, position, velocity and the current in the on phase are the only non-zero state variables. Figure II-5 shows the single step response where the non-zero state variables have been plotted in a three dimensional state space. The blue curve is the actual system response and shows both current inductive rise and the effect of the back EMF on the oscillations. The red curve is the projection of the system response back into the position-velocity plane. The projection results in a response in the position-velocity plane that is very similar to the second order, single step response shown by Gauthier.

In Figure II-6 the concept of displaying the response of a stepping motor with one phase on in three

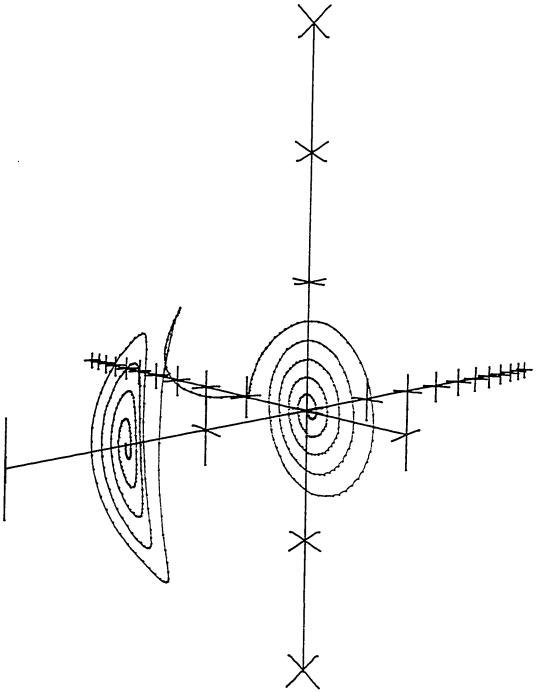

A THREE DIMENSION SINGLE STEP RESPONSE

FIGURE II-5

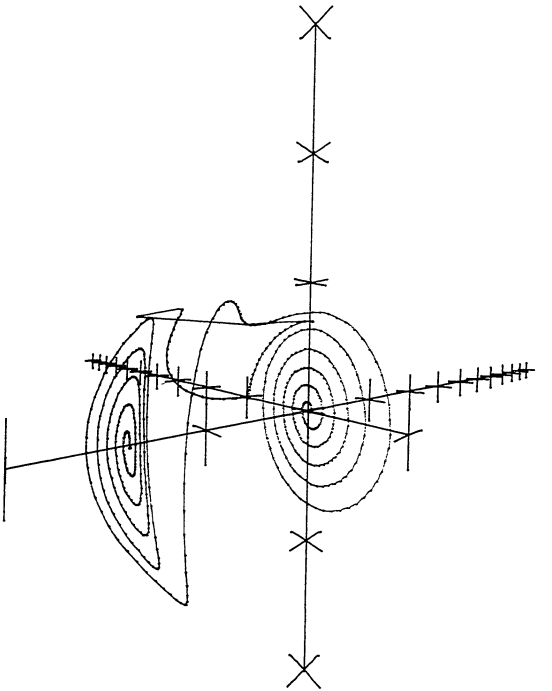

A THREE DIMENSION TWO STEP RESPONSE

FIGURE II-6

dimensions is extended to show a two step sequence. Again the position, velocity and on phase current are displayed in three dimensions. The blue curve is the three dimensional trajectory and the red curve is the projection back into the position-velocity plane. In Figure II-6 the motor starts from rest, and after .0022 seconds it is stepped. Stepping is shown as first an instantaneous shift in position equal to minus one step, and then as shift to zero current. This occurs because the current in the first phase has just been turned off, and because the initial condition of the current in the second phase is zero.

It should be noted that the currents in phase one and phase two are different state variables and plotting them on the same axis is not technically correct. However it is very useful in showing the response of the higher order system.

A four step sequence that fails at the natural frequency is shown in the three dimensional state space in Figure II-7. Figure II-7 shows that a sequence that contains more than one or two steps quickly becomes confusing to understand. However, the projection of the trajectory back into the position-velocity plane, the red curve, is very similar to sequences predicted by Gauthier using the second order model to show failure at step rates near the natural frequency. This indicates that, even though a higher order model is now being used, it should be possible to display

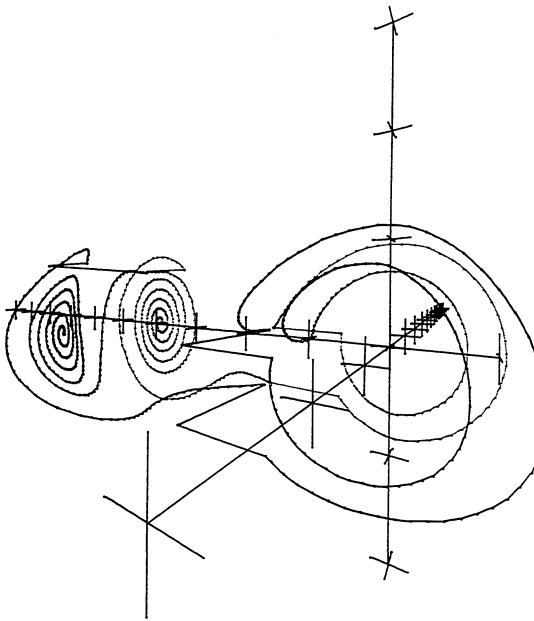

A THREE DIMENSION FOUR STEP RESPONSE

FIGURE II-7

the results as a projection back into the position-velocity plane.

Also, if the motor is being operated with more than one phase energized, the total system response cannot be shown in the three dimensional space. At least a four dimensional space would be needed. In this case projecting the response into the position-velocity plane will yield the best overall results.

Because of the problems associated with displaying the results of the higher order model in a higher order space, a projection of the higher order results will be displayed in the position-velocity plane.

Stepping is still represented by an instantaneous shift in the position equivalent to the step size. Zero velocity and zero position still represent the desired equilibrium position. This enables many of the same insights that were realized in the second order phase plane to be gained from the state space. There are however, several subtle differences between the second order velocity-error plane and the projection of the trajectory in the higher order state space into the velocity-error plane.

Because of the higher order nature of the system, the projection of the trajectory into the velocity-error plane may cause a trajectory to cross itself. The reason this crossing occurs is that the velocity and error

coordinates are the same but the stator currents are different each time the trajectory passes through that point in the projection. See Figure II-8.

Another effect is a hooking or unusual curve in the trajectory just after a step has been made. This is seen only during multiphase operation. It occurs because the location of the magnetic flux vector does not change instantaneously with the step command during multiphase operation. Rather it shifts from the old equilibrium position to the new equilibrium position at the same rate at which the current rises in the winding that has just been energized. See Figure II-9. The rotor attempts to settle on the flux vector as the vector continues to move to the new position. This results in the unusual shape of the trajectory in Figure II-9.

Figure II-7 demonstrats another point that has considerable impact on understanding the higher order state space concepts. The three dimensional trajectory crosses a separatrix during the third step. In the higher order state space, a separatrix is no longer a unique trajectory that leads to a unstable equilibrium point. Rather the separatrices are a whole family of higher order trajectories that lead to the unstable equilibrium point. This family of separatrices make up a surface in the state space.

This separatrix surface separates the higher order

JM=	3.25m	TF=	1.61	ST=	0.00	B=	11.60m	KT=	78.00
DTR=	5.50	DTRM=	4.00	KB=	448.80m	VR=	5.40	IR=	1.50
RM=	3.60	LM=	20.00m	PHZE=	4.00	STPR=	200.00		
VS=	35.40	RS=	20.00	RF=	0.00	STS=	1.00	PHO=	2.00
EQTQ=M		FD=M		FDL=M		WRW=M		DRTP=1	

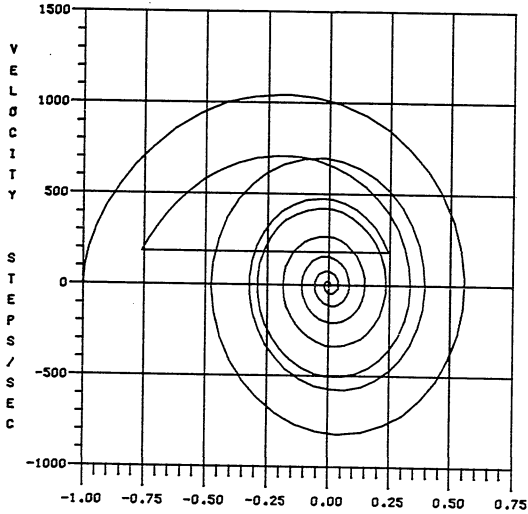

A CROSSING TRAJECTORY IN THE PHASE PLANE

FIGURE II-8

JM=	3.25m	TF=	1.61	ST=	0.00	B=	11.80m	KT=	78.00
DTR=	5.50	DTRM=	4.00	KB=	448.80m	VR=	5.40	IR=	1.50
RM=	3.80	LM=	20.00m	PHZE=	4.00	STPR=	200.00		
VS=	5.40	RS=	0.00	RF=	0.00	STS=	1.00	PHO=	2.00
EQTQ=N		FD=N		FDL=N		WRW=N		DRTP=1	

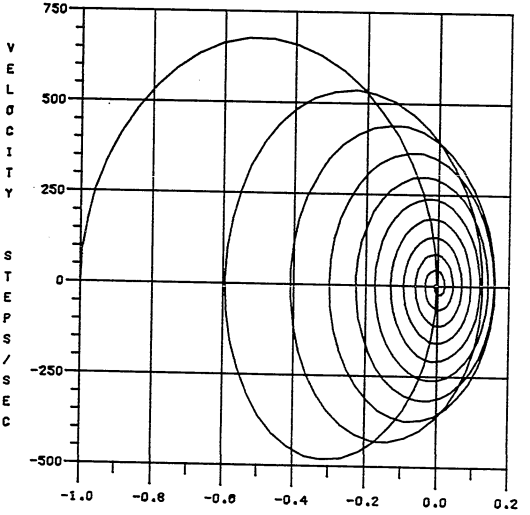

A HOOKED TRAJECTORY IN THE PHASE PLANE

FIGURE II-9

space into regions around each stable equilibrium point. Even though the separatrix is a surface, a single curve on that surface is projected and plotted in the velocity-error plane. Separatrices are calculated by using the unstable equilibrium point as the initial condition and running time backward. Because of the problem of deciding which portion of the separatrix to project into the velocity-error plane, the second order model is used for calculating the separatrix.

Because the separatrix is approximated using the second order model and the trajectories are being projected back into the position-velocity plane, it is possible for a projected trajectory to cross a projected separatrix during stepping in the velocity-error plane without losing or gaining steps. Again the position and velocity coordinates appear to cross in the two-dimension plot, however, when all six coordinates are considered, the trajectory does not cross a separatrix surface.

Conclusion

At this point it is important to recognize that even though the higher order model is more complex, it can still be easily used to obtain insights into the low speed behavior of the stepping motor/drive system. The additional differential equations are solved using the same numerical

techniques that were used to solve the original second order equation. Therefore, no new methods are required, just an increase in computation time. All the low speed failure modes can still be described by projecting the trajectory into the phase plane. In addition, by including the inductive rise time in the model, the model can be used to describe systems operating over a wider range of speeds.

Figures II-10 and 11 show two high performance, constant velocity sequences for the 90' permanent magnet stepping motor. Both sequences were designed using analytical models and the results were tested on an experimental system. Figure II-10 was designed using the second order model with the inductance neglected. In Figure II-11 the inductance was included. It is clear that by including the inductance in the model, the simulation produced obtains more satisfactory results.

As long as it is kept in mind that there are some subtle effects due to projecting the trajectory into the phase plane, all of the methods that were developed by Gauthier for analyzing a stepping motor's performance are still valid. For the higher order model the phase plane is still a very insightful and powerful method for understanding the dynamic characteristics of a stepping motor.

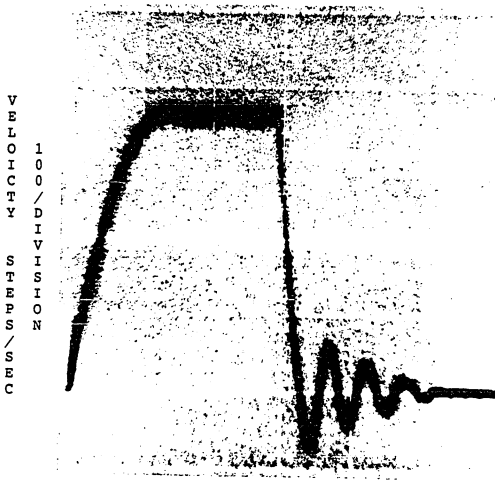

A 100 STEP SEQUENCE FOR A 90' PERMANENT MAGNET STEPPING MOTOR, L_m = 0.0 mH

FIGURE II-10

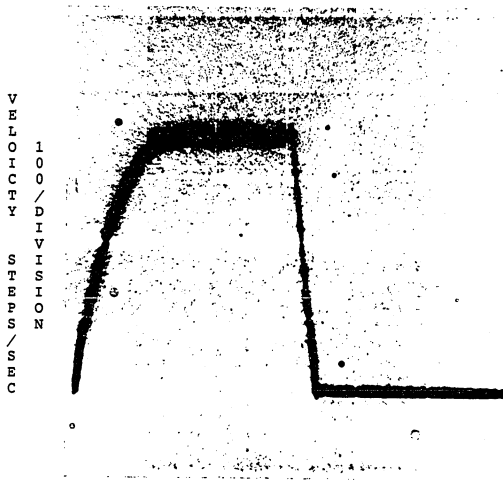

A 100 STEP SEQUENCE FOR A 90' PERMANENT MAGNET STEPPING MOTOR, L_m = 15.20 mH

FIGURE II-11

CHAPTER III

SATURATION, HYSTERESIS, AND EDDY CURRENTS IN THE HYBRID STEPPING MOTOR

Introduction

As stated earlier, Gauthier achieved considerable success in describing and predicting the low speed behavior of the permanent magnet stepping motor using the second order model. The velocity transient of a PM motor being single stepped is shown in Figure III-1. Both the analytical response as predicted by the model and the actual experimental response are shown. The figure shows the excellent correlation between the two.

In Chapter II, it was shown that when the stator winding inductance is added to the PM motor model creating a higher order model, the model can also be used to predict the high speed performance of the motor. Figure III-2a is a plot of the velocity transient of a point to point, no-over-shoot step sequence that was designed using the PM motor model. The corresponding experimental response is shown in Figure III-2b. Again, there is an excellent correlation between the analytical and experimental results. There is further documentation of high speed applications in the work conducted by Dietz.[2]

If the higher order PM motor model is used to

```
 JM= 405.00u  TF= 335.00m  ST=   0.00    B= 650.00u  KT=   0.55
DTR=   0.00 DTRM=  12.00   KB=  48.00m  VR=  11.34   IR= 900.00m
 RM=  12.00   LM=  15.20mPHZE=   4.00 STPR=   4.00
 VS=  40.00   RS=  31.66   RF=   0.00  STS=   1.00  PHO=   1.00
EQTQ=N        FD=N        FDL=N       WRW=N       DRTP=0
```

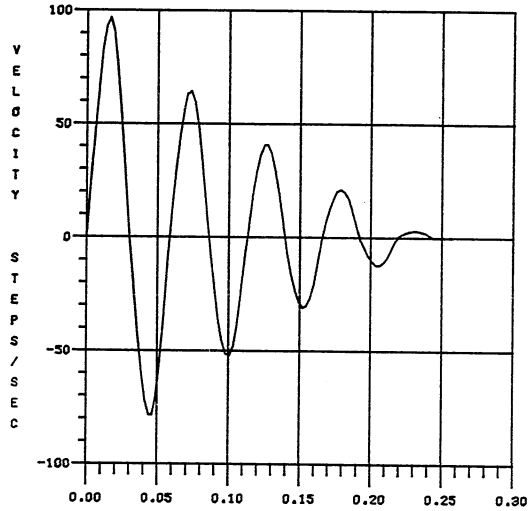

AN ANALYTICAL PM MOTOR SINGLE STEP
VELOCITY PROFILE

FIGURE III-1a

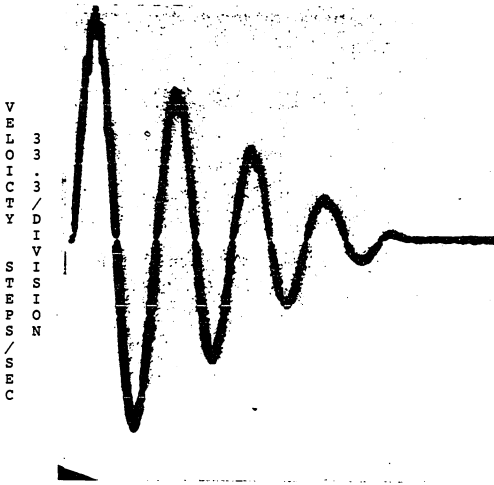

AN EXPERIMENTAL PM MOTOR SINGLE STEP
VELOCITY PROFILE

FIGURE III-1b

JM= 405.00u TF= 335.00m ST= 0.00 B= 650.00u KT= 0.55
DTR= 0.00 DTRM= 12.00 KB= 48.00m VR= 11.34 IR= 900.00m
RM= 12.60 LM= 15.20mPHZE= 4.00 STPR= 4.00
VS= 40.00 RS= 31.68 RF= 0.00 STS= 1.00 PHO= 1.00
EQTQ=N FD=N FDL=N WRW=N DRTP=1

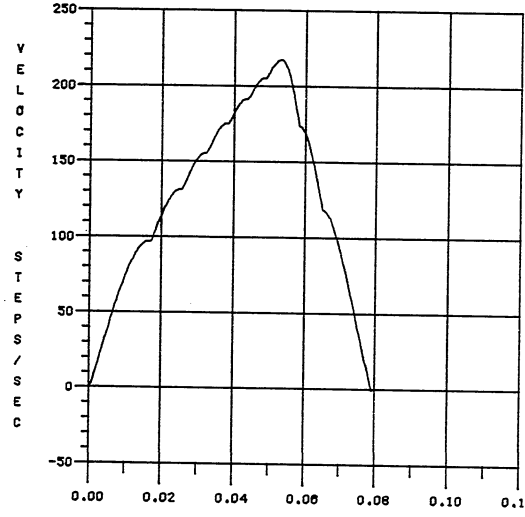

AN ANALYTICAL PM MOTOR MULTI-STEP
VELOCITY PROFILE

FIGURE III-2a

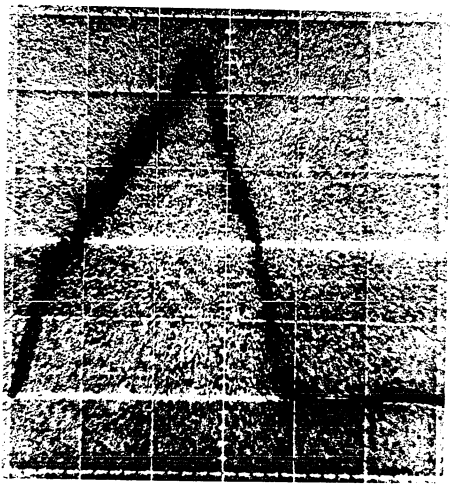

.02/ DIVISION

TIME SECONDS

AN EXPERIMENTAL PM MOTOR MULTI-STEP
VELOCITY PROFILE

FIGURE III-2b

predict the dynamic response of the hybrid stepping motor, the results are not nearly as accurate. The single step velocity response of a 1.8' hybrid motor according to the higher order PM model is shown in Figure III-3a. The actual response of an experimental system is shown in Figure III-3b. The analytical and experimental current profiles are shown in Figures III-3b and III-3c. It can be seen from these four figures that the PM motor model does not provide an accurate description of the hybrid motor. The same result can be seen in Figures III-4a and III-4b where the PM motor model was used to design a twenty-four step, point to point sequence for the hybrid motor. Figure III-4c is a compressed view of III-4b which demonstrates the extent of the ringout.

In attempting to determine the differences between the PM motor and the hybrid motor, it is their similarities which stand out. Even though the motors have two different magnetic designs, they have similar characteristics. Mechanically, the inertia, bearing friction and damping are similar. Both motors have sinusoidal stator torque and detent torque angle curves. Electrically, the resistances and inductances of the windings are similar and they have sinusoidal back EMF voltages induced in the windings. From these similarities, it follows that the more complex magnetic structure of the hybrid motor does not necessarily mean that there is a whole new phenomenon to be modeled. Rather, the different magnetic structure must have some

JM=	3.25m	TF=	1.61	ST=	0.00	B=	11.80m	KT=	78.00
DTR=	5.50	DTRM=	4.00	KB=	448.00m	VR=	5.40	IR=	1.50
RM=	3.60	LM=	13.00m	PHZE=	4.00	STPR=	200.00		
VS=	35.40	RS=	20.00	RF=	0.00	STS=	1.00	PHO=	1.00
EQTQ=N		FD=N		FDL=N		URW=N		DRTP=1	

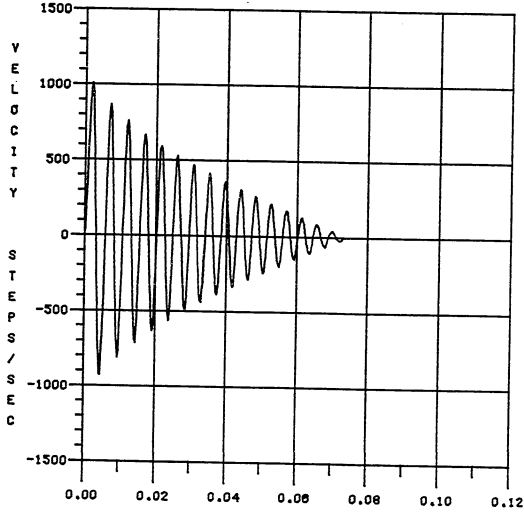

AN ANALYTICAL HYBRID MOTOR SINGLE STEP VELOCITY PROFILE

FIGURE III-3a

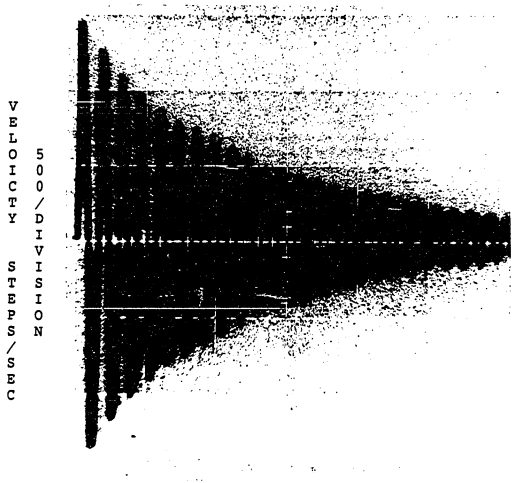

AN EXPERIMENTAL HYBRID MOTOR SINGLE STEP
VELOCITY PROFILE

FIGURE III-3b

JM=	3.25m	TF=	1.61	ST=	0.00	B=	11.80m	KT=	78.00
DTR=	5.50	DTRM=	4.00	KB=	448.80m	VR=	5.40	IR=	1.50
RM=	3.60	LM=	13.00m	PHZE=	4.00	STPR=	200.00		
VS=	35.40	RS=	20.00	RF=	0.00	STS=	1.00	PHO=	1.00
EQTQ=N		FD=N		FDL=N		WRW=N		DRTP=1	

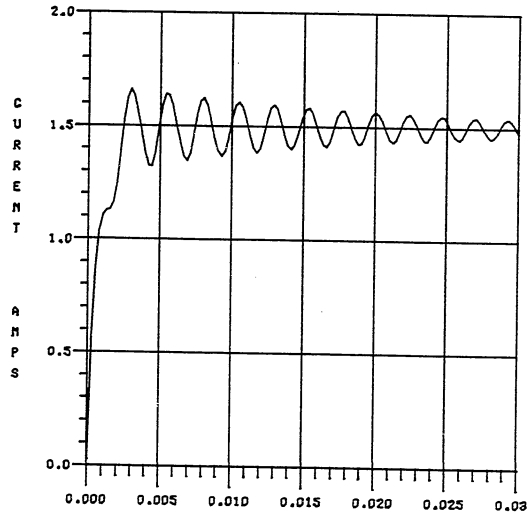

AN ANALYTICAL HYBRID MOTOR SINGLE STEP CURRENT PROFILE

FIGURE III-3c

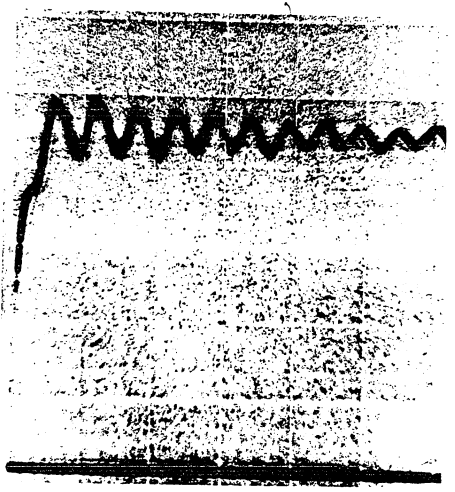

CURRENT AMPERES .6/DIVISION

.005 / DIVISION

TIME SECONDS

AN EXPERIMENTAL HYBRID MOTOR SINGLE STEP CURRENT PROFILE

FIGURE III-3d

JM=	3.25m	TF=	1.61	ST=	0.00	B=	11.80m	KT=	78.00
DTR=	5.50	DTRM=	4.00	KB=	448.00m	VR=	5.40	IR=	1.50
RM=	3.60	LM=	13.00m	PHZE=	4.00	STPR=	200.00		
VS=	35.40	RS=	20.00	RF=	0.00	STS=	1.00	PHO=	1.00
EQTQ=N		FD=N		FDL=N		WRW=N		DRTP=1	

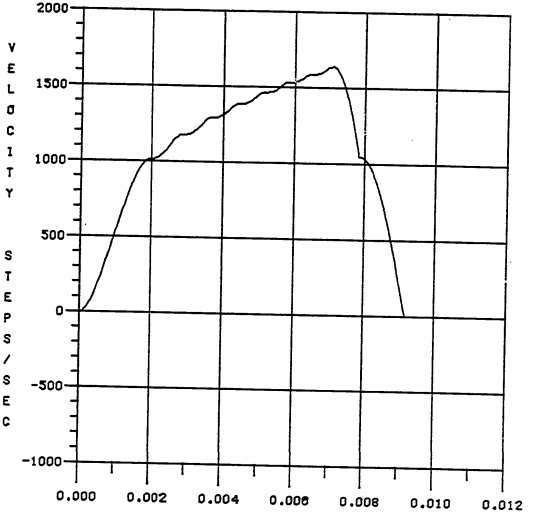

AN ANALYTICAL HYBRID MOTOR MULTI-STEP
VELOCITY PROFILE

FIGURE III-4a

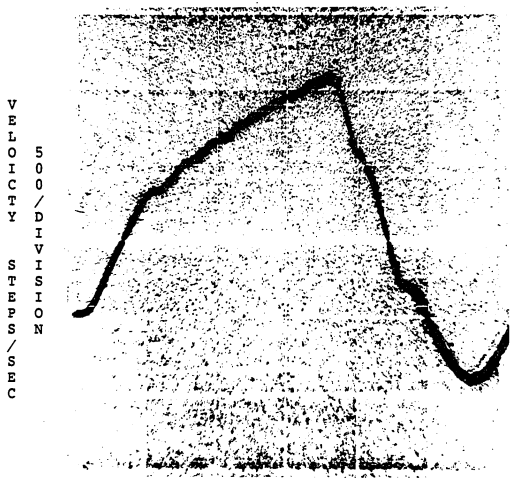

AN EXPERIMENTAL HYBRID MOTOR MULTI-STEP
VELOCITY PROFILE

FIGURE III-4b

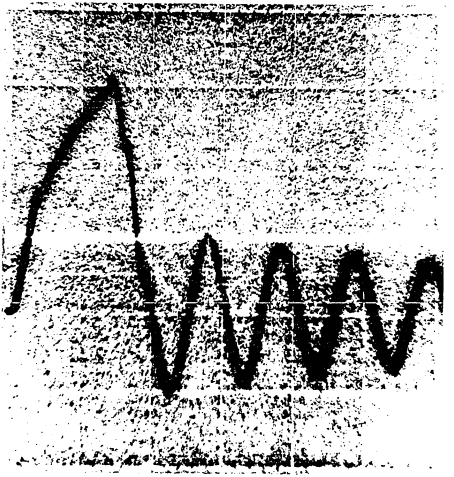

AN EXPERIMENTAL HYBRID MOTOR MULTI-STEP
VELOCITY PROFILE (COMPRESSED VIEW)

FIGURE III-4c

effect on these parameters that was not seen in the PM stepping motor.

Magnetic Saturation

In stepping motors the maximum rated current of the motor is usually determined by the motor's ability to dissipate heat. This heat comes from the I^2R losses in the stator phase winding. When compared to a comparable size PM motor, the hybrid motor will have a similar heat dissipation capability. However, it will produce larger torques at the same current level and it will magnetically saturate at a lower current level. The torque versus angle curve for a size 23, 1.8', four phase hybrid stepping motor with one phase energized at various current levels, is shown in Figure III-5a. The motor is rated at 1.5 amperes maximum current. The peaks of the torque angle curve versus current are plotted in figure III-5b. The solid curve is the actual torque produced by the stepping motor. The dashed curve is the theoretical torque that would be produced by the stepping motor if there were no magnetic saturation. This is based on the torque constant (K_t), calculated from the initial slope of the torque current curve. From this plot it can be seen that at rated current, 1.5 amperes, the torque produced is 90 oz-in, compared to a theoretical value of 105 oz-in, or 85.7% of the theoretical value.

The reason for this degradation in torque is that as

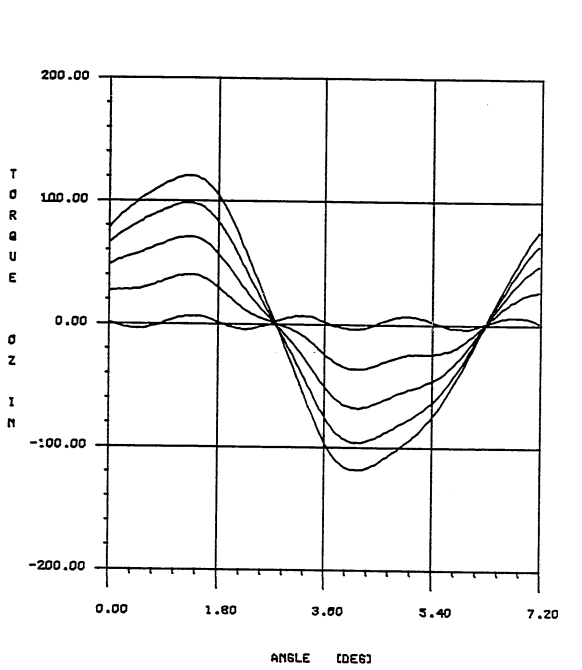

TORQUE ANGLE CURVES FOR THE 1.8°
HYBRID MOTOR, 1 PHASE ON

FIGURE III-5a

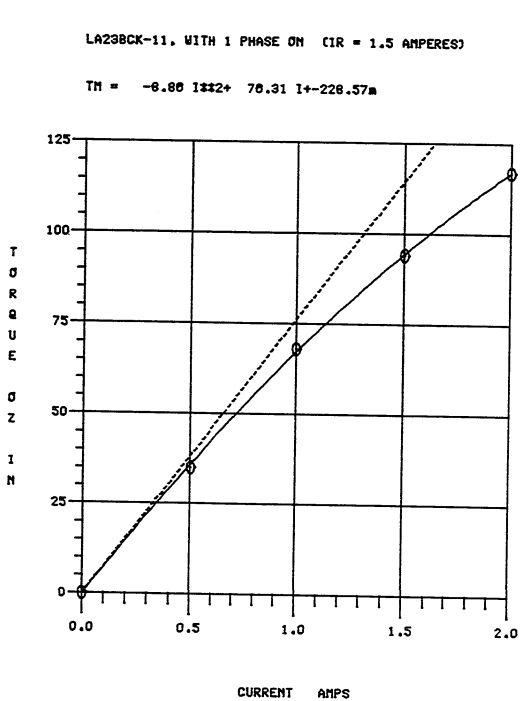

A TORQUE CURRENT CURVE FOR THE 1.8'
HYBRID MOTOR, 1 PHASE ON

FIGURE III-5b

the current is increased there are fewer and fewer magnetic domains remaining in the stator iron that can rotate and align with the induced magnetic field. This results in a decrease in the incremental change in flux produced by an incremental change in current. At any given position the torque is proportional to flux, therefore the change in torque with current is proportional to the change in flux with current. If the stator current were increased further, it would reach a point where there would be no further increase in torque with the increased current. This would be the point where the stator iron would be completely saturated. All the magnetic domains in the stator would be aligned with the magnetic field.

In the PM motor, saturation is not as severe and it is unnecessary to model the effect. In the hybrid motor, however, it is necessary to account for the magnetic saturation under normal operating conditions. Returning to Figure III-5b, it is possible to model the torque current curve with a second order polynomial. In general, the resulting polynomial would have the form shown in Equation III-1.

$$T(\Theta) = a_2 I^2 + a_1 I + a_0 \qquad \text{(III-1)}$$

Where: $T(\Theta)$ = Torque at some angle (Θ)
I = Stator current
a_2, a_1, a_0 = Polynomial coefficients

The detent torque is modeled by a separate term in

Equation II-7. Therefore the torque, T(θ), in Equation III-1 is solely dependent upon the current in the stator winding. When I equals zero, T(θ) equals zero, so that a_0 also equals zero and can be neglected. In the PM motor model a_1 would be the torque constant K_t.

In the absence of saturation, the magnetic torque term in the mechanical model is shown in Equation III-2. In

$$T = \frac{K_t}{J} \sum_{n=1}^{p} I_n \sin(A\theta-(n-1)\frac{2\pi}{p}) - \frac{D_t}{J} \sin(D_m A\theta) \quad \text{(III-2)}$$

order to keep the equations consistent in form and increase the complexity as easily as possible, it would be beneficial to develop a saturation term. Then Equation III-2 would only have an added term and not a new form. The

$$T = \frac{K_t}{J} \sum_{n=1}^{p} S_f I_n \sin(A\theta-(n-1)\frac{2\pi}{p}) - \frac{D_t}{J} \sin(D_m A\theta) \quad \text{(III-3)}$$

Where: S_f = Saturation coefficient

saturation coefficient is defined as the torque produced at the current operating point divided by the theoretical torque produced at the same operating point in the absence of saturation. The theoretical torque is the initial slope of the torque current curve times the operating current or $K_t I_n$.

$$S_f = \frac{T(\theta)}{K_t I_n} = \frac{a_2 I_n^2 + a_1 I_n}{K_t I_n} \qquad \text{(III-4)}$$

Which reduces to:

$$S_f = \frac{a_2 I_n + a_1}{K_t} \qquad \text{(III-5)}$$

It should be noted that as long as a_0 equals zero (as it should), a_1 equals the torque constant K_t. This results in the generalized saturation function shown in Equation III-6.

$$S_f = \frac{a_2 I_n}{K_t} + 1 \qquad \text{(III-6)}$$

In addition to the torque production being dependent upon saturation, the stator winding inductance, detent torque and back EMF constants are affected by saturation of the stator winding.

Ignoring saturation again for a moment, it was shown that for a constant incremental change in current, there is a corresponding proportional incremental change in the flux. See the dashed curve in Figure III-5b. When saturation occurs, the solid curve, constant increments of current no longer result in proportional increments of flux. Rather, the flux increases according to the local slope of the

saturation curve. Inductance is a measure of the change in flux generated by a change in current in the stator winding. As saturation occurs, the decreasing incremental changes in flux indicate that inductance decreases with saturation. To be specific, the change in inductance will be proportional to the change in slope of the saturation curve. At 1.5 amperes in Figure III-5 the local slope of the saturation curve is 47 oz-in/amp compared to an initial slope of 72 oz-in/amp at 0.0 amperes, or 66% of the expected value. This indicates that at rated current the winding inductance will be only 66% of its value at zero current.

Like the inductance, the change in the detent torque constant due to saturation is proportional to the change in the local slope of the torque current curve. The permanent magnet in the rotor has a magnetic motive force potential (MMF). This potential causes a small amount of flux to be established in the stator iron. In a typical hybrid motor the MMF of the magnet is 5% of the MMF of the stator winding at rated current and the MMF potential is usually assumed to be sinusoidal with position. The detent torque is proportional to the flux produced by the permanent magnet. As the stator iron saturates, the flux produced by the permanent magnet decreases, just as it would if the additional flux were being produced by additional current in the stator winding. Therefore, the change in the detent torque due to saturation will also be proportional to the

change in the slope of the saturation curve.

The back EMF voltage induced in the stator winding is due to the rate of change of flux within the winding. It is the rotating permanent magnet in the motor rotor that causes this change in flux. As the rotor rotates, the flux varies with angle, ($d\phi/d\theta$). At any given velocity, ($d\theta/dt$), the rate of change of the flux equals $d\phi/d\theta * d\theta/dt$ or $d\phi/dt$. As was reasoned with the detent torque, when the stator iron saturates, the additional flux generated by the permanent magnet decreases, just as it would if the additional flux were being generated by the stator winding. If ϕ decreases then $d\phi/dt$ must also decrease and again, it becomes obvious that the back EMF constant will also be proportional to the change in the slope of the torque current saturation curve.

Even though they are three different parameters, the inductance, detent torque and back EMF are affected in the same way by saturation. In order to model the saturation effects on these parameters properly, it is necessary to know the extent of saturation when the parameters are measured and and to what degree the level of saturation has changed for the current operating point.

Inductance is usually measured with a 1 Khz impedance bridge or a voltage square wave where the initial current rise time is measured. The detent torque is measured

with the windings unenergized. The back EMF constant is calculated by rotating the motor with its windings open circuited and measuring the induced voltage. In all the tests the stator iron is unsaturated. By returning to Figure III-5b, the effect of saturation on the back EMF, inductance and detent torque can be determined. The slope of the torque current curve at any current value can be developed from Equation III-5. See Equation III-7.

$$\frac{dS_f}{dI} = 2a_2I + a_1 \qquad \text{(III-7)}$$

As with the saturation factor, Equation III-7 is normalized with respect to the torque constant.

$$S_s = \frac{2a_2I + a_1}{K_t} \qquad \text{(III-8)}$$

Where: S_s = Saturation slope coefficient

From before, a_1 equaled K_t, therefore:

$$S_s = \frac{2a_2I}{K_t} + 1 \qquad \text{(III-9)}$$

Following this approach, a saturation slope coefficient is developed. The inductance, detent torque and back EMF at a particular operating current can now be calculated.

$$L_{ms} = L_m\left(-\frac{2a_2 I_n}{K_t} + 1\right) \qquad \text{(III-10)}$$

$$K_{bs} = K_b\left(-\frac{2a_2 I_n}{K_t} + 1\right) \qquad \text{(III-11)}$$

$$D_{ts} = D_t\left(-\frac{2a_2 I_n}{K_t} + 1\right) \qquad \text{(III-12)}$$

Where: L_{ms}= The saturated self inductance
K_{bs}= The saturated back EMF
D_{ts}= The saturated detent torque

L_m, K_b and D_t are the unsaturated values of inductance and back EMF. L_{ms}, K_{bs} and D_{ts} are the actual values due to saturation. To simplify discussion, the mutual inductance term has been ignored until this point. However, the same rationale that holds for the self-inductive term holds for the mutual inductive term. Only a_2, I_k and K_t are the parameters for the other magnetically coupled stator winding.

$$M_{ms} = M_m\left(-\frac{2a_2 I_k}{K_t} + 1\right) \qquad \text{(III-13)}$$

Where: M_{ms}= The saturated mutual inductance

Equation III-14 now describes the stator phase currents of the hybrid motor with magnetic saturation included.

$$\frac{dI_n}{dt} = \frac{V_s}{L_{ms}} - I_n\frac{(R_s+R_m)}{L_{ms}} - \sum_{\substack{k=1\\(K\neq n)}}^{p}\frac{M_{msk}}{L_{ms}}\frac{dI_k}{dt} + \frac{K_{bs}}{L_{ms}}\dot{\theta}\,\mathrm{Sin}(A\theta-(n-1)\frac{2\pi}{p}) \qquad \text{(III-14)}$$

The addition of saturation in the hybrid motor model only increases the algebraic complexity of the model. It does not affect the dynamic order of the model. Therefore, there are no new concepts or techniques required in order to use the model, simply another increase in the computer time required to solve the equations.

Hysteresis and Eddy Currents

In Figure III-3b it was seen that the oscillations of the hybrid motor decay much more slowly than the PM model indicates that they should. This suggests that the friction and damping values used in the simulation are too large. The most common method used for measuring the friction and damping of a motor is to use a dynamometer or a DC servo/tachometer with a rotary torque transducer. The measurements are made with the stator winding leads unenergized and open. The motor being tested is driven by a servo/tach and the speed versus the torque required to drive the motor at that speed is plotted. This test is conducted at a series of different steady state speeds and results in a curve similar to that in Figure III-6.

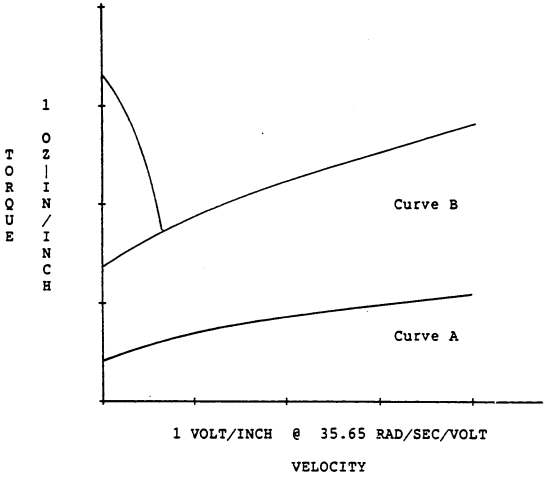

THE FRICTION AND DAMPING CURVE FOR THE
1.8' HYBRID MOTOR

FIGURE III-6

The friction (T_f) is the torque required to maintain the motor's rotation at the lowest possible speed. The damping (B) is the change in torque due to a change in the steady state speed. The initial peak torque is a result of overcoming the friction, stiction and detent torque to set the system in motion. If the friction and damping are measured for a typical hybrid motor, curve A in Figure III-6 is obtained. If the test is repeated with a motor identical except that the rotor is unmagnetized, curve B in Figure III-6 is obtained. There is a drastic difference between the two curves. The magnetized motor had the following values of friction and damping:

$$T_f = 1.40 \text{ oz-in} \qquad \text{(III-15)}$$
$$B = .0118 \text{ oz-in/rad/sec}$$

From the unmagnetized motor the following values were measured:

$$T_f = .40 \text{ oz-in} \qquad \text{(III-16)}$$
$$B = .0062 \text{ oz-in/rad/sec}$$

If the friction and damping measured in test A were strictly mechanical, one would not expect to see different values of friction and damping when the measurement was repeated with an unmagnetized motor.

There are two possible explanations for the difference between the two measurements. The first assumes

that both measurements are the mechanical friction and damping of the bearings. The increase seen in curve A is a result of an increase of the sideload on the bearings when the rotor is magnetized. When magnetized, if the rotor is not aligned exactly with the center line of the inside of the stator, radial forces will occur due to the rotor's attraction to the closest portion of the stator. These radial forces may result in increased friction and damping.

A simple experiment was devised to test this concept. One endcap of the magnetized motor was removed and the maximum radial forces possible were measured by pulling the rotor from one side of the stator to the other. The radial forces were approximately 1.5 lbs. for a size 23, 3.25 inch stack motor (the motor being tested). A third bearing was placed on the rotor shaft and the sideload on that bearing was manually applied while the friction and damping were measured. Sideloads of twenty times the magnetic radial forces were applied to the third bearing and the increases in friction and damping were less than ten percent of the original unmagnetized, curve B values. This virtually eliminates magnetic sideloads as an explanation of the differences between the two curves in Figure III-6.

The second explanation concerns magnetic hysteresis and eddy currents in the stator iron due to the rotating permanent magnet. It was stated previously that the magnetic motive force potential in the rotor's permanent magnet

causes a magnetic field to be established in the stator iron. As the rotor rotates, it causes the magnitude and direction of the magnetic field to vary, hence the flux induced depends upon the rotor's position. The effect of this is to drive the stator iron around a minor hysteresis loop. See Figure III-7. The energy losses incurred in driving the stator iron around the hysteresis loop appear as the additional "friction" in Figure III-6. These losses depend upon the area of the hysteresis loop and not on the frequency at which the loop is traversed. This is the reason it appears as a "friction" and not a damping force.

As the rotor is turned at increasing speeds, the rate of change of flux in the stator iron with time ($d\phi/dt$) increases. In addition to causing back EMF voltages in the stator windings, $d\phi/dt$ causes eddy currents to circulate in the surface of the stator iron. The eddy currents absorb energy, causing losses as did the hysteresis loop. However, the eddy current losses are velocity dependent and appear as the additional "damping" in Figure III-6.

This approach coincides with the work performed by Dahl[3] in developing a model for friction. Developing an analytical method for the determining the hysteresis and eddy currents would not be a trivial exercise so here they will be treated as "friction like" and "damping like" phenomena.

Because the hysteresis and eddy current losses

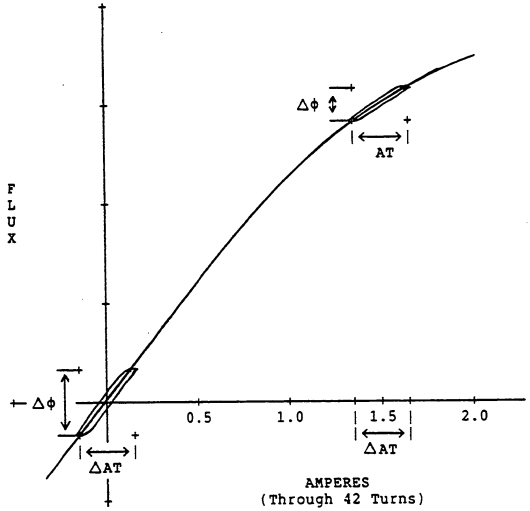

Assume the detent torque equals 10 percent of the one phase on holding torque

HYSTERESIS LOOPS INDUCED IN THE STATOR IRON DUE TO THE ROTATING PERMANENT MAGNET

FIGURE III-7

depend upon the magnitude of the flux generated in the stator iron by the permanent magnet, they are also dependent upon the effect of saturation in the stator iron. As the stator iron saturates, the magnitude of the hysteresis loop and the eddy currents decrease. See Figure III-7. This requires that the saturation slope coefficient must be included in the magnetic portions of the friction and damping terms just as it was for the inductances, detent torque and back EMF.

Therefore:

$$T_f = T_m + T_h S_s \qquad \text{(III-17)}$$
$$B = B_m + B_h S_s$$

Where: T_f = Total friction term
T_m = Mechanical friction
T_h = Hysteresis losses
B = Total damping term
B_m = Mechanical damping
B_h = Eddy current losses

The unmagnetized friction (T_m) and damping (B_m) will remain constant because they depend upon the design of the bearings and the preload.

During normal stepping motor operating conditions the motor rotor continues to travel in the same direction. The flux that is generated in the stator iron due to the permanent magnet will continue to oscillate and the

hysteresis and eddy current losses will be equal to those predicted by Equation III-17.

When the motor is being single stepped or is ringing out after a step sequence, a different phenomenon occurs. As the motor rings out, the rotor oscillates about the stable equilibrium position. The flux established in the stator iron by the permanent magnet now varies by a much smaller amount than it did when the rotor was rotating in a constant direction. This results in a small hysteresis loop. See Figure III-8. In this mode of operation it is difficult to determine the exact magnitude of the losses during the oscillations.

A small amount of trial and error experience with the single step response indicated that a sine function dependent upon the position error could be used. See Equation III-18.

$$T_f = T_m + T_h S_s \mathrm{Sin}(\theta_e)^4$$

$$B = B_m + B_h S_s \mathrm{Sin}(\theta_e)^4 \qquad \text{(III-18)}$$

Where: θ_e = The error between the rotor position and the stable equilibrium position

It should be restated that Equation III-18 is necessary only when the rotor is oscillating about a stable equilibrium point. As long as the motor is making a point to

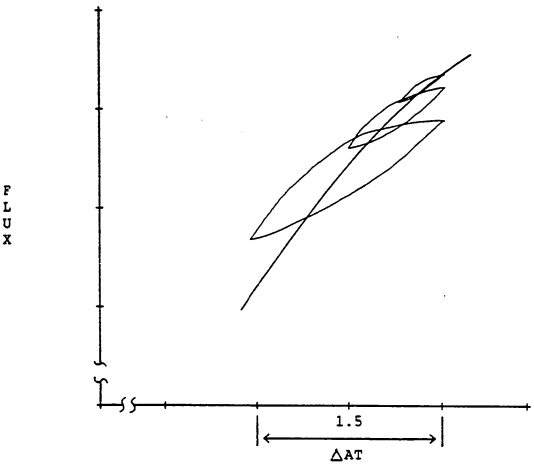

Assume the detent torque equals 10 percent of the one phase on holding torque

HYSTERESIS LOOPS INDUCED IN THE STATOR IRON DUE TO THE OSCILLATING PERMANENT MAGNET

FIGURE III-8

point or constant velocity move and the direction of motion does not change, Equation III-17 should be used. During the simulation process Equation III-18 was not used unless the velocity changed sign.

Including the saturation, hysteresis and eddy current effects into the PM motor model has resulted in Equations III-19 and III-20 which will now accurately model the hybrid stepping motor.

$$\frac{dI_n}{d\bar{T}} = \frac{V_s}{L_{ms}} - I_n\frac{(R_s+R_m)}{L_{ms}} - \sum_{k=1,(K\neq n)}^{P} \frac{M_{msk}}{L_{ms}}\frac{dI_k}{d\bar{T}} + \frac{K_{bs}}{L_{ms}}\dot{\theta}\,\mathrm{Sin}(A\theta-(n-1)\tfrac{2}{P}) \qquad \text{(III-19)}$$

and:

$$\frac{d^2\theta}{d\bar{T}^2} = -\left(\frac{B_m + B_h S_s}{J}\right)\dot{\theta} - \left(\frac{T_m + T_h S_s}{J}\right)\frac{\dot{\theta}}{|\dot{\theta}|} - \frac{K_t}{J}\sum_{n=1}^{P} S_f I_n \mathrm{Sin}(A\theta-(n-1)\tfrac{2}{P}) - \frac{D_{ts}}{J}\,\mathrm{Sin}(D_m A\theta) \qquad \text{(III-20)}$$

Like saturation, the hysteresis and eddy currents have added a degree of complexity to the model. But again, they have not added to the dynamic order of the system. The same numerical techniques can be used and the results can still be projected into the phase error plane.

The next section contains experimental comparisons with the model to demonstrate that the model accurately predicts the response of a hybrid stepping motor system.

Experimental Verification of the Hybrid Model

In any model building process, there comes a time when it is necessary to face reality. The system parameters are measured, the model that has been developed based on physical reasoning is used to simulate the real system's response and then the simulation results are compared to the real system. Often the model or the measurement techniques must be refined to obtain a more accurate correlation. Then the model can be used to investigate a range of system variations easily and quickly.

In order to verify the hybrid motor model, an experimental system was assembled. It consisted of an EAD LA23BCK-11R stepping motor driven with a zener diode clamped L/R drive. An experimental position error measurement system using a high resolution optical encoder was developed and used in conjunction with an analog tachometer. This made it possible to experimentally generate velocity-error planes for comparison with the analytical simulations. The encoder and tach became the system load. No additional load was used because the most difficult system to model is the one with a minimum of friction and damping. In a system with high

friction and damping, the more subtle effects of some of the other parameters are lost. The experimental phase plane measurement system is described in detail in Appendix B.

If the reader is unfamiliar with the measurement system it would be beneficial to read Appendix B at this time. Torsional resonance and filtering effects are discussed that make the comparison of the analytical and experimental results easier to understand.

The individual motor parameters were measured using the techniques described by Gauthier and the Stepping Motor Workshop notes.[4] The only exception is the system inertia which was calculated from the period of oscillation of torsional spring mass system. Table III-1 contains a summary of the experimental system parameters. The magnetic saturation coefficients used are the average values of the one and two phase on measurements. When measuring the torque angle curves of a hybrid motor, the torsional stiffness of the motor must not exceed the torsional stiffness of the measurement system. Otherwise the measurement system will become unstable in a region about the motor's unstable equilibrium point. Appendix A contains detailed information about the measurement of torque angle curves.

Experimental verification was conducted by comparing the analytical and experimental system responses for both one and two phase on operation. The results are presented

here in three categories: single step response, fixed period stepping and optimum step sequences.

Parameter	Symbol	Value	Units
Inertia	J	.00325	oz-in-sec^2
Friction	T_m T_h	.61 1.0	oz-in oz-in
Damping	B_m B_h	.00628 .00560	oz-in/rad/sec oz-in/rad/sec
Torque Constant	K_t	78.0	oz-in/ampere
Detent Torque	D_t	5.5	oz-in
Detent Multiplier	D_m	4	
Back EMF Constant	K_b	.4488	volts/rad/sec
Stator Resistance	R_m	3.6	ohms
Stator Inductance	L_m	.013 (1) .020 (2)	henries henries
Saturation Coefficient	a_2 a_1	-.122 1.0	
Supply Voltage	V_s	35.4	volts
Series Resistance	R_s	20.0	ohms

TABLE III-1 SYSTEM PARAMETERS

Single Step Response

The simplest comparison for a stepping motor system is the single step response. Figures III-9a and III-9b show the analytical and experimental velocity profiles for the one phase on single step response. Comparisons can be made between the period of oscillation, the ratio of amplitudes of successive oscillations and the envelope of the response. Any of these comparisons will show that there is a very good correlation between the model and the experimental results. This correlation indicates that the mechanical portion of the model, including inertia, friction, damping, hysteresis and eddy current losses, magnetic saturation, and torque production is quite accurate.

Figures III-10a and 10b are plots of the current profile for the same single step response. Comparing the current rise times, magnitudes and periods of oscillation also yields an excellent correlation. This verifies that the electrical portion of the model, specifically the back EMF and inductance during magnetic saturation, also yields accurate results.

If the process is continued with two phases energized, the experimental results again verify the model. See Figures III-11a and 11b and III-12a and 12b. Thus from the single step response, the initial conclusion is that the model for the hybrid motor yields excellent results.

JM=	3.25m	TF=	810.00m	ST=	0.00	B=	6.26m	KT=	78.00
DTR=	5.50	DTRM=	4.00	KB=	446.80m	VR=	5.40	IR=	1.50
RM=	3.60	LM=	13.00mPHZE=		4.00	STPR=	200.00		
VS=	35.40	RS=	20.00	RF=	0.00	STS=	1.00	PHO=	1.00
EQTQ=N		FD=N		FDL=N		WRW=N		DRTP=1	

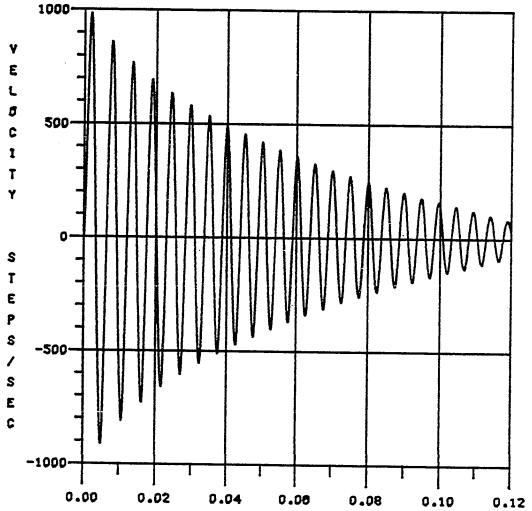

AN ANALYTICAL SINGLE STEP VELOCITY PROFILE
FOR THE 1.8' HYBRID MOTOR, 1 PHASE ON

FIGURE III-9a

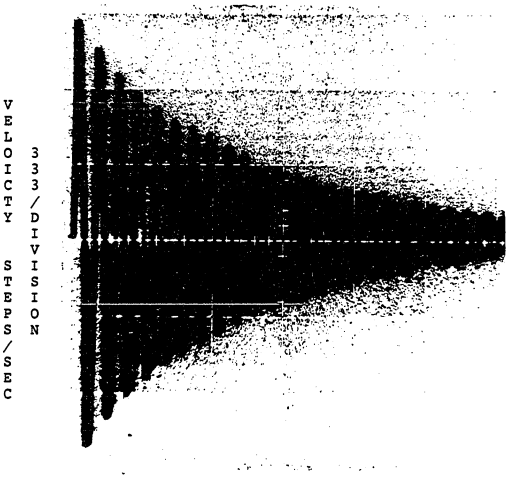

AN EXPERIMENTAL SINGLE STEP VELOCITY PROFILE
FOR THE 1.8' HYBRID MOTOR, 1 PHASE ON

FIGURE III-9b

JM=	3.25m	TF=	610.00m	ST=	0.00	B=	6.28m	KT=	76.00
DTR=	5.50	DTRM=	4.00	KB=	448.80m	VR=	5.40	IR=	1.50
RM=	3.80	LM=	13.00m	PHZE=	4.00	STPR=	200.00		
VS=	35.40	RS=	20.00	RF=	0.00	STS=	1.00	PHO=	1.00
EQTQ=N		FD=N		FDL=N		WRW=N		DRTP=1	

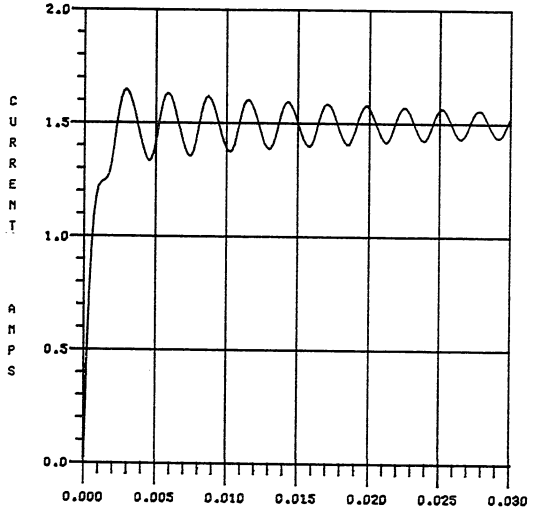

AN ANALYTICAL SINGLE STEP CURRENT PROFILE
FOR THE 1.8' HYBRID, 1 PHASE ON

FIGURE III-10a

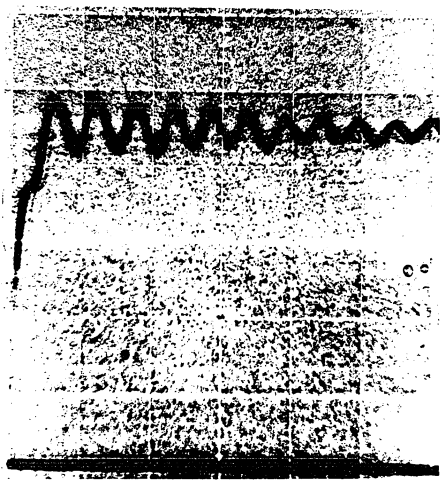

CURRENT AMPERES .3/DIVISION

.005 / DIVISION

TIME SECONDS

AN EXPERIMENTAL SINGLE STEP CURRENT PROFILE
FOR THE 1.8' HYBRID MOTOR, 1 PHASE ON

FIGURE III-10b

JM=	3.25m	TF=	610.00m	ST=	0.00	B=	6.28m	KT=	76.00
DTR=	5.50	DTRM=	4.00	KB=	448.80m	VR=	5.40	IR=	1.50
RM=	3.60	LM=	20.00m	PHZE=	4.00	STPR=	200.00		
VS=	35.40	RS=	20.00	RF=	0.00	STS=	1.00	PHO=	2.00
EQTQ=N		FD=N		FDL=N		WRW=N		DRTP=1	

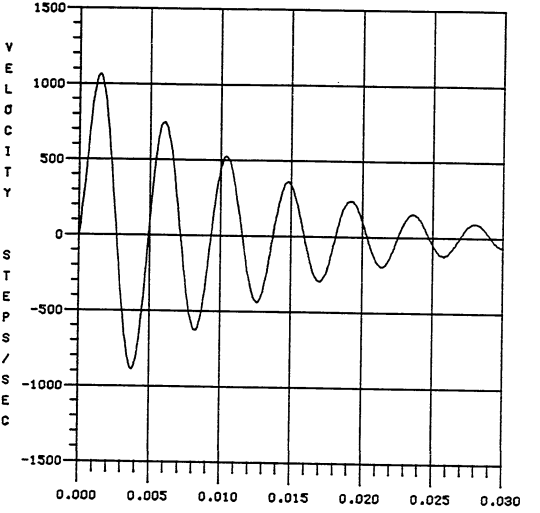

AN ANALYTICAL SINGLE STEP VELOCITY PROFILE
FOR THE 1.8' HYBRID MOTOR, 2 PHASES ON

FIGURE III-11a

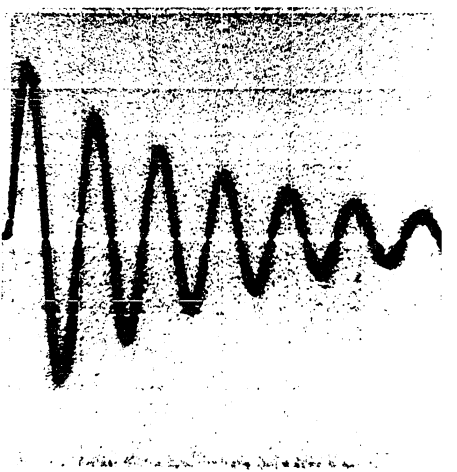

.005 / DIVISION

TIME SECONDS

AN EXPERIMENTAL SINGLE STEP VELOCITY PROFILE
FOR THE 1.8' HYBRID MOTOR, 2 PHASES ON

FIGURE III-11b

JM=	3.25m	TF=	610.00m	ST=	0.00	B=	6.26m	KT=	78.00
DTR=	5.50	DTRM=	4.00	KB=	448.80m	VR=	5.40	IR=	1.50
RM=	3.60	LM=	20.00m	PHZE=	4.00	STPR=	200.00		
VS=	35.40	RS=	20.00	RF=	0.00	STS=	1.00	PHO=	2.00
EQTQ=N		FD=N		FDL=N		WRW=N		DRTP=I	

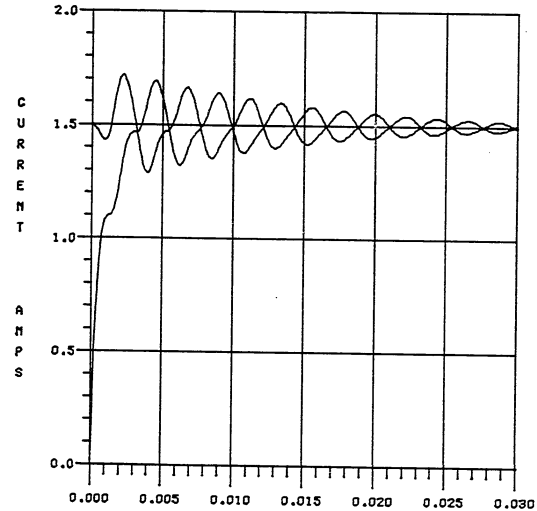

AN ANALYTICAL SINGLE STEP CURRENT PROFILE
FOR THE 1.8' HYBRID MOTOR, 2 PHASES ON

FIGURE III-12a

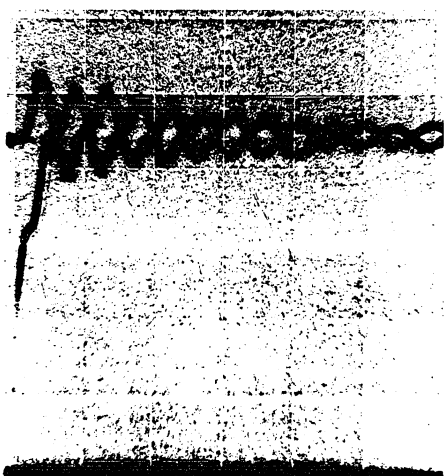

AN EXPERIMENTAL SINGLE STEP CURRENT PROFILE
FOR THE 1.8' HYBRID MOTOR, 2 PHASES ON

FIGURE III-12b

Fixed Period Stepping

For further verification of the model, several of the low speed failure modes were investigated and compared. All sequences consist of four steps at a fixed frequency. Various step frequencies were selected and simulated using the model. These step frequencies were then used to drive the experimental system. They were varied slightly until the simulated and experimental trajectories were as identical as possible. The difference between the two rates is a measure of the error in the model. Error is defined as the experimental value minus the simulated value divided by the experimental value.

$$\text{ERROR}(x) = \frac{\text{Experimental } (x) - \text{Predicted } (x)}{\text{Experimental } (x)} \qquad \text{(III-21)}$$

The first sequence to be verified is a four step sequence that does not fail. This sequence remains below the separatrix the entire time, thus the step frequency is below the no-failure rate. Figures III-13a and III-13b show that a good correlation between the the analytical and experimental trajectories was obtained.

The initial "hook" in the experimental phase plane at each step in Figure III-13b is due to the second order filter used to minimize the torsional resonance in the tachometer signal. This distortion is in the measurement system; it will occur in several of the experimental phase

JM=	3.25m	TF=	610.00m	ST=	0.00	B=	6.28m	KT=	78.00
DTR=	5.50	DTRM=	4.00	KB=	448.80m	VR=	5.40	IR=	1.50
RM=	3.60	LM=	13.00m	PHZE=	4.00	STPR=	200.00		
VS=	35.40	RS=	20.00	RF=	0.00	STS=	1.00	PHO=	1.00
EQTQ=N		FD=N		FDL=N		WRW=N		DRTP=1	

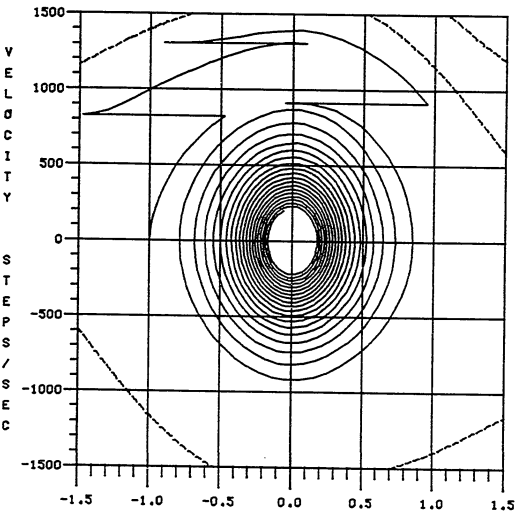

AN ANALYTICAL FOUR STEP SEQUENCE PHASE PLANE
(NO FAILURE), 1 PHASE ON

FIGURE III-13a

Analytical step period : .00145 sec

Experimental step period : .00150 sec

Error : 3.3 %

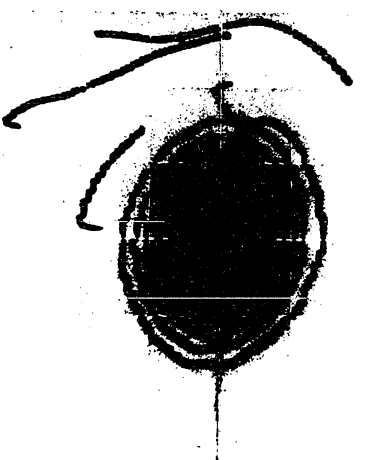

.5 / DIVISION

POSITION STEPS

AN EXPERIMENTAL FOUR STEP SEQUENCE PHASE PLANE
(NO FAILURE), 1 PHASE ON

FIGURE III-13b

planes. The full effect of the filtering is shown in Appendix B.

The step period in the analytical simulation was 1.45 msec and the step period in the experimental system was 1.5 msec. This yields an error of 3.3 percent.

The analytical and experimental current profiles for this sequence are shown in Figures III-14a and III-14b. Like the phase planes, the currents exhibit an excellent correlation between the model and the real system.

Figures III-15a and III-15b show a four step sequence that is above the no-failure rate and does not execute properly. The sequence gains four steps for a total move of eight steps. Again, a good correlation between analytical and experimental trajectories was obtained. The step periods used were the same for the experimental and analytical sequences so that the error as defined is zero percent.

Note the apparent crossing and recrossing of the separatrix by the trajectory in Figure III-15a. This is another example of the effects of projecting a higher order trajectory back into a two dimensional space.

Figures III-16a and III-16b show a sequence attempting to step at a rate above the start/stop rate. Failure occurred because the motor was unable to accelerate

JM=	3.25m	TF=	010.00m	ST=	0.00	B=	0.28m	KT=	78.00
DTR=	5.50	DTRM=	4.00	KB=	446.80m	VR=	5.40	IR=	1.50
RM=	3.80	LM=	13.00m	PHZE=	4.00	SIPR=	200.00		
VS=	35.40	RS=	20.00	RF=	0.00	STS=	1.00	PHO=	1.00
EQTQ=N		FD=N		FDL=N		WRW=N		DRTP=1	

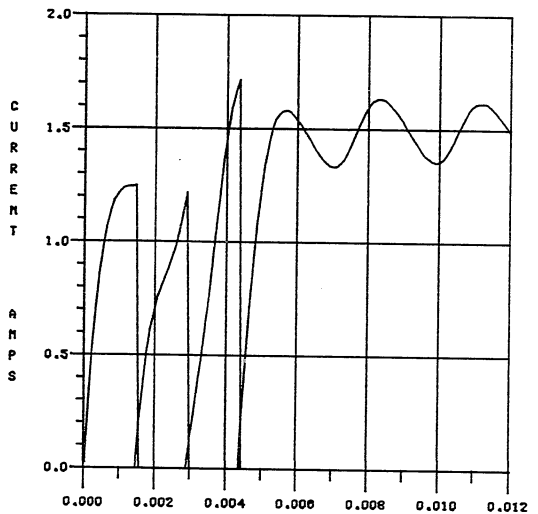

AN ANALYTICAL FOUR STEP SEQUENCE CURRENT PROFILE
(NO FAILURE), 1 PHASE ON

FIGURE III-14a

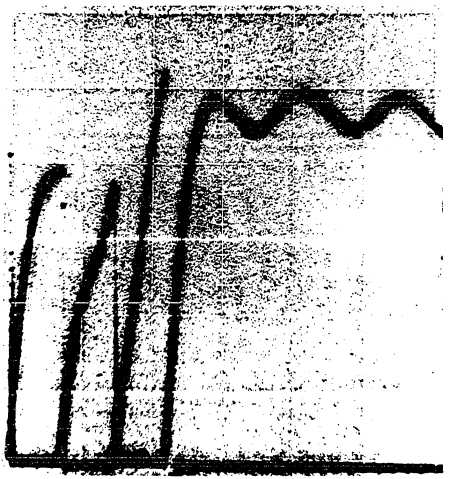

.002 / DIVISION

TIME SECONDS

AN EXPERIMENTAL FOUR STEP SEQUENCE CURRENT PROFILE
(NO FAILURE), 1 PHASE ON

FIGURE III-14b

JM=	3.25m	TF=	610.00m	ST=	0.00	B=	6.28m	KT=	78.00
DTR=	5.50	DTRM=	4.00	KB=	448.80m	VR=	5.40	IR=	1.50
RM=	3.60	LM=	13.00m	PHZE=	4.00	STPR=	200.00		
VS=	35.40	RS=	20.00	RF=	0.00	STS=	1.00	PHO=	1.00
EQTQ=N		FD=N		FDL=N		WRW=N		DRTP=1	

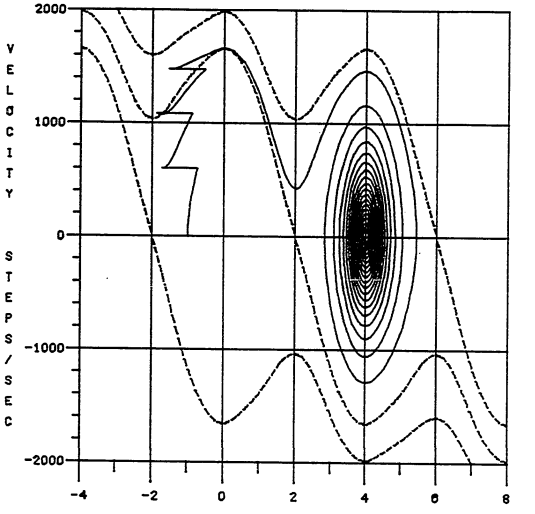

AN ANALYTICAL FOUR STEP SEQUENCE PHASE PLANE
(GAINS STEPS), 1 PHASE ON

FIGURE III-15a

Analytical step period : .00110 sec

Experimental step period : .00110 sec

Error : 0.0 %

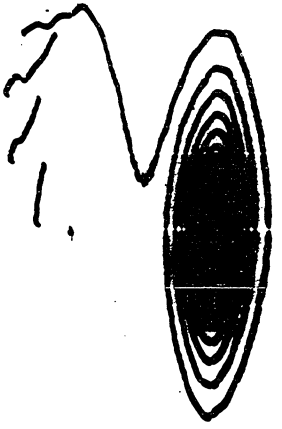

VELOCITY STEPS/SEC 66/DIVISION

2.0 / DIVISION

POSITION STEPS

AN EXPERIMENTAL FOUR STEP SEQUENCE PHASE PLANE
(GAINS STEPS), 1 PHASE ON

FIGURE III-15b

JM= 3.25m TF= 810.00m ST= 0.00 B= 0.26m KT= 78.00
DTR= 5.50 DTRM= 4.00 KB= 448.60m VR= 5.40 IR= 1.50
RM= 3.60 LM= 13.00mPHZE= 4.00 STPR= 200.00
VS= 35.40 RS= 20.00 RF= 0.00 STS= 1.00 PHO= 1.00
EQTQ=N FD=N FDL=N WRW=N DRTP=1

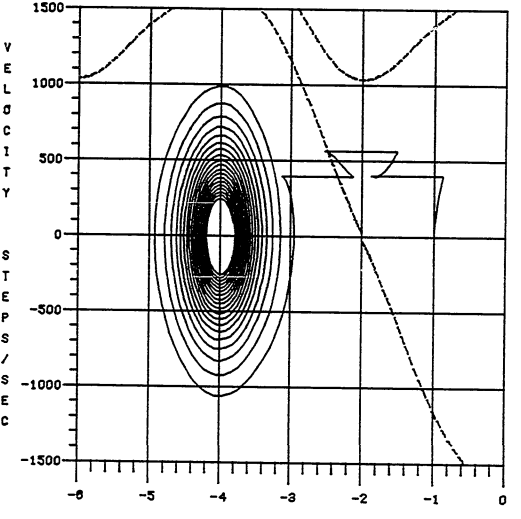

AN ANALYTICAL FOUR STEP SEQUENCE PHASE PLANE
(LOSES STEPS), 1 PHASE ON

FIGURE III-16a

Analytical step period : .00080 sec

Experimental step period : .00080 sec

Error : 0.0 %

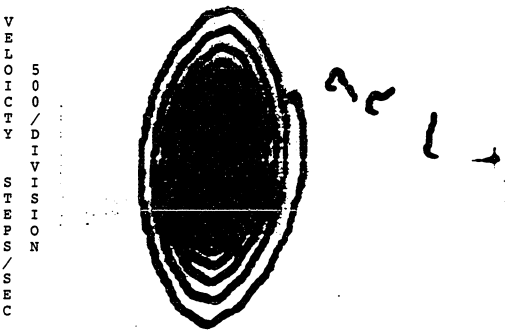

1.0 / DIVISION

POSITION STEPS

AN EXPERIMENTAL FOUR STEP SEQUENCE PHASE PLANE
(LOSES STEPS), 1 PHASE ON

FIGURE III-16b

fast enough to keep in synch with the flux vector. Again there was excellent correlation between the analytical and experimental sequences. The error between the two step rates for this sequence was also zero.

When a stepping motor system has low friction and damping, it fails at frequencies close to its natural frequency. Figures III-17a and III-17b are an example of this type of stepping failure. The error between the analytical and experimental sequences is -1.5 percent.

Investigating the low speed failure modes of the stepping motor with one phase energized, it can be seen that a very high correlation between the hybrid model and the experimental system was obtained. If the verification process using the four step sequences is repeated with two phases energized, it can be seen that the model yields excellent results for two-phase-on operation also. See Figures III-18a through III-22b.

Table III-2 is a summary of the errors for each of the step sequences with one and two phase on operation. Table III-2 shows that the hybrid model yields excellent results over a wide range of low speed operating conditions.

JM=	3.25m	TF=	610.00m	ST=	0.00	B=	0.26m	KT=	76.00
DTR=	5.50	DTRM=	4.00	KB=	446.80m	VR=	5.40	IR=	1.50
RM=	3.60	LM=	13.00m	PHZE=	4.00	STPR=	200.00		
VS=	35.40	RS=	20.00	RF=	0.00	STS=	1.00	PHO=	1.00
EQTG=N		FD=N		FDL=N		WRW=N		DRTP=1	

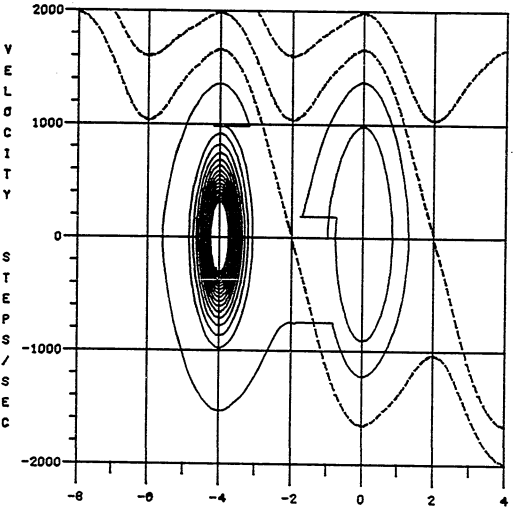

AN ANALYTICAL FOUR STEP SEQUENCE PHASE PLANE
(FAILS AT W_n), 1 PHASE ON

FIGURE III-17a

Analytical step period : .00650 sec

Experimental step period : .00640 sec

Error :-1.5 %

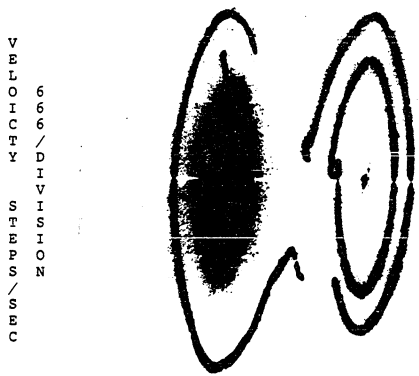

2.0 / DIVISION

POSITION STEPS

AN EXPERIMENTAL FOUR STEP SEQUENCE PHASE PLANE
(FAILS AT W_n), 1 PHASE ON

FIGURE III-17b

JM=	3.25m	TF=	610.00m	ST=	0.00	B=	6.26m	KT=	78.00
DTR=	5.50	DTRM=	4.00	KB=	448.80m	VR=	5.40	IR=	1.50
RM=	3.80	LM=	20.00m	PHZE=	4.00	STPR=	200.00		
VS=	35.40	RS=	20.00	RF=	0.00	STS=	1.00	PHO=	2.00
EQTQ=N		FD=N		FDL=N		WRW=N		DRTP=1	

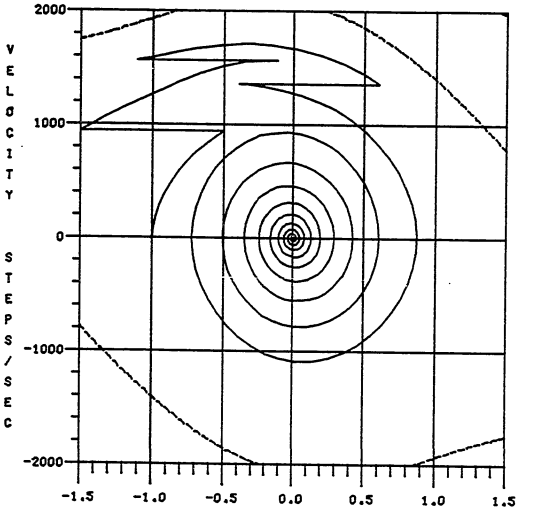

AN ANALYTICAL FOUR STEP SEQUENCE PHASE PLANE
(NO FAILURE), 2 PHASES ON

FIGURE III-18a

Analytical step period : .00105 sec

Experimental step period : .00110 sec

Error : 4.5 %

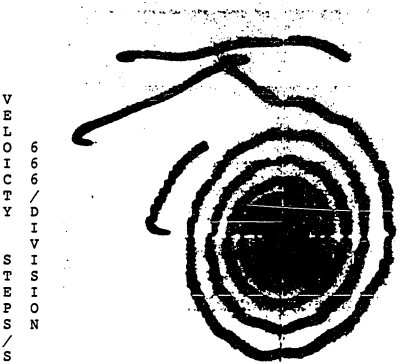

.5 / DIVISION

POSITION STEPS

AN EXPERIMENTAL FOUR STEP SEQUENCE PHASE PLANE
(NO FAILURE), 2 PHASES ON

FIGURE III-18b

JM=	3.25m	TF=	610.00m	ST=	0.00	S=	6.28m	KT=	78.00
DTR=	5.50	DTRM=	4.00	KB=	446.80m	VR=	5.40	IR=	1.50
RM=	3.60	LM=	20.00mPHZE=		4.00	STPR=	200.00		
VS=	35.40	RS=	20.00	RF=	0.00	STS=	1.00	PHS=	2.00
EQTG=N		FD=N		FDL=N		WRW=N		DRTP=1	

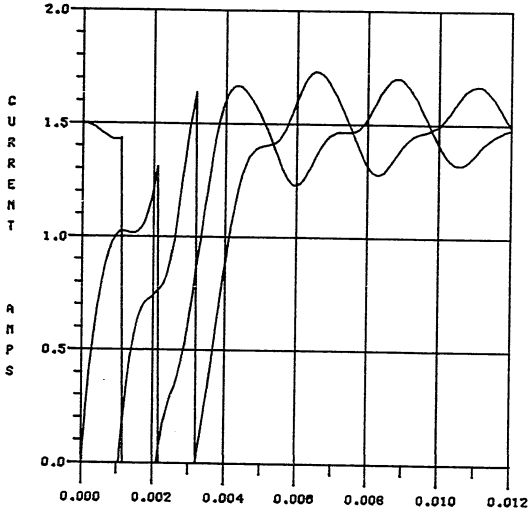

AN ANALYTICAL FOUR STEP SEQUENCE CURRENT PROFILE
(NO FAILURE), 2 PHASES ON

FIGURE III-19a

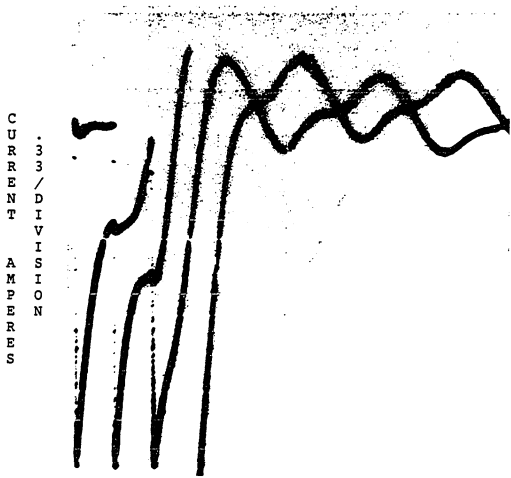

AN EXPERIMENTAL FOUR STEP SEQUENCE CURRENT PROFILE
(NO FAILURE), 2 PHASES ON

FIGURE III-19b

JM=	3.25m	TF=	610.00m	ST=	0.00	B=	6.26m	KT=	76.00
DTR=	5.50	DTRM=	4.00	KB=	448.80m	VR=	5.40	IR=	1.50
RM=	3.80	LM=	20.00m	PHZE=	4.00	STPR=	200.00		
VS=	35.40	RS=	20.00	RF=	0.00	STS=	1.00	PHO=	2.00
EQTG=M		FD=M		FDL=M		WRW=M		DRTP=1	

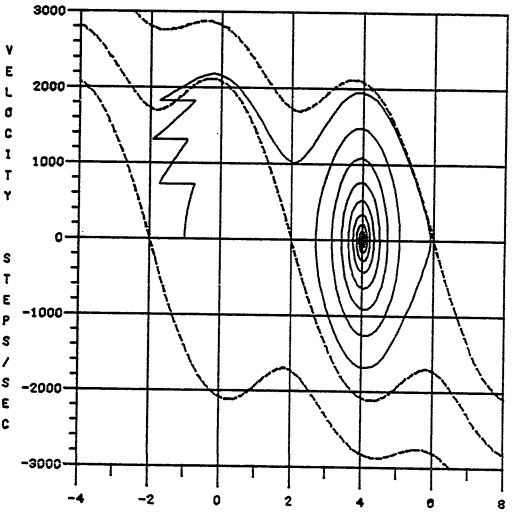

AN ANALYTICAL FOUR STEP SEQUENCE PHASE PLANE
(GAINS STEPS), 2 PHASES ON

FIGURE III-20a

Analytical step period : .00079 sec

Experimental step period : .00080 sec

Error : 1.25 %

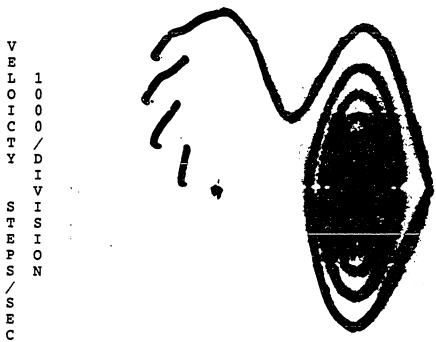

2.0 / DIVISION

POSITION STEPS

AN EXPERIMENTAL FOUR STEP SEQUENCE PHASE PLANE
(GAINS STEPS), 2 PHASES ON

FIGURE III-20b

JM=	3.25m	TF=	610.00m	ST=	0.00	B=	6.28m	KT=	78.00
DTR=	5.50	DTRM=	4.00	KB=	448.80m	VR=	5.40	IR=	1.50
RM=	3.60	LM=	20.00m	PHZE=	4.00	STPR=	200.00		
VS=	35.40	RS=	20.00	RF=	0.00	STS=	1.00	PHO=	2.00
EQTG=N		FD=N		FDL=N		WRW=N		DRTP=1	

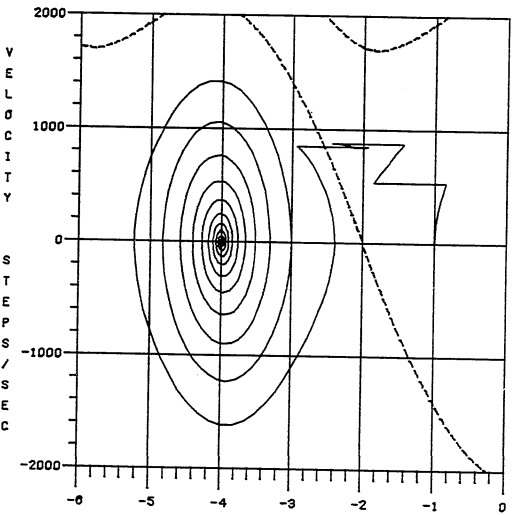

AN ANALYTICAL FOUR STEP SEQUENCE PHASE PLANE
(LOSES STEPS), 2 PHASES ON

FIGURE III-21a

Analytical step period : .00059 sec

Experimental step period : .00060 sec

Error : 1.7 %

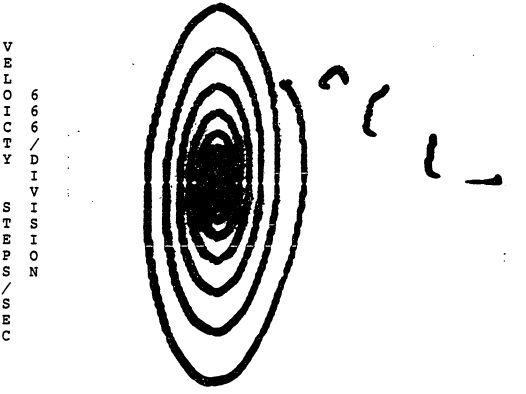

1.0 / DIVISION

POSITION STEPS

AN EXPERIMENTAL FOUR STEP SEQUENCE PHASE PLANE
(LOSES STEPS), 2 PHASES ON

FIGURE III-21b

JM=	3.25m	TF=	610.00m	ST=	0.00	B=	6.28m	KT=	78.00
DTR=	5.50	DTRM=	4.00	KB=	448.80m	VR=	5.40	IR=	1.50
RM=	3.80	LM=	20.00m	PHZE=	4.00	STPR=	200.00		
VS=	35.40	RS=	20.00	RF=	0.00	STS=	1.00	PHO=	2.00
EQTQ=N		FD=N		FDL=N		WRW=N		DRTP=1	

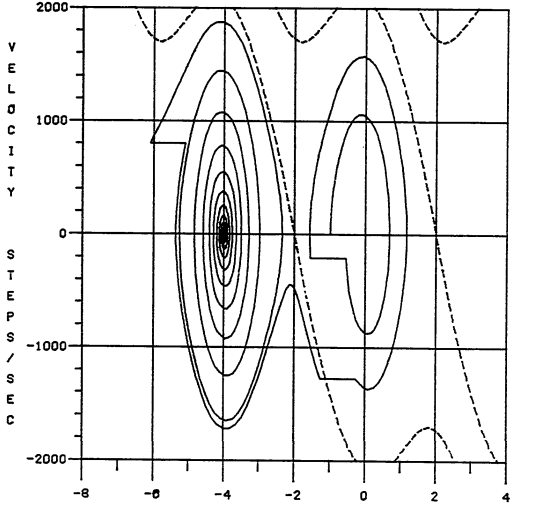

AN ANALYTICAL FOUR STEP SEQUENCE PHASE PLANE
(FAILS AT W_n), 2 PHASES ON

FIGURE III-22a

Analytical step period : .00485 sec

Experimental step period : .00500 sec

Error : 3.0 %

VELOCITY STEPS/SEC 666/DIVISION

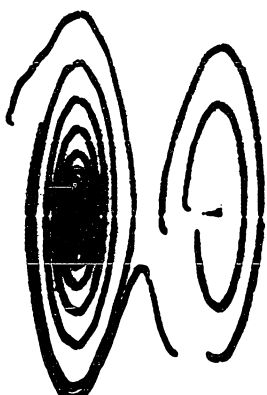

2.0 / DIVISION

POSITION STEPS

AN EXPERIMENTAL FOUR STEP SEQUENCE PHASE PLANE

(FAILS AT W_n), 2 PHASES ON

FIGURE III-22b

Optimum Step Sequences

The model verification process can be continued by comparing the model to high performance point to point and constant velocity sequences.[4] Point to point sequences are ones where the user is interested in moving from one position to another as fast as possible. The sequence consists of an acceleration ramp and a deceleration ramp that minimizes the ringout after the last step. The constant velocity sequence is similar to the point to point sequence. However, once the motor is accelerated, it then runs at a constant velocity for some number of steps until being decelerated. An example of a point to point application is the head actuator on a disk drive. The printhead actuator on a "print on the fly" dot matrix printer is an ideal example of a constant velocity application.

Figure III-23a is the velocity profile of a typical point to point move. It consists of six acceleration and two deceleration steps. The phase error plane corresponding to this sequence is shown in Figure III-23b. When this sequence was implemented on the experimental system, the phase error plane in Figure III-23c was obtained. Because fixed period stepping is not being used, it is difficult to vary the times by a constant amount to determine the error. However, the supply voltage can be used to "tune" the sequence in. By varying the supply voltage, the current and hence the torque, vary slightly. Increasing or decreasing the supply

JM=	3.25m	TF=	610.00m	ST=	0.00	B=	6.28m	KT=	78.00
DTR=	5.50	DTRM=	4.00	KB=	448.80m	VR=	5.40	IR=	1.50
RM=	3.60	LM=	13.00m	PHZE=	4.00	STPR=	200.00		
VS=	35.40	RS=	20.00	RF=	0.00	STS=	1.00	PHO=	1.00
EQTQ=N		FD=N		FDL=N		WRW=N		DRTP=1	

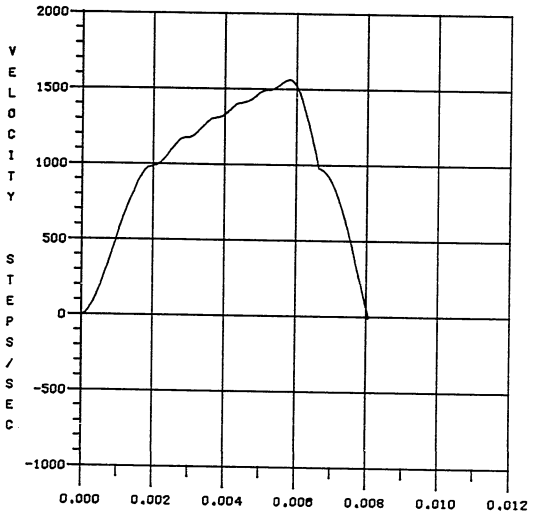

AN ANALYTICAL EIGHT STEP POINT TO POINT SEQUENCE VELOCITY PROFILE, 1 PHASE ON

FIGURE III-23a

JM= 3.25m TF= 610.00m ST= 0.00 B= 6.28m KT= 76.00
DTR= 5.50 DTRM= 4.00 KB= 448.80m VR= 5.40 IR= 1.50
RM= 3.80 LM= 13.00mPHZE= 4.00 STPR= 200.00
VS= 35.40 RS= 20.00 RF= 0.00 STS= 1.00 PHO= 1.00
EQTQ=N FD=N FDL=N WRW=N DRTP=1

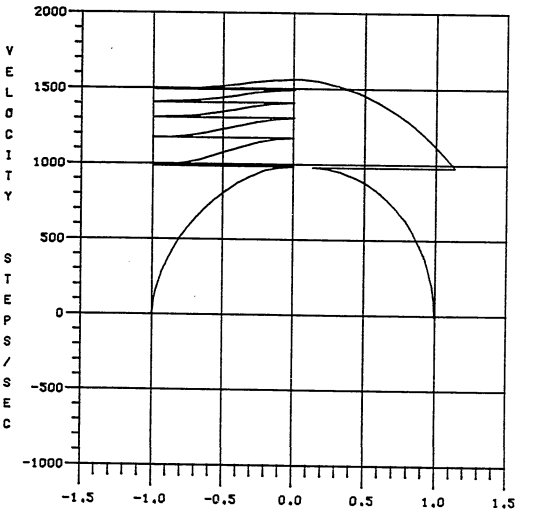

AN ANALYTICAL EIGHT STEP POINT TO POINT SEQUENCE
PHASE PLANE, 1 PHASE ON

FIGURE III-23b

Analytical current level : 1.50 amperes

Experimental current level : 1.55 amperes

Error : 3.2 %

.5 / DIVISION

POSITION STEPS

AN EXPERIMENTAL EIGHT STEP POINT TO POINT SEQUENCE
PHASE PLANE, 1 PHASE ON

FIGURE III-23c

voltage will cause the experimental sequence to match the analytical one.

In Figure III-23c the supply voltage was increased from 35.40 volts to 36.58 volts. If these values are used in Equation III-21, an error of 3.2 percent results. Figure III-23d is the experimental velocity profile for this sequence.

Figure III-24a is the velocity profile for a constant velocity sequence. As with the point to point sequence, the motor is accelerated for six steps. Once accelerated it is then stepped in to a constant velocity limit cycle for forty more steps until it is decelerated down to zero velocity. The phase error plane for the sequence is shown in Figure III-24b. The corresponding experimental phase error plane had an error of 1.6 percent. See Figure III-24c.

Like the single step and fixed period sequences, the optimum sequences can also be verified for two phase on operation. Figures III-25a and III-25b are the velocity profile and phase error plane for an eight step move with two phases on. When this sequence was implemented on the experimental system, Figure III-25c was obtained. With the exception of the ringout at the end of the move, a good correlation was found. The ringout is not due to an error in the model but rather an error in the computer algorithm that

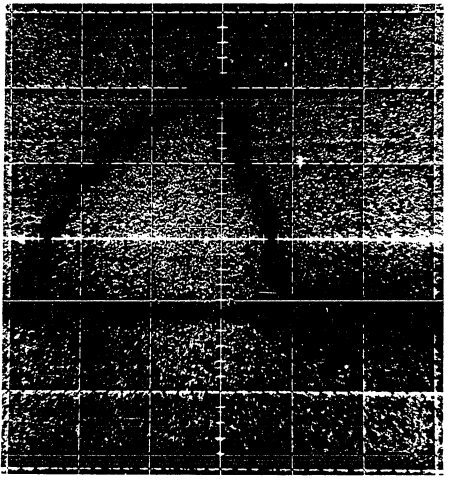

AN EXPERIMENTAL EIGHT STEP POINT TO POINT SEQUENCE
VELOCITY PROFILE, 1 PHASE ON

FIGURE III-23d

JM=	3.25m	TF=	610.00m	ST=	0.00	B=	6.26m	KT=	76.00
DTR=	5.50	DTRM=	4.00	KB=	448.80m	VR=	5.40	IR=	1.50
RM=	3.60	LM=	13.00m	PHZE=	4.00	STPR=	200.00		
VS=	35.40	RS=	20.00	RF=	0.00	STS=	1.00	PHC=	1.00
EQTQ=N		FD=N		FDL=N		WRV=N		DRTP=1	

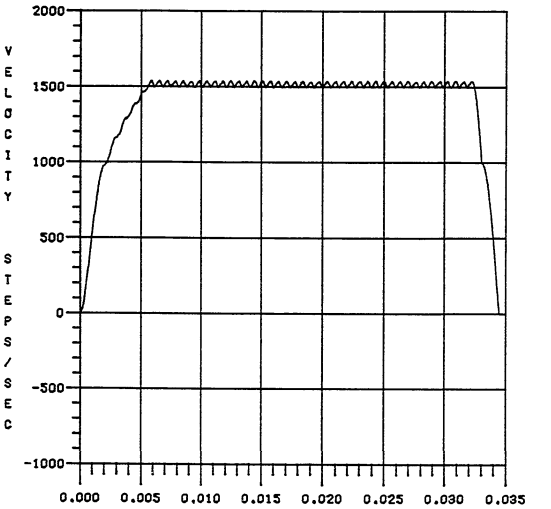

AN ANALYTICAL FORTY-EIGHT STEP CONSTANT VELOCITY SEQUENCE VELOCITY PROFILE, 1 PHASE ON

FIGURE III-24a

JM=	3.25m	TF=	610.00m	ST=	0.00	B=	6.28m	KT=	78.00
DTR=	5.50	DTRM=	4.00	KB=	448.80m	VR=	5.40	IR=	1.50
RM=	3.60	LM=	13.00m	PHZE=	4.00	STPR=	200.00		
VS=	35.40	RS=	20.00	RF=	0.00	STS=	1.00	PHC=	1.00
EQTQ=N		FD=N		FDL=N		WRW=N		DRTP=1	

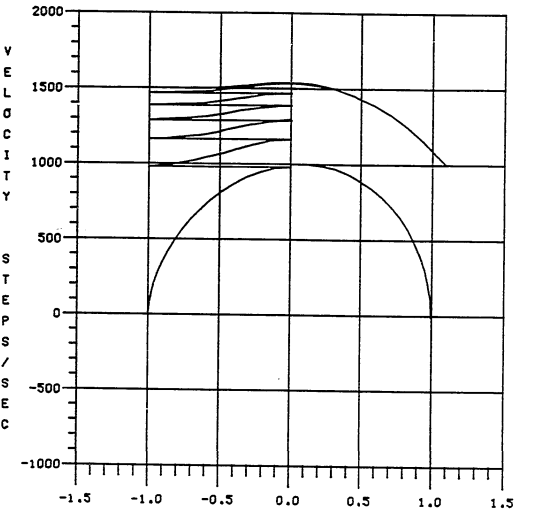

AN ANALYTICAL FORTY-EIGHT STEP CONSTANT VELOCITY SEQUENCE PHASE PLANE, 1 PHASE ON

FIGURE III-24b

Analytical current level : 1.50 amperes

Experimental current level : 1.55 amperes

Error : 1.6 %

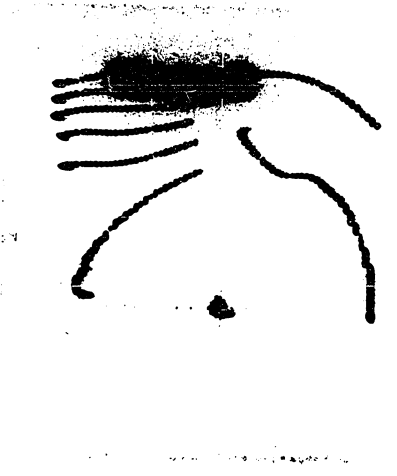

AN EXPERIMENTAL FORTY-EIGHT STEP CONSTANT VELOCITY SEQUENCE PHASE PLANE, 1 PHASE ON

FIGURE III-24d

JM=	3.25m	TF=	610.00m	ST=	0.00	B=	0.28m	KT=	78.00
DTR=	5.50	DTRM=	4.00	KB=	448.80m	VR=	5.40	IR=	1.50
RM=	3.60	LM=	20.00m	PHZE=	4.00	STPR=	200.00		
VS=	35.40	RS=	20.00	RF=	0.00	STS=	1.00	PHO=	2.00
EQTQ=N		FD=N		FDL=N		WRW=N		DRTP=1	

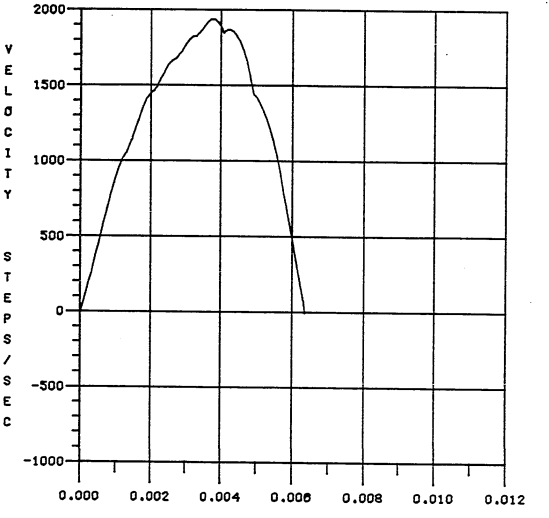

AN ANALYTICAL EIGHT STEP POINT TO POINT SEQUENCE
VELOCITY PROFILE, 2 PHASES ON

FIGURE III-25a

JM=	3.25m	TF=	610.00m	ST=	0.00	B=	6.28m	KT=	78.00
DTR=	5.50	DTRM=	4.00	KB=	448.80m	VR=	5.40	IR=	1.50
RM=	3.60	LM=	20.00m	PHZE=	4.00	STPR=	200.00		
VS=	35.40	RS=	20.00	RF=	0.00	STS=	1.00	PHC=	2.00
EQTQ=N		FD=N		FDL=N		WRW=N		DRTP=1	

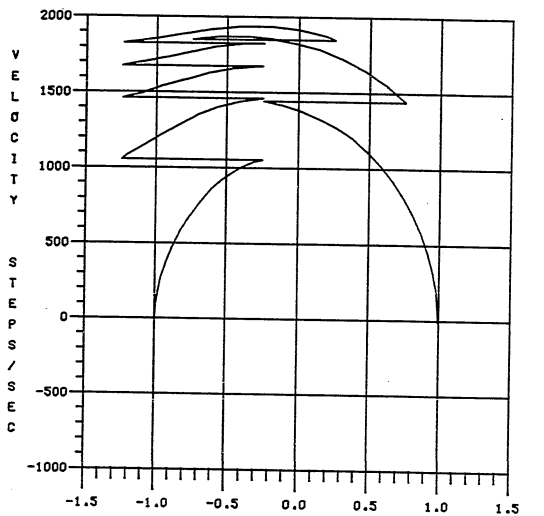

AN ANALYTICAL EIGHT STEP POINT TO POINT SEQUENCE
PHASE PLANE, 2 PHASES ON

FIGURE III-25b

Analytical current level : 1.50 amperes

Experimental current level : 1.50 amperes

Error : 0.0 %

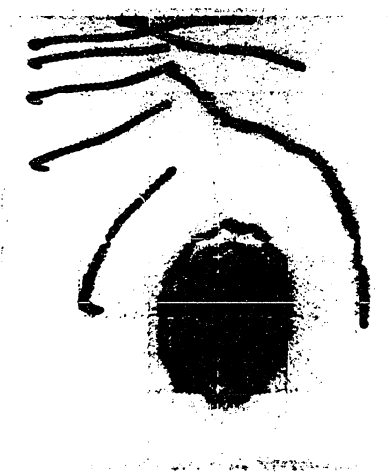

AN EXPERIMENTAL EIGHT STEP POINT TO POINT SEQUENCE
PHASE PLANE, 2 PHASES ON

FIGURE III-25c

calculates the period of the last step. It is due to the inductive rise time during the last step.

When stepping with one phase energized, the location of the magnetic flux vector shifts to its new position instantaneously. The magnitude at its new location depends upon the current and inductive rise time. When designing sequences that minimize ringout, it is the location of the flux vector that is important, not its magnitude. Stepping with two phases on causes a problem. Because the location of the flux vector depends upon the current in both phases, a change in current will cause a change in the vector's location. Consider three adjacent phases A, B and C. Prior to the last step, phases A and B are on. The equilibrium point is the midpoint between the two phases. At the moment the motor is stepped, phase A goes off, B remains on, and C begins to turn on. At this instant the flux vector and equilibrium point is aligned with phase B. As the current in phase C comes on according to the inductive time constant, the flux vector begins to slide from phase B to the midpoint between phases B and C.

This effect means that designing the last step of a two phase on optimum sequence requires that the motor be stepped so that it will be on a trajectory that will arrive at the final equilibrium point at the same moment the sliding flux vector does. While this is difficult to implement on the computer, it turns out that experimentally the last step

Analytical current level : 1.50 amperes

Experimental current level : 1.50 amperes

Error : 0.0 %

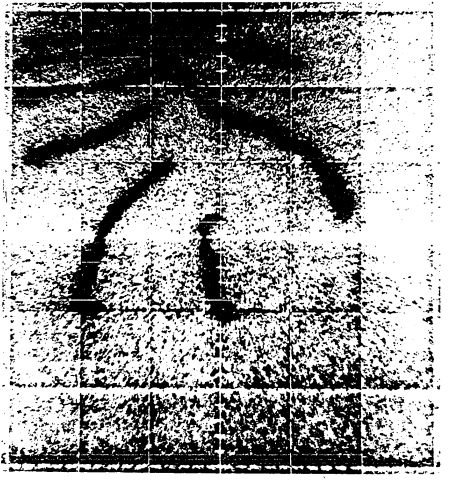

.5 / DIVISION

POSITION STEPS

AN EXPERIMENTAL EIGHT STEP POINT TO POINT SEQUENCE
PHASE PLANE, (MODIFIED), 2 PHASES ON

FIGURE III-25d

of the sequence can be shortened until a no-overshoot response is obtained. This is shown in Figure III-25d. For this sequence it was not necessary to modify the supply voltage. The experimental velocity profile of the sequence is shown in Figure III-25e.

Figures III-26 a, b and c repeat the process for the constant velocity sequence. As with the two phase on point to point sequence, it was unnecessary to modify the supply voltage for the sequence in Figure II-26c.

Table III-2 contains the summary of the errors obtained during point to point and constant velocity verification.

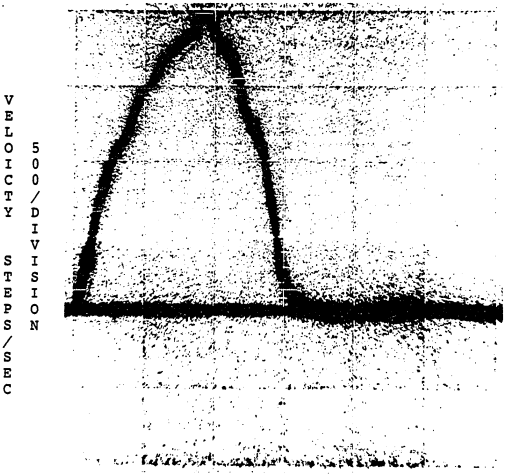

.002 / DIVISION

TIME SECONDS

AN EXPERIMENTAL EIGHT STEP POINT TO POINT SEQUENCE
VELOCITY PROFILE, (MODIFIED), 2 PHASES ON

FIGURE III-25e

JM=	3.25m	TF=	610.00m	ST=	0.00	B=	6.28m	KT=	78.00
DTR=	5.50	DTRM=	4.00	KB=	448.80m	VR=	5.40	IR=	1.50
RM=	3.80	LM=	20.00m	PHZE=	4.00	STPR=	200.00		
VS=	35.40	RS=	20.00	RF=	0.00	STS=	1.00	PHO=	2.00
EQTQ=N		FD=N		FDL=N		WRW=N		DRTP=1	

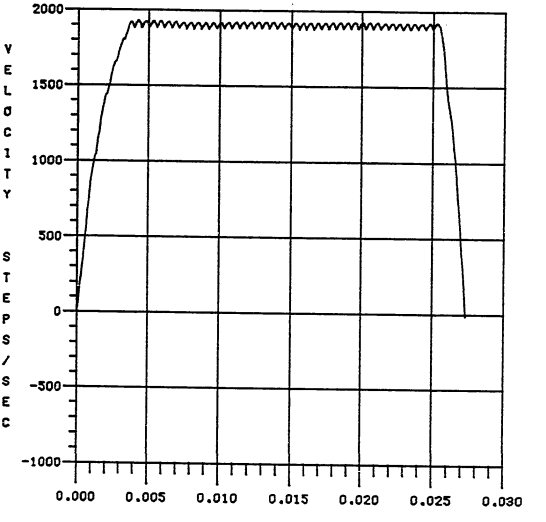

AN ANALYTICAL FORTY-EIGHT STEP CONSTANT VELOCITY SEQUENCE VELOCITY PROFILE, 2 PHASES ON

FIGURE III-26a

JM=	3.25m	TF=	610.00m	ST=	0.00	B=	6.28m	KT=	78.00
DTR=	5.50	DTRM=	4.00	KB=	448.80m	VR=	5.40	IR=	1.50
RM=	3.60	LM=	20.00m	PHZE=	4.00	STPR=	200.00		
VS=	35.40	RS=	20.00	RF=	0.00	STS=	1.00	PHC=	2.00
EQTQ=N		FD=N		FDL=N		WRW=N		DRTP=1	

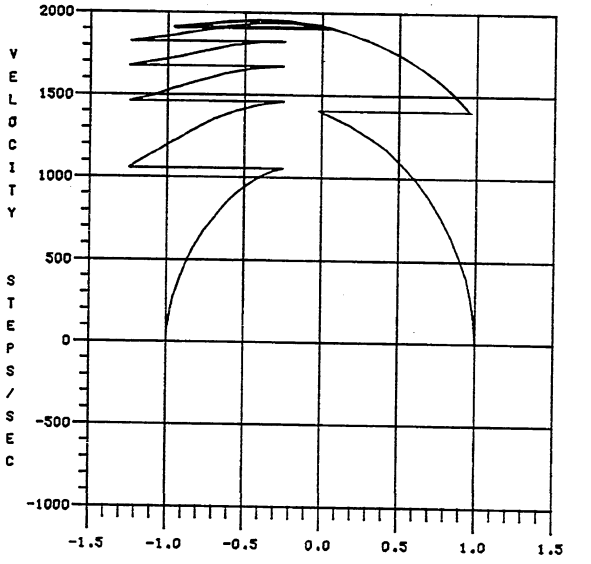

AN ANALYTICAL FORTY-EIGHT STEP CONSTANT VELOCITY SEQUENCE PHASE PLANE, 2 PHASES ON

FIGURE III-26b

Analytical current level : 1.50 amperes

Experimental current level : 1.50 amperes

Error : 0.0 %

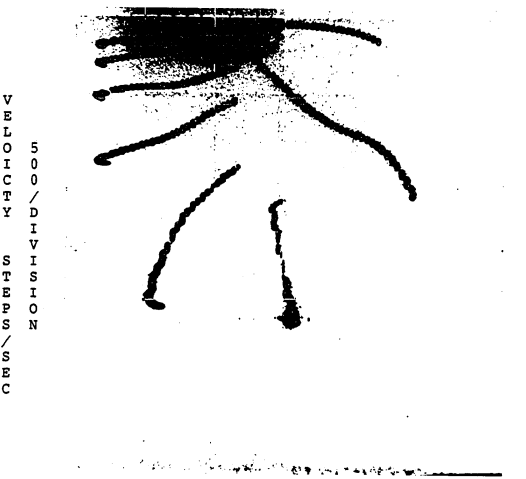

AN EXPERIMENTAL FORTY-EIGHT STEP CONSTANT VELOCITY SEQUENCE PHASE PLANE, 2 PHASES ON

FIGURE III-26c

Conclusion

Having verified the hybrid model using single step, fixed period and optimum sequences, it was seen that a good correlation was obtained in each case. Table III-2 contains a summary of the errors found during each of the tests. Having found all errors to be 4.5% or less, it follows that this model can be used to accurately describe the hybrid motor and it can be used to investigate various systems and configurations that the motor might be used in.

The hybrid model is more complex than the model Gauthier developed for the PM motor. The dynamic order of the model is increased because of the inductive nature of the windings. Several of the other physical parameters are also more complex. However, they add to the algebraic complexity, not the dynamic complexity. Even with these additions to the model, the techniques developed by Gauthier for both solving the equations and understanding the results remain basically the same. It just requires that the user have a strong understanding of the significance of projecting a higher order model into the phase plane.

Type of Stepping	Analytical Period Experimental Period Percent Error	Analytical Period Experimental Period Percent Error
	1 Phase on	2 Phases on
Fixed Period with No Failure	.00145 sec .00150 sec 3.3 %	.00105 sec .00110 sec 4.5 %
Fixed Period that Gains Steps	.00110 sec .00110 sec 0.0 %	.00079 sec .00080 sec 1.25 %
Fixed Period that Loses steps	.00080 sec .00080 sec 0.0 %	.00059 sec .00060 sec 1.7 %
Fixed Period at the Local Natural Freq.	.00650 sec .00640 sec -1.5 %	.00485 sec .00500 sec 3.0 %
Variable period 8 step Point to point	1.50 amps 1.55 amps 3.2 %	1.50 amps 1.50 amps 0.0 %
Variable Period 40 step Constant Velocity	1.50 amps 1.53 amps 1.6 %	1.50 amps 1.50 amps 0.0 %

TABLE III-2 SUMMARY OF THE EXPERIMENTAL VERIFICATION

CHAPTER IV

ANGLE ACCURACY AND REPEATABILITY IN STEPPING MOTORS

Introduction

Having developed a model that will accurately describe the hybrid stepping motor, this is an opportune time to digress from the development of the model and use the model to gain insight into the behavior of the stepping motor. As stepping motor technology has developed, the stepping motor has had to accelerate harder, run faster and position more accurately. Nowhere are these demands more apparent than in the area of disk storage technology, particularly in the positioning of the head. To people working with these applications, the position or angle accuracy of the motor has become more and more critical.

Angle accuracy is often broken down into two categories. The first is the ability of a motor to make uniform, constant steps that vary by no more than a certain percentage. For example, a five percent 1.8' stepper is a motor that steps in 1.8' increments with a variation of no more than plus or minus five percent of 1.8'. The second aspect of stepping motor accuracy is repeatability, often called angle hysteresis. This is a measure of the ability of

a stepping motor to move a given number of steps in one direction, then reverse and move back the same number of steps to the original position. The hysteresis is defined as the difference between the starting position and the final position after the motor has moved out and back without losing steps, expressed as a percentage of one step.

Hysteresis, as it is used in this chapter, describes the position error that occurs when a stepping motor approaches the same stable equilibrium point from two different directions. It is not the magnetic hysteresis of the iron in the flux paths, as described in Chapter III.

Causes of Angle Inaccuracy

In a stepping motor the angle accuracy and hysteresis are determined by two phenomena. The first is the dead zone, a region around each equilibrium position where the coulomb friction and stiction exceed the torque developed by the motor. Once the rotor falls into this region, it will not move until the torque is increased so that the rotor's position is no longer in the dead zone. The dead zone has an effect on both angle accuracy and hysteresis. The second phenomenon is the mechanical and electrical variations due to the stepping motor's construction that are found between phases over one mechanical revolution. This causes the angle between the

equilibrium positions to vary from phase to phase. The angle also varies as the motor moves through one revolution.

The Dead Zone

The mathematical model for the stepping motor developed in Chapter III is based on the following form.

$$J\ddot{\theta} + B\dot{\theta} + K_t S_f I \sin(A\theta) + D_t \sin(D_m A\theta) = T_f \frac{\dot{\theta}}{|\dot{\theta}|} \qquad \text{(IV-1)}$$

And

$$V_s = L_{ms} \frac{dI}{dt} + (R_m + R_s)I - K_{bs}\dot{\theta} \sin(A\theta) \qquad \text{(IV-2)}$$

The dead zone can be calculated at the equilibrium position because at equilibrium:

$$\ddot{\theta} = 0.0$$
$$\dot{\theta} = 0.0$$
$$\frac{dI}{dt} = 0.0$$
$$I = I_r$$

Therefore, Equations IV-1 and IV-2 result in:

$$K_t S_f I \sin(A\theta) + D_{ts} \sin(D_m A\theta) \leq T_f \qquad \text{(IV-3)}$$

Where: $I = V_s / (R_m + R_s)$

The lefthand side of Equation IV-3 is the torque angle curve for the motor. As long as $K_t S_f I \sin(A\theta) + D_{ts} \sin(D_m A\theta)$ remains less than the friction, the system remains at rest. For a

given supply voltage V_s, the static torque versus angle about the equilibrium position can be plotted. See Figure IV-1. The equilibrium position is defined as the point where the torque equals zero.

The friction for the system is plotted on the y-axis (torque). See Point A. A horizontal line is drawn to the left until the torque angle curve is intercepted at Point B. Point C on the x-axis is the corresponding angle where the positive torque developed by the stepping motor equals the friction in the system. Because friction always opposes motion, and hence torque, the process can be repeated for negative torques. A second point where the negative torque equals the friction can be found. See Point D.

The angle between Points C and D is the dead zone for this particular motor energized with a given supply voltage. If the rotor lands anywhere within this region, it will remain at that location because the motor does not develop significant torque to overcome and move the rotor closer to the equilibrium position.

It should be noted that the dead zone can be calculated from Equation IV-3 by solving for θ where the torque angle curve equals the friction.

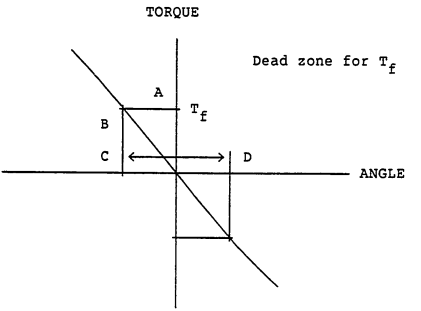

THE DEAD ZONE ABOUT THE EQUILIBRIUM POINT

FIGURE IV-1

$$\theta = \frac{\text{Sin}^{-1}}{A} \left(\frac{T_f}{K_t S_f I \, \text{Sin}(A\theta) + D_{ts} \text{Sin}(D_m A\theta)} \right) \quad \text{(IV-4)}$$

Because θ is measured from the equilibrium position, the dead zone equals two θ.

Once the dead zone about an equilibrium position is known, the maximum error in the angle accuracy of the motor due to the dead zone can be calculated. First assume the motor is being stepped one step at a time. Each phase has a dead zone about its equilibrium position. The dead zone for two adjacent phases is shown in Figure IV-2. If the motor did not have a dead zone it would step from the phase 1 equilibrium to the phase 2 equilibrium position and the error would be zero. However, because the motor does have a dead zone, there is a good chance there will be an error. The largest positive error occurs under the following conditions: phase 1 of the motor is energized and the motor is at rest at the extreme left edge of the dead zone. The motor is then stepped, turning phase 1 off and phase 2 on. The motor goes through a transient and comes to rest at the extreme right edge of the dead zone around the phase 2 equilibrium position. Therefore, the motor actually makes a move equal to its step size plus one-half of each dead zone. See Figure IV-2 and Equation IV-4.

$$A_{md} = T_{ss} + \frac{1}{2} (D_{z1} + D_{z2}) \quad \text{(IV-5)}$$

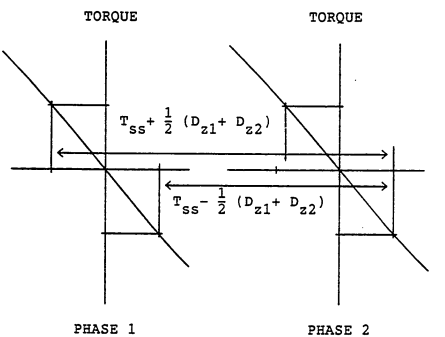

THE ANGLE ERROR DUE TO THE DEAD ZONE

FIGURE IV-2

Where: A_{md} = Actual motor displacement
T_{ss} = Theoretical step size
D_{z1} = Dead zone for phase 1
D_{z2} = Dead zone for phase 2

Likewise, the largest negative error will occur when the motor steps from the right side of dead zone 1 to the left side of dead zone 2. These two worst case examples show that the motor is capable of making steps of any size between these two values.

$$T_{ss} - \frac{1}{2}(D_{z1} + D_{z2}) \leq A_{md} \leq T_{ss} + \frac{1}{2}(D_{z1} + D_{z2}) \quad \text{(IV-6)}$$

If the motor is making a move of more than one step, the move will equal the number of steps times the theoretical step size plus or minus half the dead zone. See Equation IV-7.

$$NT_{ss} - \frac{1}{2}(D_{z1} + D_{z2}) \leq A_{md} \leq NT_{ss} + \frac{1}{2}(D_{z1} + D_{z2}) \quad \text{(IV-7)}$$

Where: N = The number of steps

So far the discussion has been with respect to the dead zone's effect on the accuracy of the step size. The dead zone will also affect the repeatability or hysteresis of the motor. If the motor is stepped from phase 1 to phase 2 and back to phase 1, there will usually be some error between the starting and final positions. This is because these positions can lie anywhere within the dead zone. The maximum hysteresis will occur when the motor is initially at

one edge of the dead zone and, after its move, it is at the other edge of the dead zone. It follows, therefore, that the maximum hysteresis at any equilibrium position equals the dead zone at that equilibrium position.

Up to this point a motor with one phase energized has been considered. If the motor is being used with several phases energized, the concepts are still valid. The torque angle curve is the sum of the torques produced by the energized stator phases. The equilibrium point will be where the torque equals zero. If the phases of the motor are unbalanced, this point may not be the midpoint between the two phases.

Construction Variations

Earlier it was mentioned that, in addition to the dead zone, variation in the construction of the stepping motor causes a reduction in the position accuracy of the stepping motor. Depending on the design and construction techniques used in manufacturing a stepping motor, the locations of the equilibrium points may vary from stator phase to stator phase around one mechanical revolution. In the hybrid motor, this occurs if the stator poles are not spaced properly. This type of error is usually very small in the hybrid motor because the stator laminations are stamped from a die. However, certain designs of the canstack

stepping motors provide an excellent example of this problem. Many canstack stepping motors are made such that each set of teeth are stamped from a separate piece of iron. During assembly if the teeth are not aligned properly, the equilibrium positions will not be the proper distance apart. See Figure IV-3. If there is a variation in the angle between the equilibrium points, these will be an additional error in the position accuracy. Figure IV-4 shows the position error as the sum of the dead zone and the alignment error. The total position error is shown in Equation IV-8.

$$NT_{ss} - E_r - \frac{1}{2}(D_{z1} + D_{z2}) \leq A_{md} \leq NT_{ss} + E_r + \frac{1}{2}(D_{z1} + D_{z2}) \quad \text{(IV-8)}$$

Where: E_r= Alignment error

The alignment or construction error does not have an effect on the hysteresis error because the hysteresis is always measured with respect to the same equilibrium point.

The alignment error can be determined by measuring the torque angle curves of each of the phases of the motor. The zero crossing points on the torque angle curve indicate the equilibrium points.

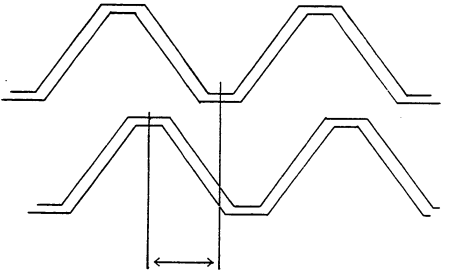

THE ALIGNMENT ERROR IN A CANSTACK MOTOR

FIGURE IV-3

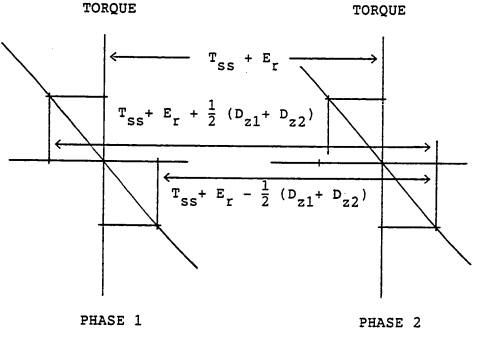

TOTAL ANGLE ERROR DUE TO THE DEAD ZONE AND THE ALIGNMENT ERROR

FIGURE IV-4

Measurement Techniques

The angle accuracy can be determined from Equations IV-4, IV-5, and IV-7. It is necessary to measure the torque angle curve, and the unmagnetized and magnetized frictions. When using the equations that determine the errors, it is necessary to consider the effects of saturation, hysteresis and eddy currents. Saturation will reduce the torque angle curve of the motor and therefore increase the dead zone.

The actual friction can be very difficult to determine. As mentioned in Chapter III, when the motor is oscillating in very small amplitudes about the equilibrium point, the actual friction becomes quite small. This occurs because the bearings are now riding back and forth on the lubrication film inside the bearing housing and the balls are not turning as they would if the motor were continuing to turn in the same direction.

The hysteresis losses also effect the dead zone because torque must be developed to move the rotor, which in turn causes the magnetic hysteresis loop to be traversed. The size of the hysteresis loop is difficult to determine while the motor is oscillating about the equilibrium point. The sine function used with the position error in Equation III-17 must also be used.

The method currently used most often in the industry is that of attaching a high resolution optical

JM=	3.25m	TF=	20.00	ST=	0.00	B=	11.80m	KT=	78.00
DTR=	5.50	DTRM=	4.00	KB=	448.80m	VR=	5.40	IR=	1.50
RM=	3.80	LM=	20.00mPHZE=		4.00	STPR=	200.00		
VS=	35.40	RS=	20.00	RF=	0.00	STS=	1.00	PHO=	2.00
EQTQ=N		FD=N		FDL=N		WRW=N		DRTP=1	

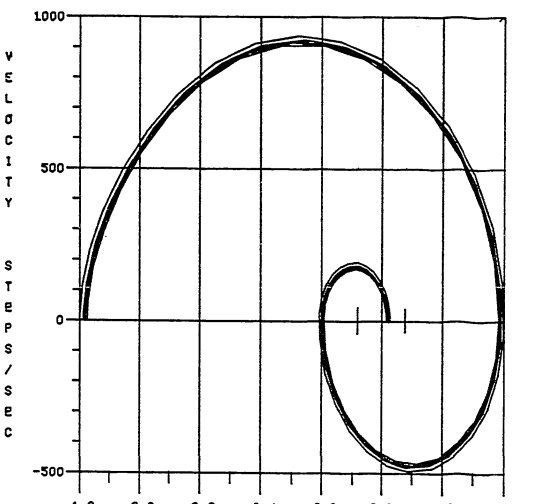

A SINGLE STEP CONVERGING LIMIT CYCLE

T_f = 20.0 oz-in

FIGURE IV-5

JM=	3.25m	TF=	25.00	ST=	0.00	B=	11.80m	KT=	78.00
DTR=	5.50	DTRM=	4.00	KB=	448.80m	VR=	5.40	IR=	1.50
RM=	3.60	LM=	20.00m	PHZE=	4.00	STPR=	200.00		
VS=	35.40	RS=	20.00	RF=	0.00	STS=	1.00	PHO=	2.00
EQTQ=N		FD=N		FDL=N		URW=N		DRTP=1	

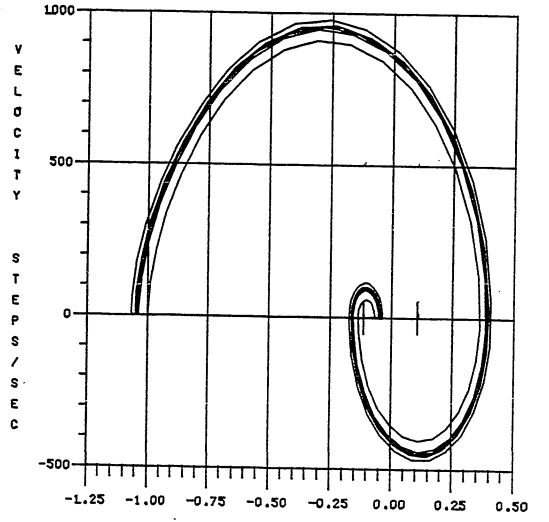

A SINGLE STEP CONVERGING LIMIT CYCLE

T_f = 25.0 oz-in

FIGURE IV-6

encoder to the stepping motor. The motor is stepped out one revolution and then back to the starting point. The output of the encoder is monitored and each step size and location is recorded. At the conclusion of the test, the largest step error and hysteresis are obtained.

The fault of this test is that it is a statistical one. There is no guarantee that the absolute maximum error will be found. In fact, the phase plane shows that the maximum errors usually will not be found.

While the motor is single stepped out and back it converges on a single step limit cycle. Once the limit cycle is found, each subsequent step is identical to the one before it. This is the exact opposite of what is desired by someone who is looking for the limits of the dead zone.

The limit cycle converges in one of two ways. When looking at the dead zone about an equilibrium point, the motor's trajectory can approach it from four directions, one in each quadrant. Trajectories that approach from quadrants I and II can converge to some limit cycle anywhere within the dead zone. See Figures IV-5 and 6.

The first step always starts at the origin for simplicity. Subsequent steps alternate on each side of the limit cycle until the trajectory converges on the single step limit cycle. Figures IV-5 and IV-6 show that this test is not going to find the extremes of the dead zone. Rather,

after the first few steps no new information will be obtained.

When the trajectory approaches the dead zone from quadrants III and IV a different phenomenon occurs. This time the limit cycle converges on one edge of the dead zone. See Figures IV-7 and 8. Again the first step starts at the origin. However, each subsequent step moves to the edge of the dead zone that was closest to the first step.

Under these conditions, the test yields better results. Still, in both cases the final errors depend upon where the motor is when the test is started, compared to the location of the limit cycle. If the motor is already very close to the limit cycle position, very small errors will occur. Often when this test is conducted, the motor is stepped several times to get the motor traveling in the correct direction before the test is actually started. In this case, an even smaller error will be detected because the motor has already begun to converge upon the limit cycle.

Conclusion

The stepping motor model can be used to determine the angle accuracy of a stepping motor. It is necessary to carefully consider the measurement of the model parameters to be used.

JM=	3.25m	TF=	30.00	ST=	0.00	B=	11.80m	KT=	78.00
DTR=	5.50	DTRM=	4.00	KB=	448.80m	VR=	5.40	IR=	1.50
RM=	3.60	LM=	20.00m	PHZE=	4.00	STPR=	200.00		
VS=	35.40	RS=	20.00	RF=	0.00	STS=	1.00	PHO=	2.00
EQTQ=N		FD=N		FDL=N		WRW=N		DRTP=1	

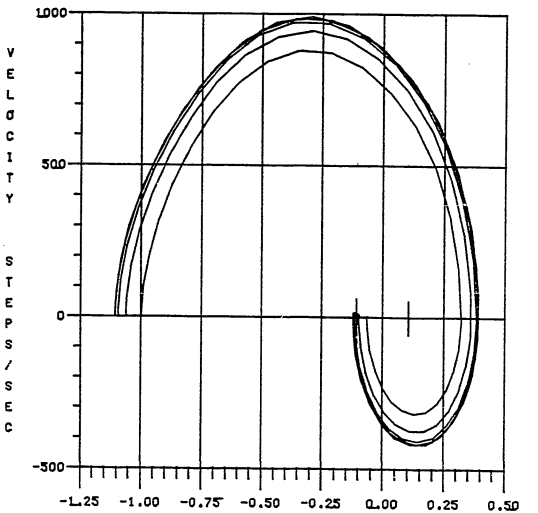

A SINGLE STEP CONVERGING LIMIT CYCLE

T_f = 30.0 oz-in

FIGURE IV-7

JM=	3.25m	TF=	40.00	ST=	0.00	B=	11.80m	KT=	78.00
DTR=	5.50	DTRM=	4.00	KB=	448.80m	VR=	5.40	IR=	1.50
RM=	3.60	LM=	20.00m	PHZE=	4.00	STPR=	200.00		
VS=	35.40	RS=	20.00	RF=	0.00	STPS=	1.00	PHO=	2.00
EQTQ=N		FD=N		FDL=N		WRW=N		DRTP=1	

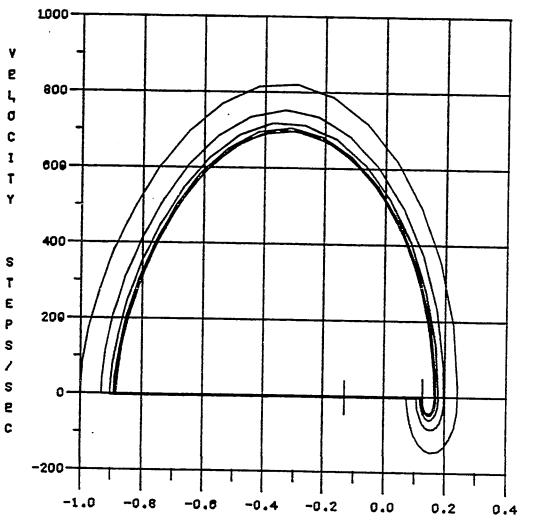

A SINGLE STEP CONVERGING LIMIT CYCLE

T_f = 40.0 oz-in

FIGURE IV-8

The model can also show that the test methods currently used by many yield a statistical result at best, and in no way measure the actual position error in the motor under test.

CHAPTER V

THE HYBRID MOTOR AS A SYNCHRONOUS DEVICE

Introduction

When the hybrid motor was first developed by General Electric Company, it was designed to be operated as a synchronous device. It can be run as a two phase motor energized by two AC voltages ninety degrees out of phase. When the hybrid motor is operated in this fashion it becomes a smooth running, low speed device. If a 1.8' hybrid is run with 60 Hz AC, the motor will have a shaft speed of seventy-two revolutions per minute. This makes the motor a very attractive low speed actuator.

The model just developed, with one modification, can also be used to describe the behavior of the hybrid motor when it is being run synchronously. The phase supply voltage V_s, is replaced with a $V_s \text{Cos } A\dot{\theta}_s t$ and a $V_s \text{Sin } A\dot{\theta}_s t$ term to represent the AC phase voltages. When displaying the simulation solution, a new set of state variables will be defined in the phase plane. Instead of using position error and velocity, the position error and velocity error between the rotor and the rotating voltage vector will be used. This allows the synchronous behavior of the motor to be displayed in a compact and insightful manner similar to the step

response of the stepping motor.

Synchronous Model Development

Equation III-18 can be modified to represent the stator phase circuit with AC excitation.

$$\frac{dI_n}{dt} = \frac{V_s}{L_{ms}} \text{Cos}(A\dot{\theta}_s t - (n-1)\frac{2\pi}{P}) - I_n \frac{(R_s + R_m)}{L_{ms}} - \left(\sum_{\substack{k=1 \\ k\neq n}}^{P} \frac{M_{msk}}{L_{ms}} \frac{dI_k}{dt} + \frac{K_{bs}}{L_{ms}} \dot{\theta} \text{Sin}(A\theta - (n-1)\frac{2\pi}{P})\right) \quad \text{(V-1)}$$

Where: $\dot{\theta}_s$ = Synchronous velocity
t = Time

This equation, along with the mechanical system equation, III-19, now represents the hybrid motor when it is being operated synchronously. The solution to these equations is obtained by the same numerical simulation techniques that were used with Equations III-18 and III-19.

Because the input synchronous velocity (AC frequency $\dot{\theta}_s$) is known, it is easy to calculate the position error and velocity error of the synchronous motor. The position error is the difference between the actual rotor position and the synchronous velocity times time. Likewise the velocity error is the error between the rotor velocity and the synchronous velocity.

$$\Psi = A\Theta - A\dot{\theta}_s t \qquad \text{(V-2a)}$$

$$\dot{\Psi} = A\dot{\theta} - A\dot{\theta}_s \qquad \text{(V-2b)}$$

Where: Ψ = Synchronous position error
$\dot{\Psi}$ = Synchronous velocity error

The position error and velocity error can be plotted as X and Y respectively in the phase or error plane. Figure V-1a shows a typical startup transient of the motor. Notice the initial condition is $\Psi = 0$ and $\dot{\Psi} = -\dot{\theta}_s$. This assumes that at $t = 0+e$, the rotor is aligned with the voltage vector. The velocity initial condition assumes the rotor is still stationary. However, the voltage vector has just begun to rotate at synchronous speed. It will be shown later what occurs when other initial conditions are used. Starting at $\Psi = 0$ and $\dot{\Psi} = -\dot{\theta}_s$, the motor goes through a transient and comes to a point, $\Psi = \psi$ and $\dot{\Psi} = 0$ in the plane. This corresponds to the motor having reached steady state velocity or synchronous speed. The rotor is trailing the voltage vector at some angle. This angle is often called the power angle. It is at this angle that the motor load equals the torque produced by the motor. The point $\Psi = \psi$, $\dot{\Psi} = 0$ is a stable equilibrium point in this plane.

In addition to plotting the position and velocity errors in the error plane, it is also possible to plot the currents in a current plane. By plotting the current in one

JM= 3.25m TF= 1.61 ST= 0.00 B= 11.60m KT= 76.00
DTR= 0.00 DTRM= 4.00 KB= 446.60m VR= 5.40 IR= 1.50
RM= 3.60 LM= 20.00mPHZE= 4.00 STPR= 200.00

VS= 35.40 RS= 20.00 RF= 0.00 STS= 1.00 PHO= 2.00
EQTB=M FD=M FDL=M WRW=M DRTP=1
DVFB= 100.00

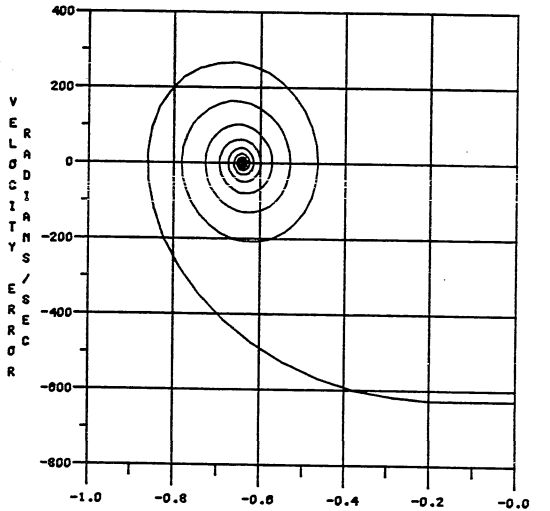

A TYPICAL ERROR PLANE START-UP TRANSIENT

FIGURE V-1a

phase versus the current in the other phase, it is possible to investigate the current transients. See Figure V-1b. In Figure V-1b the response has an initial condition of I_1 equal to 1.5 amperes and I_2 equal to 0.0 amperes. The currents go through a dynamic transient and converge on a forced oscillation due to the excitation voltages.

Returning to Figure V-1a and considering that the motor has a sinusoidal torque angle curve, it follows that there is an unstable equilibrium point as well as the stable equilibrium point in the error plane. In addition, there are separatrices that travel through the state space and terminate at the unstable equilibrium point, and there is a zero slope isocline that separates regions of positive acceleration from regions of negative acceleration.

To simplify the calculation of the equilibrium points, separatrices and zero slope isocline, it would be advantageous to develop a second order model that describes the synchronous motor error plane. Because the majority of hybrid motors are four phase unipolar or two phase bipolar designs, the second order model will be developed for that motor design. It is then possible to follow the same approach for motors with a different number of phases.

For this motor the stator winding equations are:

JM= 3.25m TF= 1.61 ST= 0.00 B= 11.80m KT= 78.00
DTR= 0.00 DTRM= 4.00 KB= 446.80m VR= 5.40 IR= 1.50
RM= 3.60 LM= 20.00mPHZE= 4.00 STPR= 200.00

VS= 35.40 RS= 20.00 RF= 0.00 STS= 1.00 PHO= 2.00
EQTG=M FD=M FDL=M WRW=M DRTP=1
DVFG= 100.00

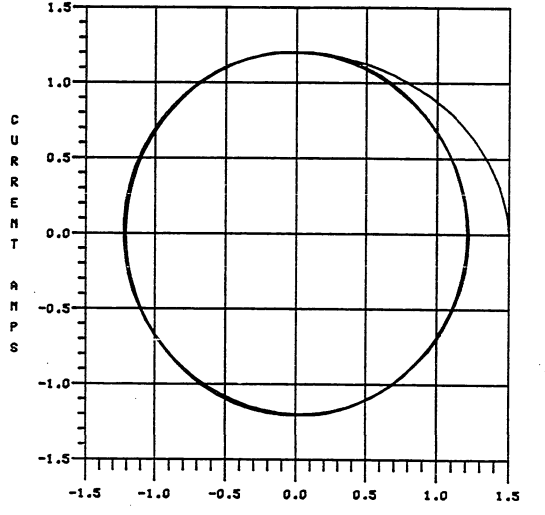

A TYPICAL CURRENT PLANE START-UP TRANSIENT

FIGURE V-1b

$$\frac{dI_1}{dt} = \frac{V_s}{L_{ms}} \text{CosA}\dot{\theta}_s t - I_1\left(\frac{R_s + R_m}{L_{ms}}\right) - \frac{M_{ms2}}{L_{ms}} \frac{dI_2}{dt} + \frac{K_{bs}}{L_{ms}} \dot{\theta} \text{ SinA}\theta \quad \text{(V-3a)}$$

$$\frac{dI_2}{dt} = \frac{V_s}{L_{ms}} \text{SinA}\dot{\theta}_s t - I_2\left(\frac{R_s + R_m}{L_{ms}}\right) - \frac{M_{ms1}}{L_{ms}} \frac{dI_1}{dt} - \frac{K_{bs}}{L_{ms}} \dot{\theta} \text{ CosA}\theta \quad \text{(V-3b)}$$

For the two phase hybrid motor design and many synchronous motors, the mutual inductive term approximately equals zero. Therefore, the following equations describe the phase currents for the synchronous motor.

$$\frac{dI_1}{dt} = \frac{V_s}{L_{ms}} \text{CosA}\dot{\theta}_s t - I_1\left(\frac{R_s + R_m}{L_{ms}}\right) + K_{bs}\dot{\theta} \text{ Sin A}\theta \quad \text{(V-4a)}$$

$$\frac{dI_2}{dt} = \frac{V_s}{L_{ms}} \text{SinA}\dot{\theta}_s t - I_2\left(\frac{R_s + R_m}{L_{ms}}\right) - K_{bs}\dot{\theta} \text{ Cos A}\theta \quad \text{(V-4b)}$$

When the motor is traveling at or near synchronous speed, both the back EMF voltage and the AC excitation voltage are sinusoids at the same frequency but at different phase angles. Consequently the phase currents can be assumed to be nearly sinusoidal in this region. While this seems like a gross assumption, several simulations will be shown later where this assumption has not been made and the

results agree quite closely. Based on this assumption, it is possible to consider the currents as phasors. The currents will be related to the drive voltages by some amplitude ratio and phase angle.

$$\text{Let: } R_t = R_s + R_m$$

$$\text{From Equation V-2a: } \dot{\Psi}_s = A\dot{\Theta} - A\dot{\Theta}\,t$$

$$\text{And: } R_t + L_{ms}A\dot{\theta}_s j = \sqrt{R_t^2 + L_{ms}^2 A^2 \dot{\theta}_s^2}\ \angle \text{Tan}^{-1}\frac{L_{ms}A\dot{\theta}_s}{R_t} \qquad \text{(V-5a)}$$

$$\text{Tan } \Psi_e = \frac{L_{ms}A\dot{\theta}_s}{R_t} \qquad \text{(V-5b)}$$

Using these identities and placing Equations V-4a and V-4b in a phasor format yields Equation V-6.

$$I_1 = \frac{V_s \cos(A\dot{\theta}_s t - \Psi_e) + K_{bs}(\dot{\Psi}_A + \dot{\theta}_s)\sin(A\dot{\theta}_s t + \Psi - \Psi_e)}{\sqrt{R_t^2 + L_{ms}^2 A^2 \dot{\theta}_s^2}} \qquad \text{(V-6a)}$$

$$I_2 = \frac{V_s \sin(A\dot{\theta}_s t - \Psi_e) - K_{bs}(\dot{\Psi}_A + \dot{\theta}_s)\cos(A\dot{\theta}_s t + \Psi - \Psi_e)}{\sqrt{R_t^2 + L_{ms}^2 A^2 \dot{\theta}_s^2}} \qquad \text{(V-6b)}$$

For this two phase motor, the stator torque portion of Equation III-19 can be rewritten in the following form.

$$T(\Theta) = K_t S_f (I_1 \sin A\Theta - I_2 \cos A\Theta) \qquad \text{(V-7)}$$

Substituting for I_1 and I_2 yields:

$$T = \frac{K_t S_f V_s}{\sqrt{R_t^2 + L_{ms}^2 A^2 \dot{\theta}_s^2}} \left[\cos(A\dot{\theta}_s t - \psi_e) \sin A\theta - \sin(A\dot{\theta}_s t - \psi_e) \cos A\theta \right]$$

$$+ \frac{K_t S_f K_{bs} (\dot{\Psi} + \dot{\theta}_s)}{\sqrt{R_t^2 + L_{ms}^2 A^2 \dot{\theta}_s^2}} \left[\sin(A\dot{\theta}_s t + \Psi - \psi_e) \sin A\theta + \cos(A\dot{\theta}_s t + \Psi - \psi_e) \cos A\theta \right] \quad \text{(V-8)}$$

Which reduces to:

$$T = \frac{K_t S_f V_s}{\sqrt{R_t^2 + L_{ms}^2 A^2 \dot{\theta}_s^2}} \sin(A\theta - A\dot{\theta}_s t + \psi_e)$$

$$+ \frac{K_t S_f K_{bs} (\dot{\Psi} + \dot{\theta}_s)}{\sqrt{R_t^2 + L_{ms}^2 A^2 \dot{\theta}_s^2}} \cos(A\theta - A\dot{\theta}_s t - \Psi + \psi_e) \quad \text{(V-9)}$$

Remember Equation V-2 and from the phasor:

$$\cos \psi_e = \frac{R_t}{\sqrt{R_t^2 + L_{ms}^2 A^2 \dot{\theta}_s^2}}$$

Equation V-9 reduces to:

$$T = \frac{K_t S_f V_s}{\sqrt{R_t^2 + L_{ms}^2 A^2 \dot{\theta}_s^2}} \sin(\Psi + \psi_e) \quad \text{(V-10)}$$

$$+ \frac{K_t S_f K_{bs} (\dot{\Psi}/A + \dot{\theta}_s) R_t}{A(R_t^2 + L_{ms}^2 A^2 \dot{\theta}_s^2)}$$

The torque equation shown in V-10 has two components. The first term is due to the power angle or the angular difference between the location of the rotor and the synchronous magnetic field. The second term is a back EMF term which results because the voltages induced in the stator phases cause currents to flow which reduce the torque in proportion to motor speed.

Equation V-10, in conjunction with the remaining terms in Equation III-19, forms a second order differential equation that describes the synchronous hybrid motor.

$$\frac{d^2\theta}{dt^2} = -\left(\frac{B_m + B_h}{J}\right)\dot{\theta} - \left(\frac{T_m + T_h}{J}\right)\frac{\dot{\theta}}{|\dot{\theta}|}$$

$$- \frac{K_t S_f}{J} \frac{V_s}{\sqrt{R_t^2 + L_{ms}^2 A^2 \dot{\theta}_s^2}} \sin(\Psi + \Psi_e) \qquad \text{(V-11)}$$

$$- \frac{K_t S_f}{J} \frac{K_{bs}(\dot{\Psi}/A + \dot{\theta}_s) R_t}{A(R_t^2 + L_{ms}^2 A^2 \dot{\theta}_s^2)} + \frac{D_{ts}}{J} \sin(D_m A\Theta)$$

Equation V-11 can be completely rewritten in terms of Ψ, the synchronous position error as shown in Equation V-12.

$$\frac{d^2\Psi}{dt^2} = -\left(\frac{B_m + B_h}{J}\right) A\left(\dot{\frac{\Psi}{A}}+\dot{\theta}_s\right) - \left(\frac{T_m + T_h}{J}\right) A\frac{\left(\dot{\frac{\Psi}{A}}+\dot{\theta}_s\right)}{\left|\dot{\frac{\Psi}{A}}+\dot{\theta}_s\right|}$$

$$- \frac{K_t S_f}{J} \frac{V_s A}{\sqrt{R_t^2 + L_{ms}^2 A^2 \dot{\theta}_s^2}} \sin(\Psi+\psi_e) \qquad \text{(V-12)}$$

$$- \frac{K_t S_f}{J} \frac{K_{bs} A\left(\dot{\frac{\Psi}{A}}+\dot{\theta}_s\right) R_t}{R_t^2 + L_{ms}^2 A^2 \dot{\theta}_s^2} + \frac{D_{ts} A}{J} \sin(D_m(A\dot{\theta}_s t + \Psi))$$

The effects of saturation, hysteresis and eddy currents have been included in this derivation for the sake of consistency with the hybrid model. This AC model can be used to study the performance of other designs of synchronous devices. In those cases it is necessary to determine the magnitude of the saturation, hysteresis and eddy currents. If they are to be included, Equations V-6a and V-6b must be evaluated to determine the current in each of the windings. The saturation and saturation slope factors (S_f and S_s) can then be determined.

Equation V-12 has equilibrium points or singularities which can be found by assuming that the motor has reached steady state and the rate of change of error is zero. This results in Equation V-13.

$$0 = -(B_m + B_h)A\dot{\theta}_s - (T_m + T_h)A$$

$$- K_t S_f \frac{V_s A}{\sqrt{R_t^2 + L_{ms}^2 A^2 \dot{\theta}_s^2}} \sin(\Psi + \Psi_e) \qquad \text{(V-13)}$$

$$- K_t S_f \frac{K_{bs} A \dot{\theta}_s R_t}{\sqrt{R_t^2 + L_{ms}^2 A^2 \dot{\theta}_s^2}}$$

Where: $\Psi = \dot{\Psi}$ and $\dot{\Psi} = 0$ defines the equilibrium point.

In Equation V-13 the detent torque is temporarily ignored. The detent torque can be considered as a sinusoidal disturbance to the system at some multiple of the drive frequency. This multiple is D_m and depends upon the magnetic design of the motor. The effect of the detent torque will be considered in a later section.

The singularities can be found by solving for Ψ in Equation V-13.

$$\Psi = \sin^{-1} \left\{ -[(B_m + B_h) A \dot{\theta}_s + (T_m + T_h) A \right.$$

$$+ K_t S_f \frac{K_{bs} A \dot{\theta}_s R_t}{\sqrt{R_t^2 + L_{ms}^2 A^2 \dot{\theta}_s^2}} \Bigg] \qquad \text{(V-14)}$$

$$\left. \frac{\sqrt{R_t^2 + L_{ms}^2 A^2 \dot{\theta}_s^2}}{K_t S_f V_s A} \right\} - \Psi_e$$

These equilibrium points exist in pairs +/- 2π electrical radians apart. They are the steady state operating points of the system. They can be stable or

unstable, as was the case with phase plane for the stepping motor. Stable and unstable singularities also alternate in this phase plane as they did for the stepping motor.

Having developed the second order model, it is now possible to easily calculate the equilibrium points, the separatrices and the zero slope isocline. The fourth order model in Equations V-1 and III-19 can still be used to calculate the dynamic response of the synchronous motor. The resulting trajectory is projected back into the error plane just as it was for the motor when it was being stepped. As with the stepping motor, the separatrices are used to demonstrate the failure modes of the synchronous motor.

Results of the Synchronous Model

Figure V-2 is the phase plane plot for a 1.8' hybrid motor running as a synchronous motor with a drive frequency of 100 Hz. Position error in radians is plotted versus velocity error in radians per second. The zero slope isocline is the sinusoidal curve. This function is periodic and repeats every 2~ radians. In the region below the zero slope isocline, the trajectories have a positive slope and the motor accelerates. Above the zero slope isocline, the slope is negative and the motor decelerates. Notice that unlike the zero slope isocline for a stepping motor, this zero slope isocline is shifted downward. This occurs because of the damping loads present at synchronous speed.

JM= 3.25m TF= 1.61 ST= 0.00 B= 11.60m KT= 76.00
DTR= 0.00 DTRM= 4.00 KB= 448.60m VR= 5.40 IR= 1.50
RM= 3.80 LM= 20.00mPHZE= 4.00 STPR= 200.00

VS= 35.40 RS= 20.00 RF= 0.00 STS= 1.00 PHO= 2.00
EQTG=M FD=M FDL=M WRW=M DRTP=1
DVFG= 100.00

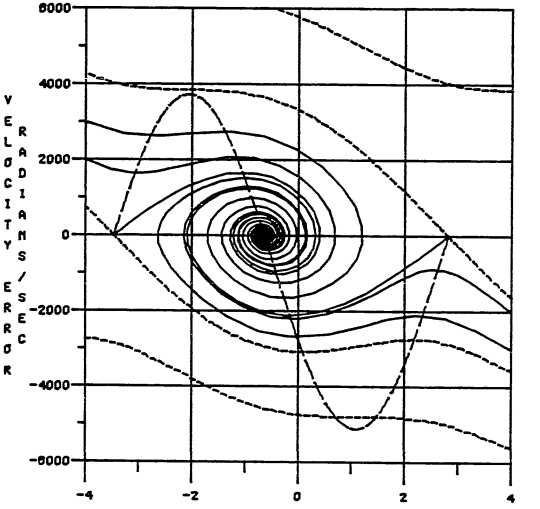

A SYNCHRONOUS PHASE PLANE AT 100 Hz

FIGURE V-2

Also shown on this plot are four separatrices. The separatrices divide the plane up into regions about a stable singularity as they did for a stepping motor. In Figure V-2, the two separatrices nearest to the middle of the plot bound a region where trajectories travel to the stable singularity at (-.64, 0.0). Outside of that region the trajectories go to another stable singularity. As time increases, in the top half plane the trajectories travel to the right and in the bottom half plane they travel to the left.

The trajectories represent the solutions to the synchronous motor equations for an initial position and velocity error. The four trajectories shown start with an error of +/-4 radians and an initial velocity error of +/-2000 and +/-3000 radians per second. The upper portion of the plane represents a region in which the motor is running faster than the drive frequency, and the bottom half of the plane is the region in which it is running slower. The equilibrium point shown at approximately -0.64 radians is the steady state operating point for the motor. After all the transients die out, the motor operates with a position error of 0.64 radians at 100 Hz excitation frequency.

If the drive frequency is increased, it is possible to obtain an entirely different phase plane. See Figure V-3. In this phase plane the drive frequency is increased to 250 Hz. The separatrices in the lower half plane now wrap around

below the stable singularity and come back up into the top half of the phase plane. This creates regions in the phase plane that do not contain a stable singularity. Therefore, it is possible to have an initial condition for a trajectory that nevers lead to a stable singularity. This is the condition where the load is large enough or the drive frequency is high enough so that the motor is unable to gain synchronous speed. Instead the motor goes through a transient and eventually comes to rest at some position while the voltage vector continues to rotate.

Figures V-2 and 3 were developed using the second order model to calculate the trajectories, separatrices and zero slope isocline. While this model doesnot always accurately describe a synchronous motor because of the restriction that the velocity must vary slowly compared to the drive frequency, it still provides good insight and understanding about the different characteristics that the synchronous motors have.

In order to obtain results that are a bit more exact, the trajectories will be calculated using Equation V-4. Because this is the actual winding equation there is no restriction on how the velocity may vary. The second order model will still be used to calculate the separatrices and the zero slope isolcine.

The remainder of this chapter will consist of the

JM= 3.25m TF= 1.81 ST= 0.00 B= 11.80m KT= 78.00
DTR= 0.00 DTRM= 4.00 KB= 446.60m VR= 5.40 IR= 1.50
RM= 3.80 LM= 20.00mPHZE= 4.00 STPR= 200.00

VS= 35.40 RS= 20.00 RF= 0.00 STS= 1.00 PHO= 2.00
EQTQ=M FD=M FDL=M WRW=M DRTP=1
DVFQ= 250.00

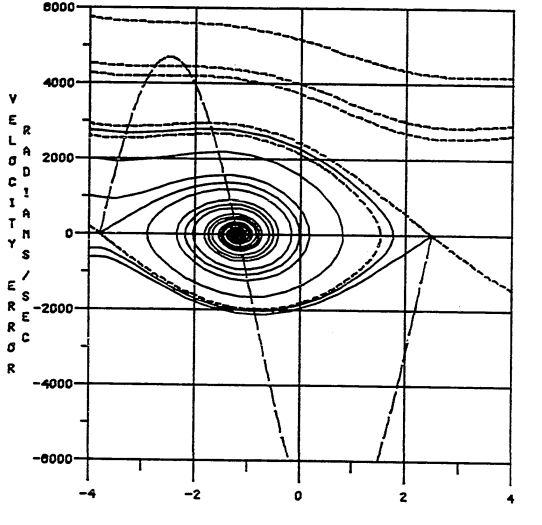

A SYNCHRONOUS PHASE PLANE AT 250 Hz

FIGURE V-3

investigation of several different phenomena that occur during the various modes of synchronous motor operation. Startup, reversal and detent torque, as well as the AC zero work curve and parameter variations will be discussed. The same motor, load and drive that was used in the verification of the hybrid model in Chapter III will be used in the discussion in this chapter.

Start-up

Figure V-4 shows the phase plane for the same motor and drive frequency that was used in Figure V-2, only now the motor is starting from rest. The initial position error is zero and, since it is at rest, there is a negative velocity error equal to 2π times 100 Hz or 628 radians per second. The motor goes through a transient of over- and under-shooting the stable equilibrium point before it pulls into synchronous speed. At synchronous speed the motor lags the voltage vector at a power angle of -0.64 radians while rotating at a constant velocity equal to the drive frequency.

Figure V-5 displays the same motor starting from rest at an excitation frequency of 200 Hz. This increase in frequency causes the separatrices in the lower half plane to move much closer together and to move closer to the origin, while the separatrices in the top half plane move only

JM= 9.25m TF= 1.61 ST= 0.00 B= 11.80m KT= 78.00
DTR= 0.00 DTRM= 4.00 KB= 448.80m VR= 5.40 IR= 1.50
RM= 9.60 LM= 20.00mPHZE= 4.00 STPR= 200.00

VS= 95.40 RS= 20.00 RF= 0.00 STS= 1.00 PHO= 2.00
EGTQ=M FD=M FDL=M WRW=M DRTP=1
DVFQ= 100.00

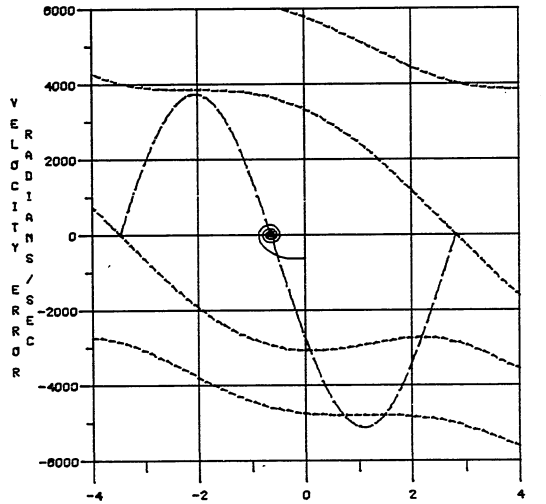

A SYNCHRONOUS START-UP AT 100 Hz

FIGURE V-4

JM= 3.25m TF= 1.61 ST= 0.00 B= 11.60m KT= 78.00
DTR= 0.00 DTRM= 4.00 KB= 446.80m VR= 5.40 IR= 1.50
RM= 3.60 LM= 20.00mPHZE= 4.00 STPR= 200.00

VS= 35.40 RS= 20.00 RF= 0.00 STS= 1.00 PHO= 2.00
EQTG=N FD=N FDL=N WRW=N DRTP=1
DVFG= 200.00

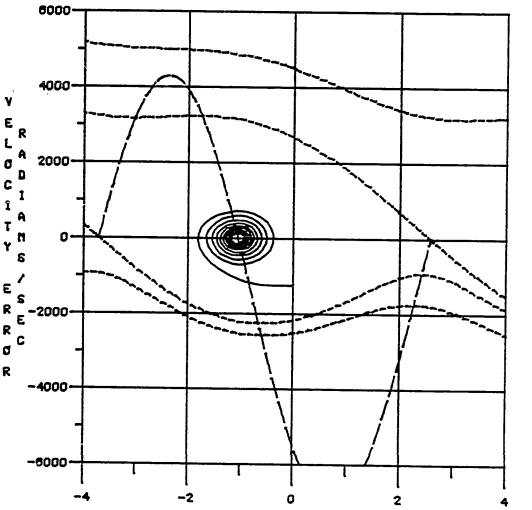

A SYNCHRONOUS START-UP AT 200 Hz

FIGURE V-5

slightly closer together. As the drive frequencey of the motor increases, the start-up transient has larger velocity and position error overshoot. The trajectories during start-up fall entirely within the separatrices so that no failure can occur. Thus in Figures V-4 and V-5 the motor will start and come up to speed without a problem. Figure V-6 shows that only a slight increase in the drive frequency to 225 Hz causes the the separatrices to pinch off in the bottom half of the plane. Figure V-7 shows a further increase in the drive frequency causes the pinching off to grow. Note, however, that the trajectories still lie within the separatrices so that the motor still obtain synchronous speed without incident.

In Figures V-4 through V-7 the start-up transients for various speeds are shown. It was assumed that the rotor was aligned with the voltage vector at t = 0+e. This is not always true and the error plane can be used to investigate the start-up transient from various initial conditions. In Figure V-8 at a motor excitation frequency of 100 Hz, the start-up transient is shown for several initial errors. These represent different rotor positions relative to the drive voltage vector and can all occur for a given drive frequency. The initial error can be any value from -2~ to +2~. The initial position of the voltage vector is always $\Psi = 0$. At a drive frequencey of 100 Hz the motor pulls into synchronous speed from any of the initial conditions.

```
 JM=   3.25m  TF=   1.61   ST=   0.00    B=  11.60m  KT=  76.00
DTR=   0.00 DTRM=   4.00   KB= 446.60m  VR=   5.40   IR=   1.50
 RM=   3.60   LM= 20.00mPHZE=   4.00 STPR= 200.00

 VS=  35.40   RS=  20.00   RF=   0.00  STS=   1.00  PHO=   2.00
EQTQ=M        FD=M         FDL=M       WRW=M       DRTP=1
DVFQ= 225.00
```

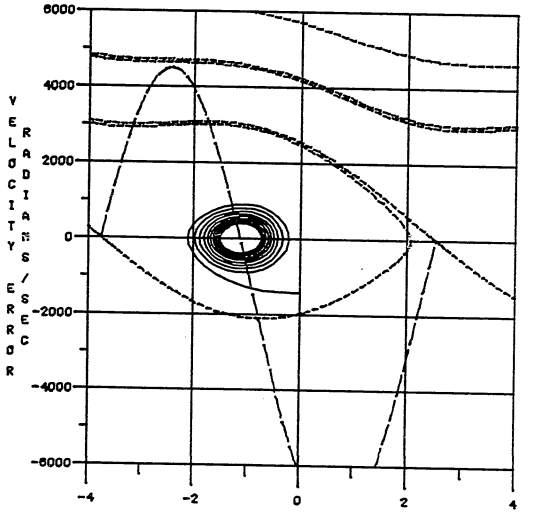

A SYNCHRONOUS START-UP AT 225 Hz

FIGURE V-6

JM= 3.25m TF= 1.61 ST= 0.00 B= 11.80m KT= 78.00
DTR= 0.00 DTRM= 4.00 KB= 446.80m VR= 5.40 IR= 1.50
RM= 3.80 LM= 20.00mPHZE= 4.00 STPR= 200.00

VS= 35.40 RS= 20.00 RF= 0.00 STS= 1.00 PHO= 2.00
EQTQ=M FD=M FDL=M WRW=M DRTP=1
DVFQ= 250.00

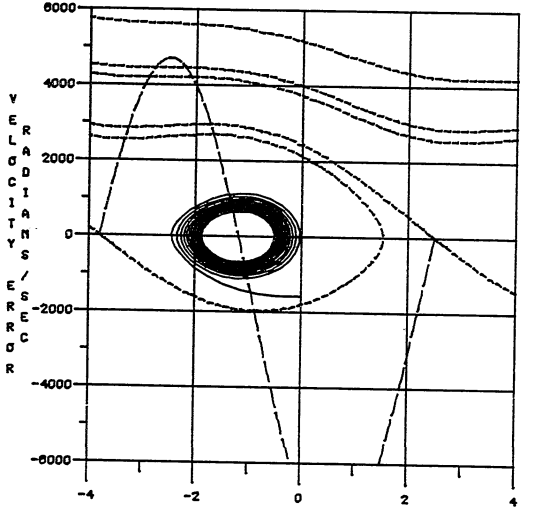

A SYNCHRONOUS START-UP AT 250 Hz

FIGURE V-7

JM= 3.25m TF= 1.61 ST= 0.00 B= 11.60m KT= 76.00
DTR= 0.00 DTRM= 4.00 KB= 446.80m VR= 5.40 IR= 1.50
RM= 3.60 LM= 20.00mPHZE= 4.00 STPR= 200.00

VS= 35.40 RS= 20.00 RF= 0.00 STS= 1.00 PHO= 2.00
EQTR=M FD=M FDL=M WRW=M DRTP=1
DVFR= 100.00

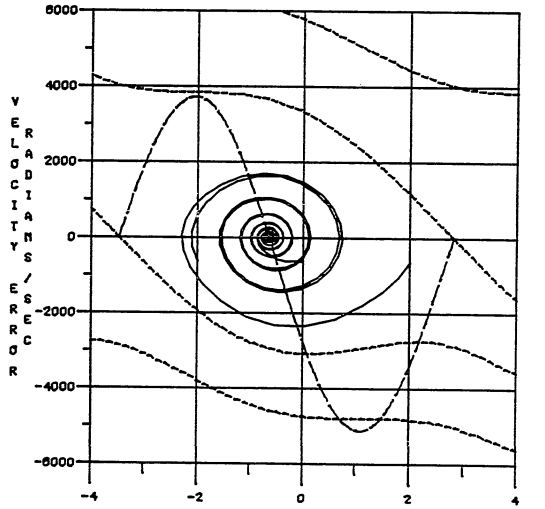

SYNCHRONOUS START-UP AT 100 Hz FOR
VARIOUS INITIAL CONDITIONS

FIGURE V-8

In Figure V-9 the drive frequency is increased to 200 Hz. Notice that two of these initial positions lead to the stable equilibrium point. The other trajectory is across a separatrice and travels to a different stable equilibrium point causing a negative position error. This indicates that the motor is able to come to synchronous speed for all initial conditions. However, for some initial conditions the rotor will "slip" one cycle of the torque angle curve before it gains synchronous speed.

The trajectory that "slips" has an initial condition outside of one of the separatrices. This indicates that before the motor even starts, it can be determined that it will fail to start. The trajectory then crosses and recrosses the second trajectory before pulling into the singularity at -8.0 radians. The cause of this crossing and recrossing is the assumption made about the rate of change of the velocity of the motor when developing the second order model. In this case the variation in the velocity leads to an inaccuracy in the results when the second order model is used to calculate the separatrices. Because of this inaccuracy the separatrix can not always predict the exact point of failure. However, any time the trajectory is in a region close to the separatrix, it becomes a point of serious concern because a minor variation in a system paramater could greatly affect the response of the system.

In Figure V-10 the start-up transients for the same

JM= 3.25m TF= 1.61 ST= 0.00 B= 11.80m KT= 78.00
DTR= 0.00 DTRM= 4.00 KB= 448.80m VR= 5.40 IR= 1.50
RM= 3.60 LM= 20.00mPHZE= 4.00 STPR= 200.00

VS= 35.40 RS= 20.00 RF= 0.00 STS= 1.00 PHO= 2.00
EQTQ=N FD=N FDL=N WRW=N DRTP=1
DVFQ= 200.00

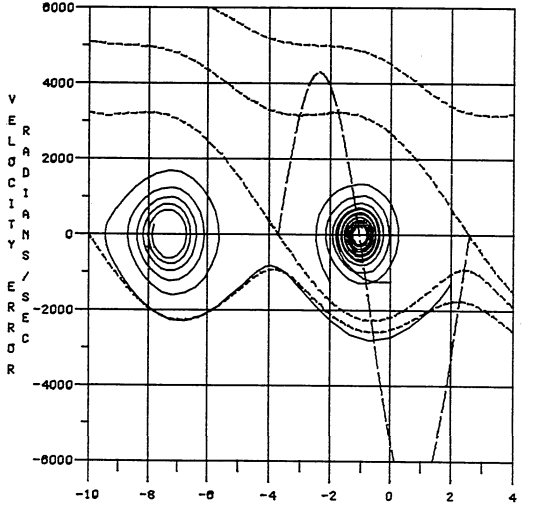

SYNCHRONOUS START-UP AT 200 Hz FOR
VARIOUS INITIAL CONDITIONS

FIGURE V-9

initial conditions are shown again except the drive frequency has been increased from 200 Hz to 250 Hz. In Figure V-10 the motor does not always pick up because the trajectories which now fall outside the separatrix never lead to a stable singularity. Consequently, the motor is not able to come up to synchronous speed from all initial position errors. While it appears that the motor should be able to pick up easily if the position error is equal to zero, at other initial positions the response lies totally outside the separatrices. When this condition occurs the motor follows a trajectory that has an average velocity error equal to minus synchronous speed, i.e., zero velocity. It oscillates slightly about this point due to its reaction to the flux vector that continues to rotate.

If the rotor is aligned with the flux vector, it is also possible to determine the maximum drive frequency at which the rotor will pull into synchronous speed. This is shown in Figure V-11. It is the speed where the initial condition and the separatrix just coincide at $\Psi = 0$.

Reversal

Figure V-12 shows a reversal sequence for excitation frequency of 160 Hz. During start-up the motor starts from rest and goes to some initial equilibrium point shown at a location of $-\Psi$ radians in the phase plane. On reversal,

JM= 3.25m TF= 1.61 ST= 0.00 B= 11.80m KT= 78.00
DTR= 0.00 DTRM= 4.00 KB= 448.80m VR= 5.40 IR= 1.50
RM= 3.60 LM= 20.00mPHZE= 4.00 STPR= 200.00

VS= 35.40 RS= 20.00 RF= 0.00 STS= 1.00 PHO= 2.00
EQTQ=N FD=N FDL=N WRW=N DRTP=1
DVFQ= 250.00

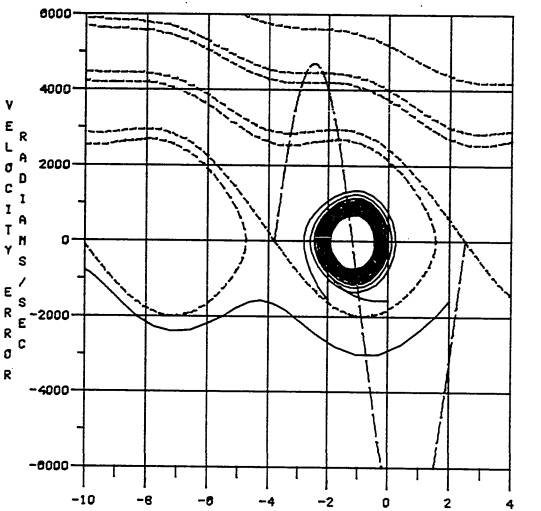

SYNCHRONOUS START-UP AT 250 Hz FOR
VARIOUS INITIAL CONDITIONS

FIGURE V-10

JM= 3.25m TF= 1.61 ST= 0.00 B= 11.80m KT= 78.00
DTR= 0.00 DTRM= 4.00 KB= 448.80m VR= 5.40 IR= 1.50
RM= 3.60 LM= 20.00mPHZE= 4.00 STPR= 200.00

VS= 35.40 RS= 20.00 RF= 0.00 STS= 1.00 PHO= 2.00
EQTQ=N FD=N FDL=N WRW=N DRTP=1
DVFQ= 275.00

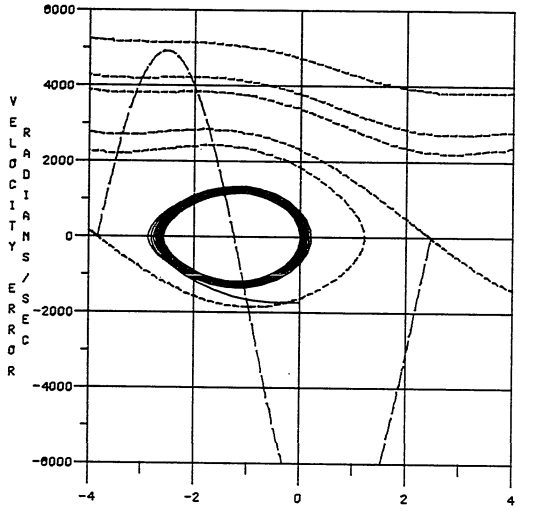

MAXIMUM SYNCHRONOUS START-UP FREQUENCY

FIGURE V-11

JM= 3.25m TF= 1.61 ST= 0.00 S= 11.60m KT= 78.00
DTR= 0.00 DTRM= 4.00 KS= 446.60m VR= 5.40 IR= 1.50
RM= 3.60 LM= 20.00mPHZE= 4.00 STPR= 200.00

VS= 35.40 RS= 20.00 RF= 0.00 STS= 1.00 PHS= 2.00
EQTG=1 FD=1 FDL=1 VRV=1 DRTP=1
DVFG= 180.00

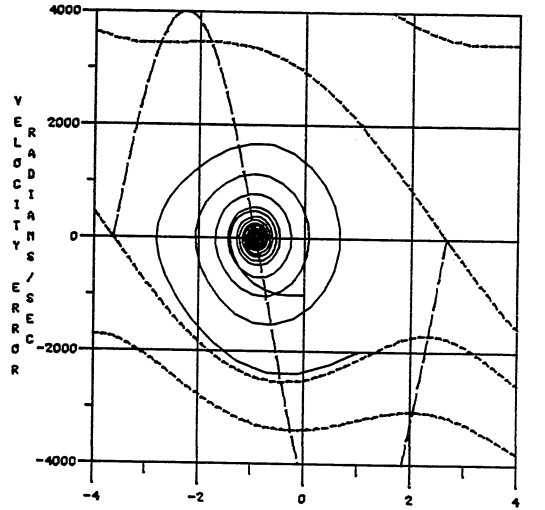

MAXIMUM NO-SLIP REVERSAL FREQUENCY

FIGURE V-12

the position error initial condition now occurs at plus Ψ and the rate of change of error ($\dot{\Psi}$) is minus 2 times the synchronous speed, or $-2\dot{\theta}s$. This puts the system just inside the separatrix so that after the reversal transient, it comes back to the equilibrium point at $-\Psi$. However, now it is operating in the opposite direction.

Notice that the trajectories cross in this phase plane. This is the same condition that occurs in the higher order stepping motor phase plane. During the startup transient the position and velocity coordinates are identical while the currents have different values.

In Figure V-13, a reversal is shown for a higher synchronous speed in which the motor fails to pick up at the original equilibrium point but does pick up at some later equilibrium point after having slipped one cycle of the torque angle curve. In Figure V-14 the system is being operated at a still greater speed during a power reversal which causes it to fall outside the separatrices. The separatrices pinch off and consequently the motor fails to execute this power reversal. This occurs at a drive frequency of 220 Hz.

JM= 3.25m TF= 1.61 ST= 0.00 B= 11.80m KT= 76.00
DTR= 0.00 DTRM= 4.00 KB= 446.80m VR= 5.40 IR= 1.50
RM= 3.60 LM= 20.00mPHZE= 4.00 STPR= 200.00

VS= 35.40 RS= 20.00 RF= 0.00 STS= 1.00 PHO= 2.00
EQTQ=M FD=M FDL=M WRW=M DRTP=1
DVFQ= 215.00

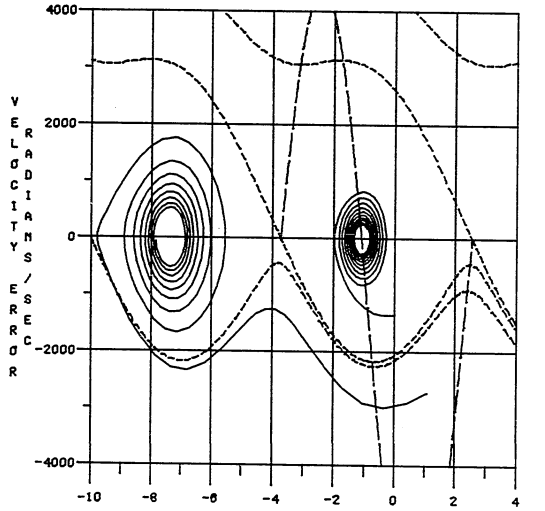

MAXIMUM REVERSAL FREQUENCY

FIGURE V-13

JM= 3.25m TF= 1.61 ST= 0.00 B= 11.80m KT= 78.00
DTR= 0.00 DTRM= 4.00 KB= 448.80m VR= 5.40 IR= 1.50
RM= 3.60 LM= 20.00mPHZE= 4.00 STPR= 200.00

VS= 35.40 RS= 20.00 RF= 0.00 STS= 1.00 PHO= 2.00
EQTQ=N FD=N FDL=N WRW=N DRTP=1
DVFQ= 220.00

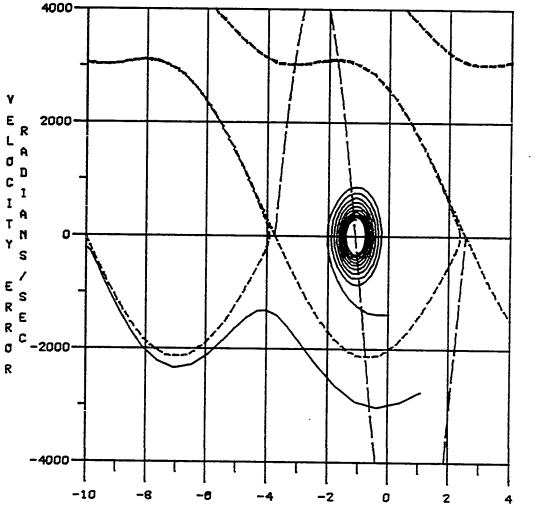

REVERSAL FAILURE

FIGURE V-14

The Zero Work and Torque Speed Curves

In addition to using the synchronous phase plane to investigate the dynamic performance of a synchronous permanent magnet motor, it is also possible to gain other insights into the performance of these motors from the model developed.

In Figures V-15, 16, and 17 several phase planes are shown for various synchronous speeds. These are frequencies above which the motor can pull in and it is necessary to ramp the motor up to these speeds. The shaded area shows regions in the phase plane where trajectories will never come to an equilibrium point. At these higher drive frequencies, the regions of synchronous operation of the motor become smaller and smaller. In Figure V-17 the region of operation is quite small compared to the entire plane. Most of the plane is occupied by trajectories for which the motor will not run at synchronous speed.

It is possible to combine a series of error plane plots at various speeds as in Figures V-15 through V-17, into one more compact plot. By calculating the stable and unstable equilibrium points at many synchronous speeds for the same system, a zero work curve (ZWC) for the motor can be developed. See Figure V-18. At any speed on the vertical axis, the position error coordinates for the stable (right curve) and unstable (left curve) equilibrium points can be

JM= 3.25m TF= 1.61 ST= 0.00 B= 11.80m KT= 76.00
DTR= 0.00 DTRM= 4.00 KB= 448.80m VR= 5.40 IR= 1.50
RM= 3.60 LM= 20.00mPHZE= 4.00 STPR= 200.00

VS= 35.40 RS= 20.00 RF= 0.00 STS= 1.00 PHO= 2.00
EQTG=N FD=N FDL=N WRW=N DRTP=1
DVFQ= 400.00

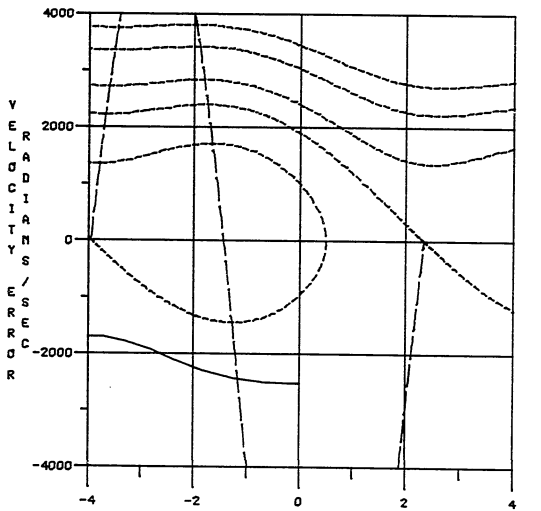

SYNCHRONOUS PHASE PLANE AT 400 Hz

FIGURE V-15

JM= 3.25m TF= 1.61 ST= 0.00 B= 11.60m KT= 78.00
DTR= 0.00 DTRM= 4.00 KB= 448.80m VR= 5.40 IR= 1.50
RM= 3.60 LM= 20.00mPHZE= 4.00 STPR= 200.00

VS= 35.40 RS= 20.00 RF= 0.00 STS= 1.00 PHO= 2.00
EQTQ=N FD=N FDL=N WRW=N DRTP=1
DVFQ= 800.00

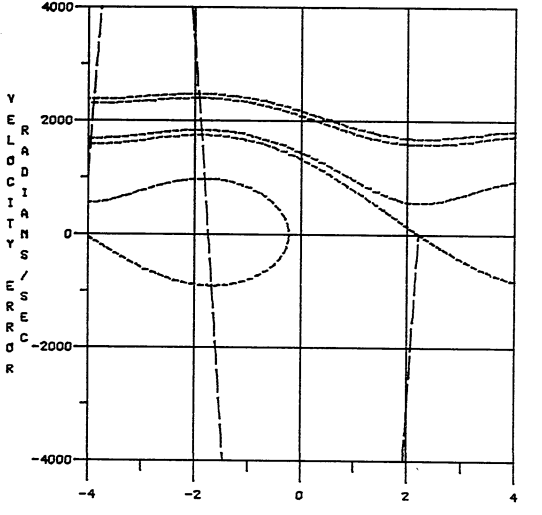

SYNCHRONOUS PHASE PLANE AT 800 Hz

FIGURE V-16

JM= 3.25m TF= 1.61 ST= 0.00 B= 11.80m KT= 78.00
DTR= 0.00 DTRM= 4.00 KB= 448.80m YR= 5.40 IR= 1.50
RM= 3.60 LM= 20.00mPHZE= 4.00 STPR= 200.00

VS= 35.40 RS= 20.00 RF= 0.00 STS= 1.00 PHO= 2.00
EQTQ=M FD=M FDL=M WRW=M DRTP=1
DVFQ= 1.60k

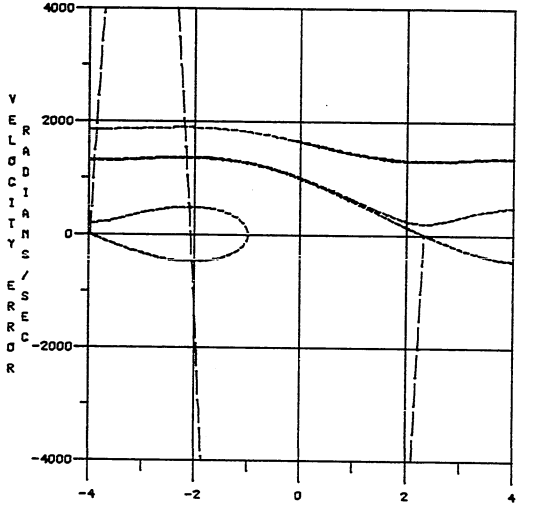

SYNCHRONOUS PHASE PLANE AT 1600 Hz

FIGURE V-17

JM= 3.25m TF= 1.61 ST= 0.00 B= 11.80m KT= 76.00
DTR= 0.00 DTRM= 4.00 KB= 448.80m VR= 5.40 IR= 1.50
RM= 3.60 LM= 20.00mPHZE= 4.00 STPR= 200.00

VS= 35.40 RS= 20.00 RF= 0.00 STS= 1.00 PHO= 2.00
EQTQ=M FD=M FDL=M WRW=M DRTP=1
DVFQ= 2.79k

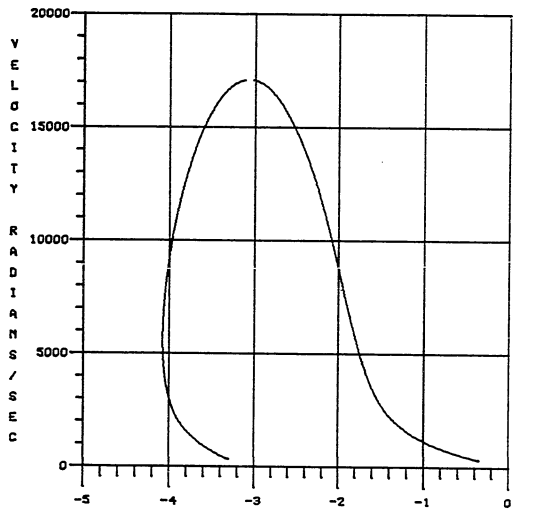

SYNCHRONOUS ZERO WORK CURVE

FIGURE V-18

calculated and plotted. The name zero work curve was taken from stepping motor terminology and signifies that while at a steady state velocity, the net work done on the rotor by external forces equals zero.

The peak of the curve is the point where the load, friction and damping equal the torque generated by the motor, above which the motor is unable to travel any faster. Thinking back to the phase error planes that the ZWC curves came from, the distance between the stable and unstable curves can be used as an approximate measure of the size of the region surrounding the stable equilibrium point. The larger the area of the stable region about the stable equilibrium point, the larger a disturbance must be to push the motor outside this region. Therefore, the distance between the two curves at a specific speed in Figure V-18 yields an insight to the relative sensitivity of the system.

While this curve is not identical to the ZWC curve for the stepping motor, it is quite similar. The ZWC for the stepping motor is the midpoint of the step for a single step limit cycle at a particular step rate. At low speeds the stepping motor is fundamentally being driven by a voltage square wave while, the synchronous motor is being driven by a sine wave. This, combined with the nonlinearities of the system, causes the stepping motor's ZWC to differ slightly from the ZWC of the synchronous motor. However, as the speed is increased, the back EMF and inductance cause the currents

in the stepper and synchronous motor to become similar and the differences between the two curves is minimized.

Even with the low speed differences, the ZWC in both cases still defines the stable equilibrium or lag angle at any speed. The peaks of the curves represent the maximum speed of the system; and the horizontal distance between the stable and unstable curves yields a general idea of the system's sensitivity to external disturbances. Because of these characteristics, the ZWC can be used as an aid to understanding the effects of variations in the system parameters.

The ZWC curve was developed from Equation V-12 in the steady state. If Equation V-12 is rearranged slightly it is also possible to calculate the frequency and damping ratio for small oscillations about the stable equilibrium point. See Equation V-15.

$$\frac{d^2\Psi}{dt^2} = -\left(\frac{B_m + B_h}{J} + \frac{K_t S_f}{J}\,\frac{K_{bs} R_t}{R_t^2 + L_{ms}^2 A^2 \dot{\theta}_s^2}\right)\dot{\Psi}$$

$$- \frac{K_t S_f}{J}\,\frac{V_s A}{\sqrt{R_t^2 + L_{ms}^2 A^2 \dot{\theta}_s^2}}\,\mathrm{Sin}(\Psi + \dot{\gamma}_e)$$

$$-\left(\frac{B_m + B_h}{J} + \frac{K_t S_f}{J}\,\frac{K_{bs} R_t}{R_t^2 + L_{ms}^2 A^2 \dot{\theta}_s^2}\right) A\dot{\theta}_s \qquad \text{(V-15)}$$

$$-\left(\frac{T_m + T_h}{J}\right)\frac{(A\dot{\theta}_s + \dot{\Psi})}{|A\dot{\theta}_s + \dot{\Psi}|}$$

$$+\ \frac{D_{ts} A}{J}\ \mathrm{Sin}(D_m(A\dot{\theta}_s t + \Psi))$$

In Equation V-15 the Ψ terms and the $\dot{\theta}_s$ terms have been grouped. The first two lines of V-15 are the dynamic portion of the equation. The second two lines represent a load torque that remains constant for a particular synchronous speed. The last term, the detent torque, takes the form of an external disturbance.

Simplified, Equation V-15 has the form of:

$$-\frac{\overline{T}}{\overline{J}} = \frac{\ddot{\Psi}}{} + \frac{\overline{B}\dot{\Psi}}{\overline{J}} + \frac{\overline{K}}{\overline{J}}\sin(\Psi+\dot{\gamma}) \qquad \text{(V-16)}$$

Where: $\overline{T}$ = External torques

$\overline{J}$ = Inertia

$\overline{B}$ = Effective damping coefficient

$\overline{K}$ = Effective spring constant

Equation V-16 can be linearized for small disturbances about $\dot{\gamma}$ and a second order linear transfer function can be developed. This transfer function is of the form:

$$\frac{\hat{\Psi}}{T} = \frac{1}{s^2 + 2\zeta_j W_n s + W_n^2} \qquad \text{(V-17)}$$

Where : W_n = Natural frequency

ζ_j = Damping ratio

$\hat{\Psi} = \Psi - \dot{\Psi}$

Returning to Equation V-15 and equating the terms in V-15 to the terms in V-17, expressions for the natural frequency and damping ratio can be obtained. See Equations V-18 and V-19. Note that the $\cos(\Psi+\dot{\Psi})$ is used in Equation V-18. This is the slope or stiffness of the torque angle curve about the stable equilibrium point, $\Psi = \dot{\Psi}$.

$$W_n = \sqrt{\frac{K_t S_f}{J} - \frac{V_s A}{\sqrt{R_t^2 + L_{ms}^2 A^2 \dot{\theta}_s^2}} \cos(\Psi+\dot{\Psi}_e)} \qquad \text{(V-18)}$$

$$\zeta_j = \frac{\left(\frac{B_m + B_h}{J} + \frac{K_t S_f}{J} \frac{K_{bs} R_t}{\sqrt{R_t^2 + L_{ms}^2 A^2 \dot{\theta}_s^2}}\right)}{2 W_n} \qquad \text{(V-19)}$$

$$\bar{T} = -\left(\frac{B_m + B_h}{J} + \frac{K_t S_f}{J} \frac{K_{bs} R_t}{R_t^2 + L_{ms}^2 A^2 \dot{\theta}_s^2}\right) A\dot{\theta}_s$$

$$- \left(\frac{T_m + T_h}{J}\right) \frac{(A\dot{\theta}_s + \dot{\Psi})}{|A\dot{\theta}_s + \dot{\Psi}|} \qquad \text{(V-20)}$$

$$+ \frac{D_{ts} A}{J} \sin(D_m(A\dot{\theta}_s t + \Psi))$$

From Equations V-18 and V-19 it is possible to plot the natural frequency and damping ratio as a function of speed. See Figure V-19. It must be remembered that these values are exact only at the equilibrium point about which the system was linearized. As the position error moves from the equilibrium point the values will become inaccurate.

As seen in Equations V-18 and V-19 and Figure V-19, the natural frequency and damping ratio also depend upon the synchronous drive frequency. Once calculated they will only be valid for a small, local variation in the drive frequency.

Keeping in mind that the local natural frequency and local damping ratio are dependent upon the drive frequency and equilibrium point, considerable insight into the response of the system at higher synchronous speeds can be obtained. In particular, the frequency, amplitude and rate of decay of any oscillations that are a result of external disturbances can be determined. From Figure V-19 it can be

JM= 9.25m TF= 1.61 ST= 0.00 B= 11.80m KT= 78.00
DTR= 0.00 DTRM= 4.00 KB= 448.80m VR= 5.40 IR= 1.50
RM= 3.80 LM= 20.00mPHZE= 4.00 STPR= 200.00

VS= 95.40 RS= 20.00 RF= 0.00 STS= 1.00 PHO= 2.00
EQTS=M FD=M FDL=M WRW=M DRTP=1
DVFS= 2.75k

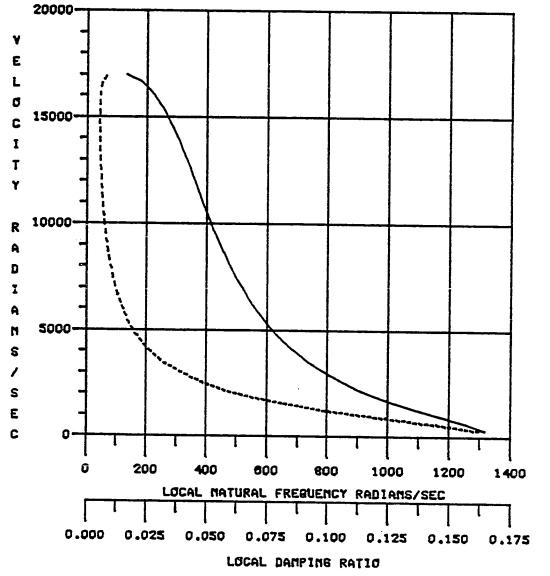

THE LOCAL NATURAL FREQUENCY AND DAMPING
RATIO FOR THE SYNCHRONOUS PHASE PLANE

FIGURE V-19

seen that as the drive frequency, increases both the natural frequency and the damping ratio decrease.

Having developed expressions for the local natural frequency and local damping ratio for any point on the ZWC, it is also possible to determine the maximum torque the motor can develop at any speed from the ZWC. Returning to Figure V-18, it was noted earlier that the peak of the ZWC is the point at which the load torques equals the torque the motor is able to develop at that speed. If the friction torque is increased in discrete increments and the peak of the ZWC is recalculated for each increment of friction torque, it is possible to plot the torque versus the peak speed of the ZWC for each torque. See Figure V-20.

This curve is referred to as the slew torque speed curve for a synchronous permanent magnet motor. It represents the maximum friction load the motor can move in the steady state. However, it does not include the inertial torques developed during a dynamic transient. Even with this limitation the torque speed curve is widely used in industry as an evaluation and design tool.

In addition to plotting the torque versus speed, it is also possible to plot the position error coordinate of the peak of the ZWC for each of the points on the torque speed curve. This resulting curve is shown in Figure V-21 along with the ZWC. This new curve could be called the

JM= 3.25m TF= 1.61 ST= 0.00 B= 11.80m KT= 78.00
DTR= 0.00 DTRM= 4.00 KB= 448.80m VR= 5.40 IR= 1.50
RM= 3.80 LM= 20.00mPHZE= 4.00 STPR= 200.00

VS= 35.40 RS= 20.00 RF= 0.00 STS= 1.00 PHO= 2.00
EQTG=M FD=M FDL=M WRV=M DRTP=1
DYFQ= 2.75k

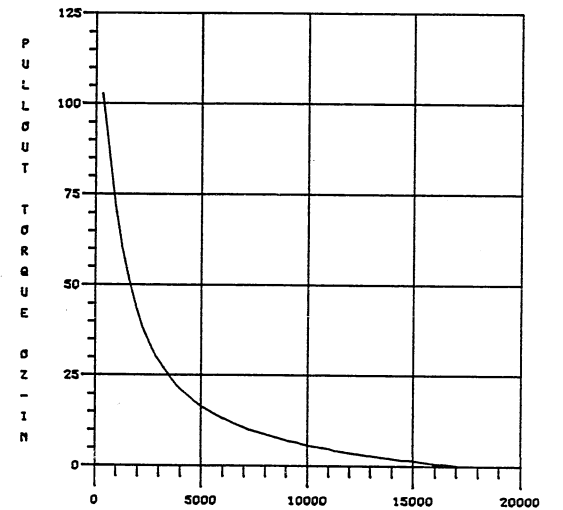

THE TORQUE SPEED CURVE FOR THE SYNCHRONOUS PHASE PLANE

FIGURE V-20

JM= 3.25m TF= 1.61 ST= 0.00 B= 11.60m KT= 78.00
DTR= 0.00 DTRM= 4.00 KB= 446.80m VR= 5.40 IR= 1.50
RM= 3.60 LM= 20.00mPHZE= 4.00 STPR= 200.00

VS= 35.40 RS= 20.00 RF= 0.00 STS= 1.00 PHO= 2.00
EQTQ=M FD=M FDL=M WRW=M DRTP=1
DVFQ= 2.75k

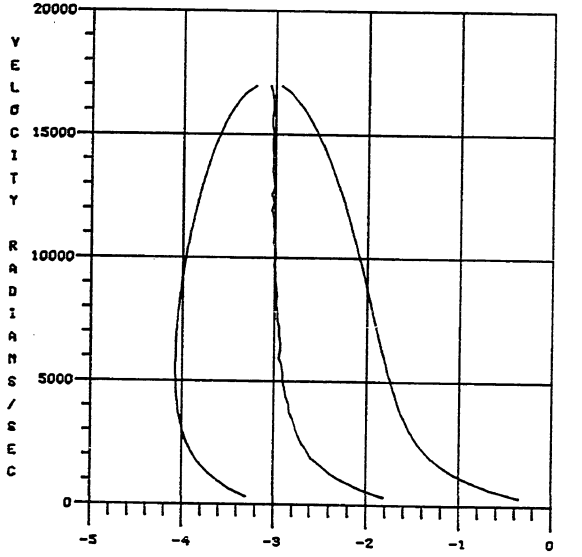

THE ZERO AND MAXIMUM WORK CURVES FOR THE SYNCHRONOUS PHASE PLANE

FIGURE V-21

maximum work curve (MWC) because it represents the equilibrium point at which the motor is moving the maximum possible load torque for a given drive frequency.

Parameter Variations

Once a motor and drive for a system have been selected, their parameters usually vary only a slight amount. It is friction, damping, and inertia of the load that may vary widely. In order to gain insight into these effects, it would be beneficial to vary those parameters and look at the resulting phase error planes, ZWC and MWC, torque speed, natural frequency and damping ratio curves.

Figures V-22 through V-24 show the effects on the phase plane of increasing friction. The equilibrium points move closer together and the zero slope isocline moves down in the phase plane. As one might expect, the increase in the friction reduces the torque available to accelerate the motor. This results in a smaller region of positive acceleration. Except for the inner most separatrix in the quadrant III, the separatrices move further away from the stable equilibrium point and each other, causing the regions around the singularities to grow. This increase makes the system less sensitive to external disturbances. In quadrant III the trajectory and the inner most separatrix move closer together as the friction is increased. This decreases the

JN= 3.25m TF= 1.61 ST= 0.00 B= 11.80m KT= 78.00
DTR= 0.00 DTRM= 4.00 KB= 448.80m VR= 5.40 IR= 1.50
RN= 3.60 LM= 20.00mPHZE= 4.00 STPR= 200.00

VS= 35.40 RS= 20.00 RF= 0.00 STS= 1.00 PHD= 2.00
EQTG=N FD=N FDL=N WRW=N DRTP=1
DVFG= 200.00

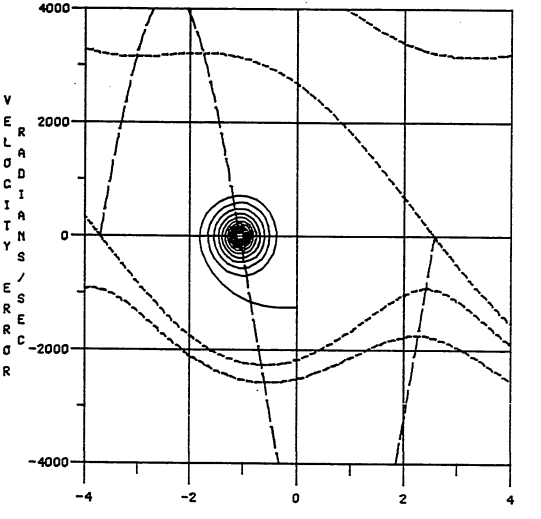

SYNCHRONOUS PHASE PLANE AT 200 Hz WITH
T_f = 1.61 oz-in

FIGURE V-22

JM= 3.25m TF= 3.22 ST= 0.00 B= 11.80m KT= 78.00
DTR= 0.00 DTRM= 4.00 KB= 448.80m VR= 5.40 IR= 1.50
RM= 3.60 LM= 20.00mPHZE= 4.00 STPR= 200.00

VS= 35.40 RS= 20.00 RF= 0.00 STS= 1.00 PHC= 2.00
EQTG=N FD=N FDL=N WRW=N DRTP=1
DVFG= 200.00

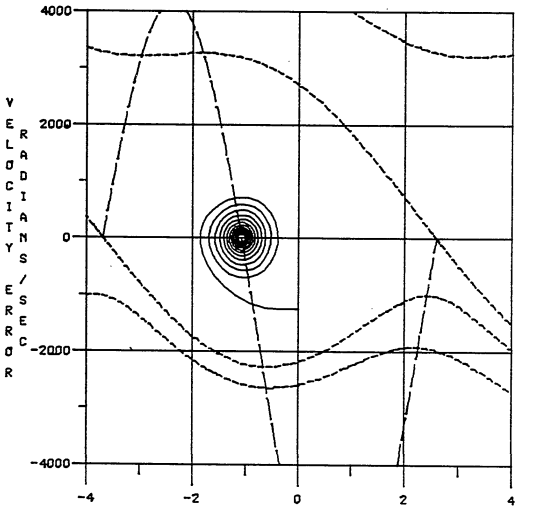

SYNCHRONOUS PHASE PLANE AT 200 Hz WITH
T_f = 3.22 oz-in

FIGURE V-23

JM= 3.25m TF= 12.88 ST= 0.00 B= 11.80m KT= 78.00
DTR= 0.00 DTRM= 4.00 KB= 448.80m VR= 5.40 IR= 1.50
RM= 3.60 LM= 20.00mPHZE= 4.00 STPR= 200.00

VS= 35.40 RS= 20.00 RF= 0.00 STS= 1.00 PHO= 2.00
EQTQ=N FD=N FDL=N WRW=N DRTP=1
DVFQ= 200.00

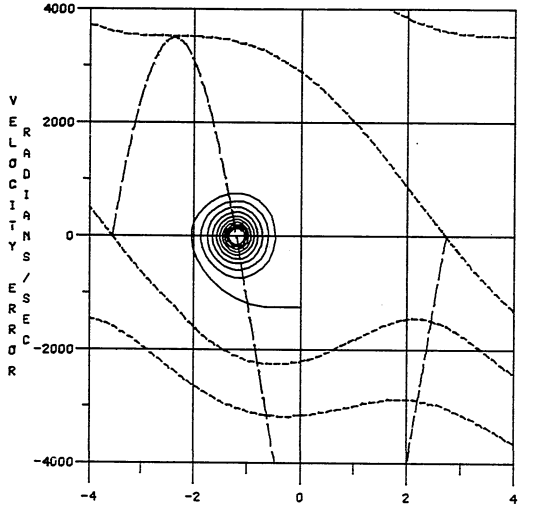

SYNCHRONOUS PHASE PLANE AT 200 Hz WITH
T_f = 12.88 oz-in

FIGURE V-24

maximum frequency the system can start at without failure.

Figure V-25 through V-27 show the work curves, torque speed, natural frequency and damping ratio for the various values of friction. The increase in friction causes a reduction in the maximum speed of the system because there is less torque available to accelerate and maintain high velocities. The torque speed curve shows a constant change between the curves equal to the increase in the friction, as expected. The local natural frequency and damping ratio have the same general shape, just a different velocity scale. This is also expected because the natural frequency and damping ratio are not functions of the friction.

Figures V-28 through V-33 show the effects of increasing damping. As with the friction, the equilibrium points move closer together and the zero slope isocline is shifted downward. The separatrices also move further away from the stable singularity. The zero work curves show the same decrease in maximum speeds. The torque speed curves separate as the speed increases due to the increase in the damping torques with speed. As was true for the friction, the damping has a very small effect on the natural frequency and the damping ratio. This is because the first portion of Equation V-19, which contains B, is small compared to the second term which is the electrical damping due to the back EMF. In general the response of the motor to increases in damping is just about the same as it is for the increases

JM= 3.25m TF= 12.88 ST= 0.00 B= 11.80m KT= 78.00
DTR= 0.00 DTRM= 4.00 KB= 448.80m VR= 5.40 IR= 1.50
RM= 3.60 LM= 20.00mPHZE= 4.00 STPR= 200.00

VS= 35.40 RS= 20.00 RF= 0.00 STS= 1.00 PHO= 2.00
EQTQ=N FD=N FDL=N WRW=N DRTP=1
DYFQ= 1.10k

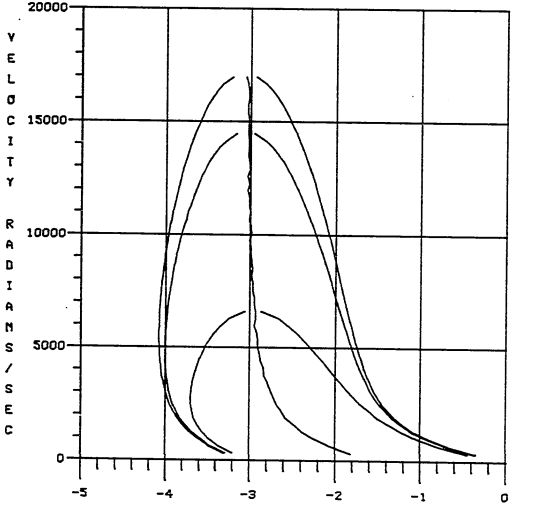

SYNCHRONOUS WORK CURVES FOR T_f = 1.61,
3.22 and 12.88 oz-in

FIGURE V-25

JM= 3.25m TF= 12.88 ST= 0.00 B= 11.60m KT= 76.00
DTR= 0.00 DTRM= 4.00 KB= 446.60m VR= 5.40 IR= 1.50
RM= 3.60 LM= 20.00mPHZE= 4.00 STPR= 200.00

VS= 35.40 RS= 20.00 RF= 0.00 STS= 1.00 PHO= 2.00
EQTG=M FD=M FDL=M WRV=M DRTP=1
DVFG= 1.10k

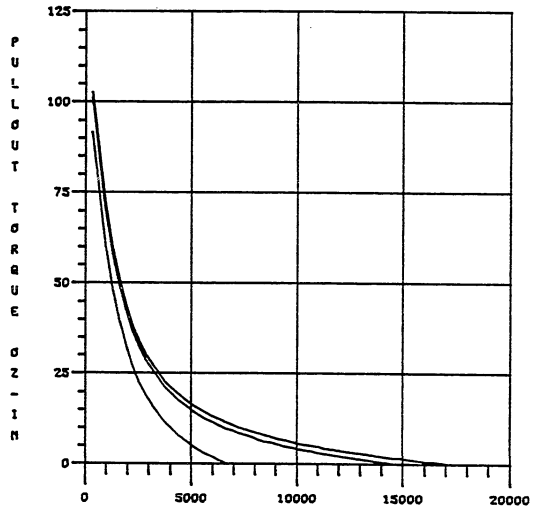

SYNCHRONOUS TORQUE SPEED CURVE FOR T_f = 1.61, 3.22 AND 12.88 oz-in

FIGURE V-26

JM= 3.25m TF= 12.88 ST= 0.00 B= 11.80m KT= 78.00
DTR= 0.00 DTRM= 4.00 KB= 448.80m VR= 5.40 IR= 1.50
RM= 3.80 LM= 20.00mPHZE= 4.00 STPR= 200.00

VS= 35.40 RS= 20.00 RF= 0.00 STS= 1.00 PHO= 2.00
EQTQ=M FD=M FDL=M WRW=M DRTP=1
DVFQ= 1.10k

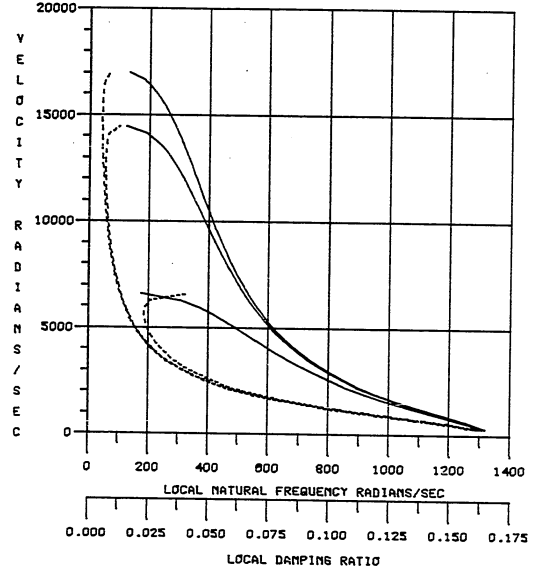

SYNCHRONOUS NATURAL FREQUENCY AND DAMPING RATIO CURVES FOR T_f = 1.61, 3.22 and 12.88 oz-in

FIGURE V-27

JM= 3.25m TF= 1.61 ST= 0.00 B= 11.80m KT= 78.00
DTR= 0.00 DTRM= 4.00 KB= 446.80m VR= 5.40 IR= 1.50
RM= 3.60 LM= 20.00mPHZE= 4.00 STPR= 200.00

VS= 35.40 RS= 20.00 RF= 0.00 STS= 1.00 PHO= 2.00
EQTG=N FD=N FDL=N WRW=N DRTP=1
DVFG= 200.00

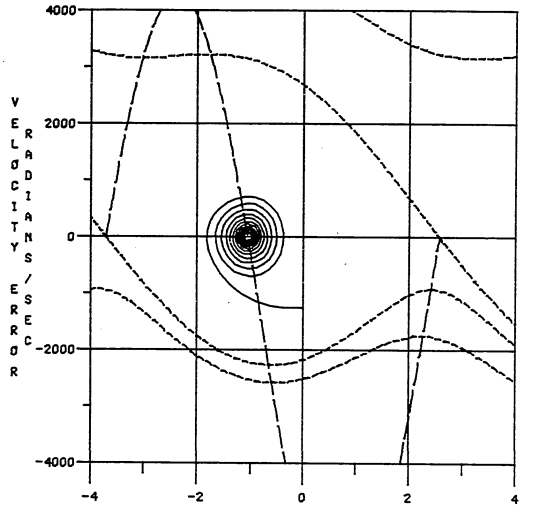

SYNCHRONOUS PHASE PLANE AT 200 Hz WITH
B = .0118 oz-in/rad/sec

FIGURE V-28

JM= 3.25m TF= 1.61 ST= 1.00 B= 23.60m KT= 78.00
DTR= 0.00 DTRM= 4.00 KB= 448.80m VR= 5.40 IR= 1.50
RM= 3.60 LM= 20.00mPHZE= 4.00 STPR= 200.00

VS= 35.40 RS= 20.00 RF= 0.00 STS= 1.00 PHO= 2.00
EQTQ=N FD=N FDL=N WRW=N DRTP=1
DVFQ= 200.00

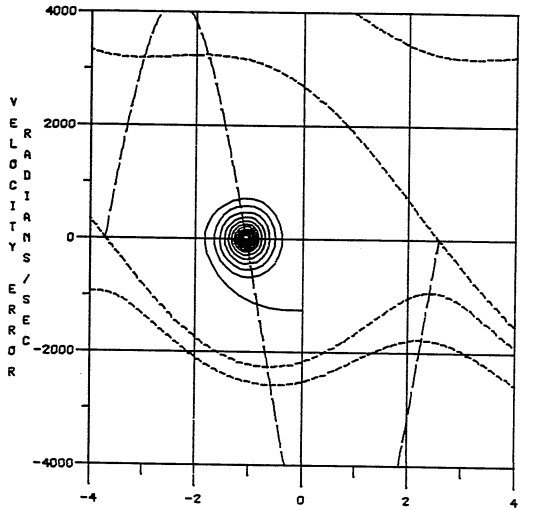

SYNCHRONOUS PHASE PLANE AT 200 Hz WITH
B = .0236 oz-in/rad/sec

FIGURE V-29

JM= 3.25m TF= 1.61 ST= 1.00 B= 54.20m KT= 78.00
DTR= 0.00 DTRM= 4.00 KB= 446.80m VR= 5.40 IR= 1.50
RM= 9.60 LM= 20.00mPHZE= 4.00 STPR= 200.00

VS= 35.40 RS= 20.00 RF= 0.00 STS= 1.00 PHO= 2.00
EQTQ=N FD=N FDL=N WRW=N DRTP=1
DVFQ= 200.00

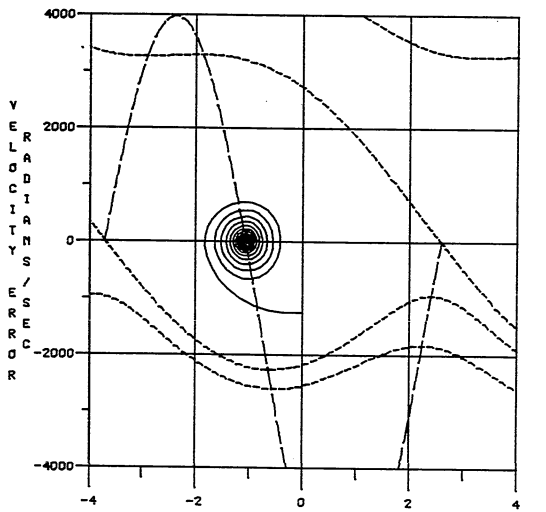

SYNCHRONOUS PHASE PLANE AT 200 Hz WITH
B = .0542 oz-in/rad/sec

FIGURE V-30

JM= 3.25m TF= 1.61 ST= 0.00 B= 54.20m KT= 78.00
DTR= 0.00 DTRM= 4.00 KB= 448.80m VR= 5.40 IR= 1.50
RM= 3.60 LM= 20.00mPHZE= 4.00 STPR= 200.00

VS= 35.40 RS= 20.00 RF= 0.00 STS= 1.00 PHO= 2.00
EQTQ=N FD=N FDL=N WRW=N DRTP=1
DVFQ= 1.40k

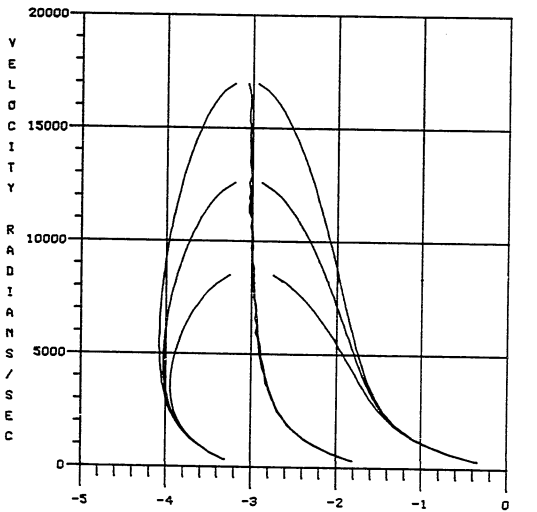

SYNCHRONOUS WORK CURVES FOR B =.0188, .0236
and .0542 oz-in/rad/sec

FIGURE V-31

JM= 3.25m TF= 1.61 ST= 0.00 B= 54.20m KT= 78.00
DTR= 0.00 DTRM= 4.00 KB= 448.80m VR= 5.40 IR= 1.50
RM= 3.60 LM= 20.00mPHZE= 4.00 STPR= 200.00

VS= 35.40 RS= 20.00 RF= 0.00 STS= 1.00 PHO= 2.00
EQTQ=N FD=N FDL=N WRW=N DRTP=1
DYFQ= 1.40k

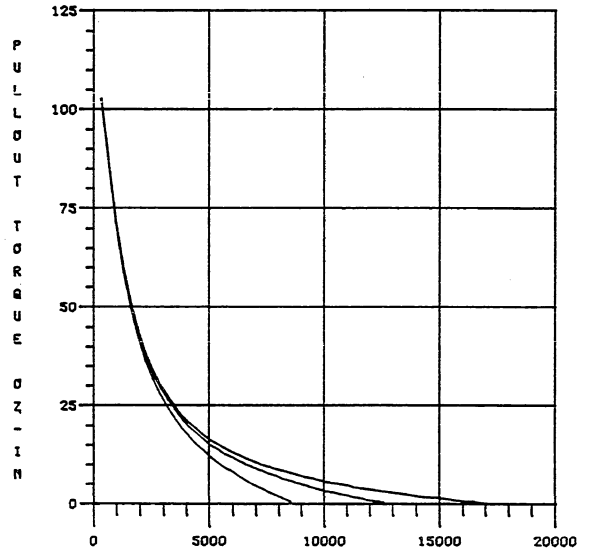

SYNCHRONOUS TORQUE SPEED CURVES FOR B =.0118,
.0236 and .0542 oz-in/rad/sec

FIGURE V-32

JM= 3.25m TF= 1.61 ST= 0.00 B= 54.20m KT= 78.00
DTR= 0.00 DTRM= 4.00 KB= 446.80m VR= 5.40 IR= 1.50
RM= 3.60 LM= 20.00mPHZE= 4.00 STPR= 200.00

VS= 35.40 RS= 20.00 RF= 0.00 STS= 1.00 PHO= 2.00
EQTQ=N FD=N FDL=N WRW=N DRTP=1
DVFQ= 1.40k

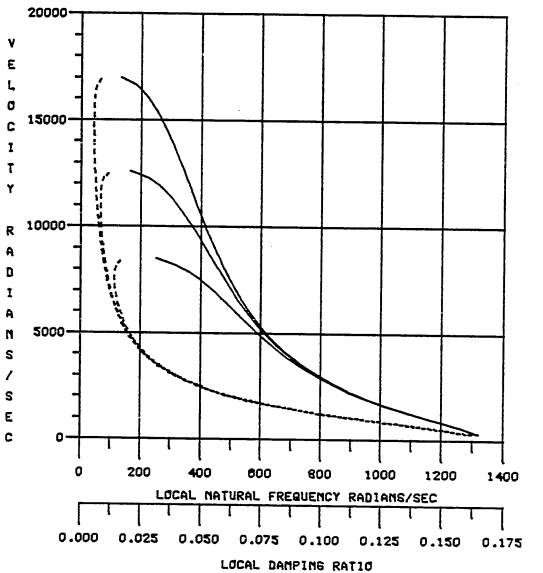

SYNCHRONOUS NATURAL FREQUENCY AND DAMPING
RATIO CURVES FOR B =.0118, .0236
and .0542 oz-in/rad/sec

FIGURE V-33

in friction.

Figures V-34 through V-39 show the effects of increasing the inertia. Inertia has the most pronounced effect on the response of the system. The separatrices move closer to the zero velocity error axis and pinch off. However, the equilibrium points remain stationary and the zero slope isocline does not change. The trajectories show much more oscillation due to the increased inertia. The system has a much harder time coming up to synchronous speed, but once obtained, the motor is less sensitive to external disturbances. The work curves and torque speed curves show no difference between the different inertias. This is expected because the work curves and torque speed curves are steady state concepts and the inertia, while greatly affecting dynamic response, has no effect on the steady state response. The natural frequency and damping ratio show significant changes. This would also be expected because Equations V-18 and V-19 are highly dependent upon the system inertia.

JM= 3.25m TF= 1.61 ST= 0.00 B= 11.80m KT= 78.00
DTR= 0.00 DTRM= 4.00 KB= 448.80m VR= 5.40 IR= 1.50
RM= 3.60 LM= 20.00mPHZE= 4.00 STPR= 200.00

VS= 35.40 RS= 20.00 RF= 0.00 STS= 1.00 PHO= 2.00
EQTQ=N FD=N FDL=N WRW=N DRTP=1
DVFQ= 200.00

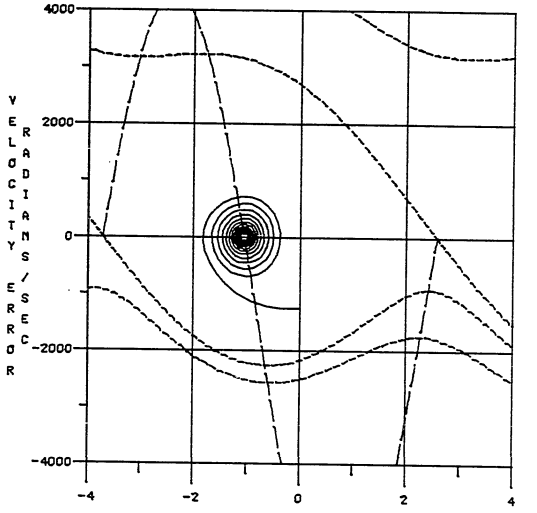

SYNCHRONOUS PHASE PLANE AT 200 Hz WITH
J_m = .00325 oz-in-sec^2

FIGURE V-34

JM= 6.50m TF= 1.61 ST= 1.00 B= 11.80m KT= 78.00
DTR= 0.00 DTRM= 4.00 KB= 448.80m VR= 5.40 IR= 1.50
RM= 3.60 LM= 20.00mPHZE= 4.00 STPR= 200.00

VS= 35.40 RS= 20.00 RF= 0.00 STS= 1.00 PHO= 2.00
EQTQ=N FD=N FDL=N WRW=N DRTP=1
DVFQ= 200.00

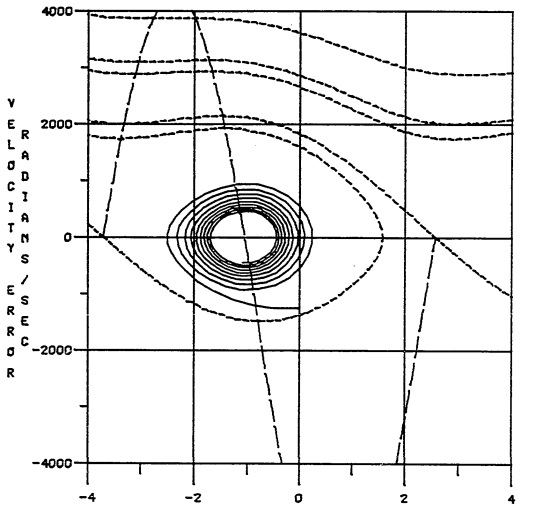

SYNCHRONOUS PHASE PLANE AT 200 Hz WITH
J_m = .00650 oz-in-sec^2

FIGURE V-35

JM= 13.00m TF= 1.61 ST= 1.00 B= 11.80m KT= 78.00
DTR= 0.00 DTRM= 4.00 KB= 448.80m VR= 5.40 IR= 1.50
RM= 3.60 LM= 20.00mPHZE= 4.00 STPR= 200.00

VS= 35.40 RS= 20.00 RF= 0.00 STS= 1.00 PHO= 2.00
EQTG=M FD=M FDL=M WRW=M DRTP=1
DVFG= 200.00

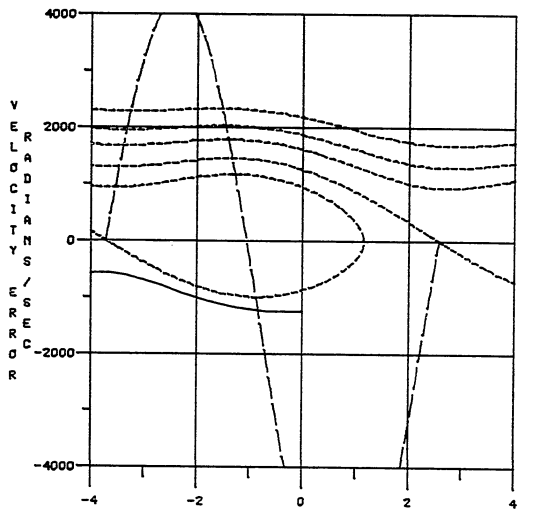

SYNCHRONOUS PHASE PLANE AT 200 Hz WITH
J_m = .01300 oz-in-sec^2

FIGURE V-36

JN= 13.00m TF= 1.61 ST= 0.00 B= 11.80m KT= 78.00
DTR= 0.00 DTRM= 4.00 KB= 446.80m VR= 5.40 IR= 1.50
RM= 3.60 LM= 20.00mPHZE= 4.00 STPR= 200.00

VS= 35.40 RS= 20.00 RF= 0.00 STS= 1.00 PHO= 2.00
EQTQ=M FD=M FDL=M WRW=M DRTP=1
DVFQ= 2.75k

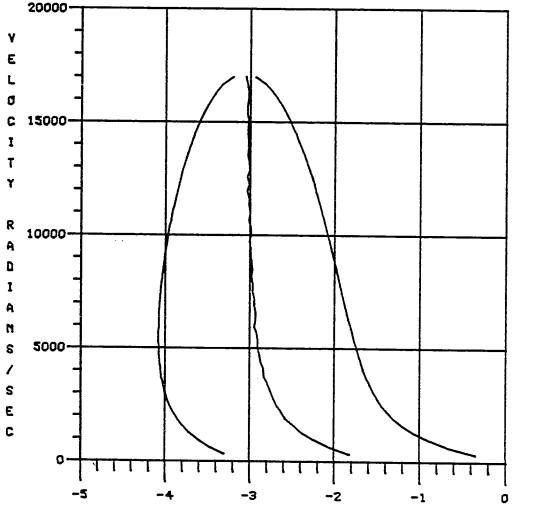

SYNCHRONOUS WORK CURVES FOR J_m =.00325,
.00650 and .01300 oz-in-sec^2

FIGURE V-37

JM= 13.00m TF= 1.61 ST= 0.00 B= 11.60m KT= 76.00
DTR= 0.00 DTRM= 4.00 KB= 448.80m VR= 5.40 IR= 1.50
RM= 3.60 LM= 20.00mPHZE= 4.00 STPR= 200.00

VS= 95.40 RS= 20.00 RF= 0.00 STS= 1.00 PHO= 2.00
EQTQ=M FD=M FDL=M WRW=M DRTP=1
DVFQ= 2.75k

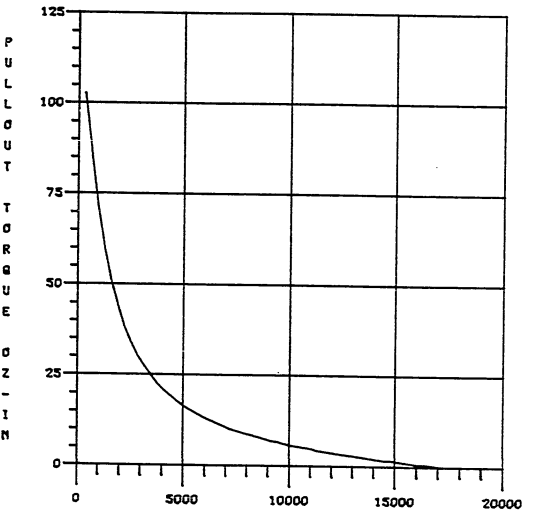

SYNCHRONOUS TORQUE SPEED CURVES FOR J_m =.00325, .00650 and .01300 oz-in-sec^2

FIGURE V-38

JM= 13.00m TF= 1.61 ST= 0.00 B= 11.80m KT= 78.00
DTR= 0.00 DTRM= 4.00 KB= 448.80m VR= 5.40 IR= 1.50
RM= 3.60 LM= 20.00mPMZE= 4.00 STPR= 200.00

VS= 35.40 RS= 20.00 RF= 0.00 STS= 1.00 PHO= 2.00
EQTG=M FD=M FDL=M WRW=M DRTP=1
DYFG= 2.75k

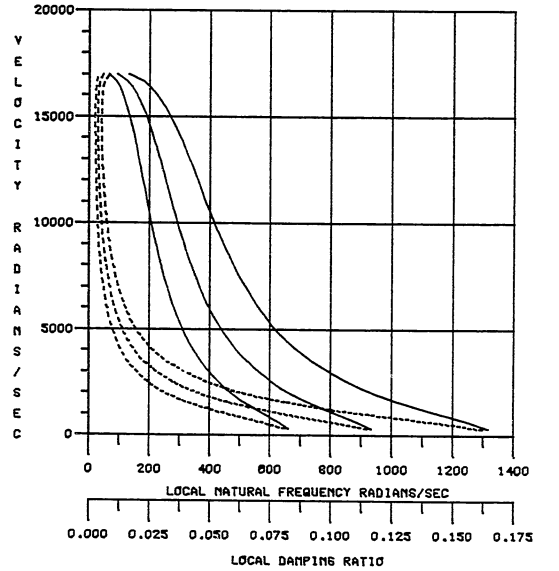

SYNCHRONOUS NATURAL FREQUENCY AND DAMPING RATIO CURVES FOR J_m=.00325, .00650 and .01300 oz-in-sec^2

FIGURE V-39

Detent Torque

When the model for the synchronous motor was developed, the detent torque was neglected. Because the detent torque is produced by a magnetic interaction with the stator and is dependent upon the mechanical structure of the motor, it looks like a periodic disturbance to the rotating mechanical system. The frequency of the detent torque depends upon the motor speed and the structure of the motor. The actual frequency is the product of the motor velocity and the number of cycles of the detent torque angle curve during one cycle of the stator torque angle curve.

The effect of the detent torque, or any similar periodic disturbance, is easily seen in the phase plane. Figure V-40 is the start-up transient at 50 Hz with the detent torque equal to zero. Figure V-41 shows the same start-up transient with a detent torque of 5.5 oz-in. The figure shows that, instead of the system settling in at the stable equilibrium point, it settles into a limit cycle about the stable equilibrium point. The size of the limit cycle is +/-0.2 radians and +/-200 radians per second.

This limit cycle occurs because, to the system, the detent torque appears to be a torque oscillation that causes the stable equilibrium point to vary slightly about the original stable equilibrium point. The motor tries to track to the varying equilibrium point and as a result, settles into the limit cycle.

JM= 3.25m TF= 1.61 ST= 0.00 B= 11.80m KT= 78.00
DTR= 0.00 DTRM= 4.00 KB= 448.80m VR= 5.40 IR= 1.50
RM= 3.60 LM= 20.00mPHZE= 4.00 STPR= 200.00

VS= 35.40 RS= 20.00 RF= 0.00 STS= 1.00 PHO= 2.00
EQTQ=N FD=N FDL=N WRW=N DRTP=1
DVFQ= 50.00

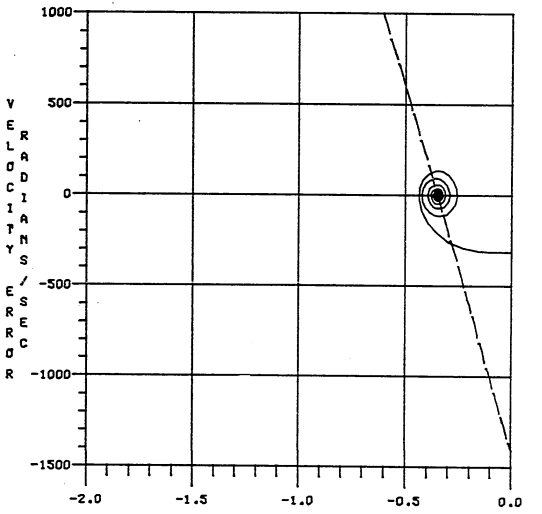

SYNCHRONOUS PHASE PLANE AT 50 Hz WITH D_t = 0.0

FIGURE V-40

JM= 3.25m TF= 1.61 ST= 0.00 B= 11.80m KT= 76.00
DTR= 5.50 DTRM= 4.00 KB= 448.80m VR= 5.40 IR= 1.50
RM= 3.80 LM= 20.00mPHZE= 4.00 STPR= 200.00

VS= 35.40 RS= 20.00 RF= 0.00 STS= 1.00 PHS= 2.00
EQTS=N FD=N FDL=N WRW=N DRTP=1
DVFS= 50.00

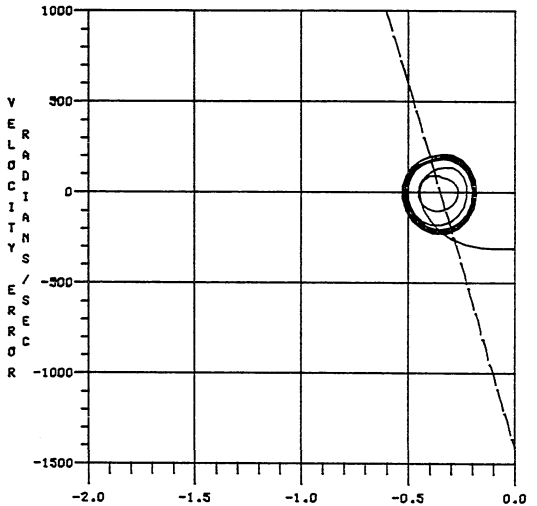

SYNCHRONOUS PHASE PLANE AT 50 Hz WITH D_t = 5.5

FIGURE V-41

If the detent torque is removed and the drive frequency is increased to 200 Hz, the phase error plane in Figure V-42 is obtained. If the detent torque is returned to the simulation, the response shown in Figure V-43 obtained. Again a limit cycle is formed; however, the amplitude is reduced to +/-0.05 radians and +/-50 radians per second, about one-quarter of the size of the 50 Hz limit cycle.

A second way to look at and explain this limit cycle, as well as the change in the limit cycle amplitude, comes from linear system theory. As was stated earlier, the synchronous model can be linearized for small regions about the equilibrium point. In this small region which contains the limit cycle, the motor can be thought of as a linear, second order system. The detent torque is a periodic input of some amplitude and frequency. The motor responds to the detent torque just as any second order system would respond to the periodic input. It oscillates at an amplitude and phase determined by the system's Bode plot. There is some break frequency where the maximum oscillation amplitude occurs and then the amplitude falls off at 20 db per decade.

Using this approach it is possible to calculate the amplitude of the limit cycle due to the detent torque at any drive frequency. Figure V-44 shows an expanded view of the lower portion of the natural frequency and damping ratio curves. At a drive frequency of 50 Hz the natural frequency

JM= 3.25m TF= 1.61 ST= 0.00 B= 11.80m KT= 78.00
DTR= 0.00 DTRM= 4.00 KB= 448.80m VR= 5.40 IR= 1.50
RM= 3.60 LM= 20.00mPHZE= 4.00 STPR= 200.00

VS= 35.40 RS= 20.00 RF= 0.00 STS= 1.00 PHO= 2.00
EQTQ=N FD=N PDL=N WRW=N DRTP=1
DVFQ= 200.00

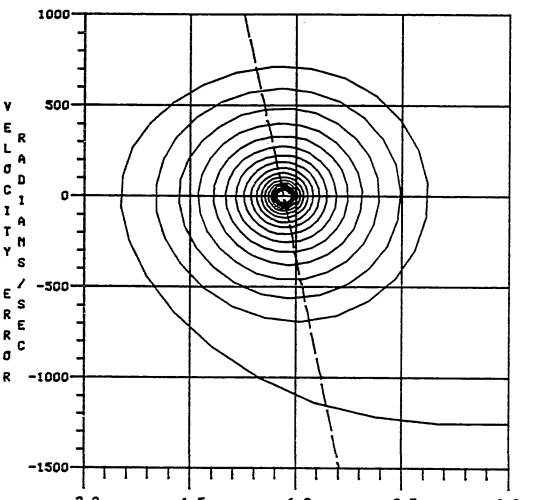

SYNCHRONOUS PHASE PLANE AT 200 Hz WITH D_t = 0.0

FIGURE V-42

JM= 3.25m TF= 1.61 ST= 0.00 B= 11.80m KT= 78.00
DTR= 5.30 DTRM= 4.00 KB= 448.80m VR= 5.40 IR= 1.50
RM= 3.60 LM= 20.00mPHZE= 4.00 STPR= 200.00

VS= 35.40 RS= 20.00 RF= 0.00 STS= 1.00 PHO= 2.00
EQTG=N FD=N FDL=N WRW=N DRTP=1
DVFG= 200.00

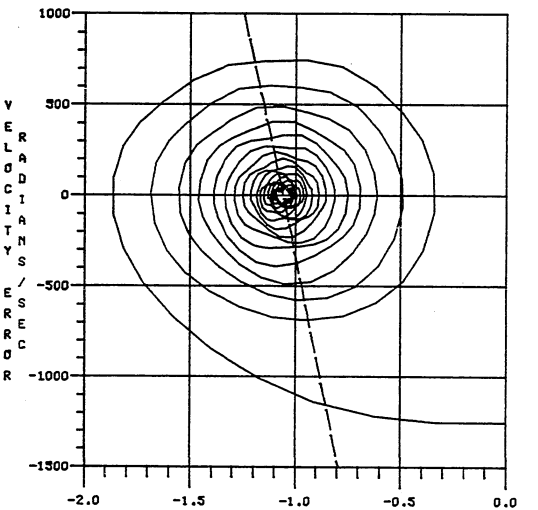

SYNCHRONOUS PHASE PLANE AT 200 Hz WITH D_t = 5.5

FIGURE V-43

JM= 3.25m TF= 1.61 ST= 0.00 B= 11.80m KT= 76.00
DTR= 0.00 DTRM= 4.00 KB= 446.80m VR= 5.40 IR= 1.50
RM= 3.60 LM= 20.00mPHZE= 4.00 STPR= 200.00

VS= 35.40 RS= 20.00 RF= 0.00 STS= 1.00 PHO= 2.00
EQTG=M FD=M FDL=M VRV=M DRTP=1
DVFG= 2.75k

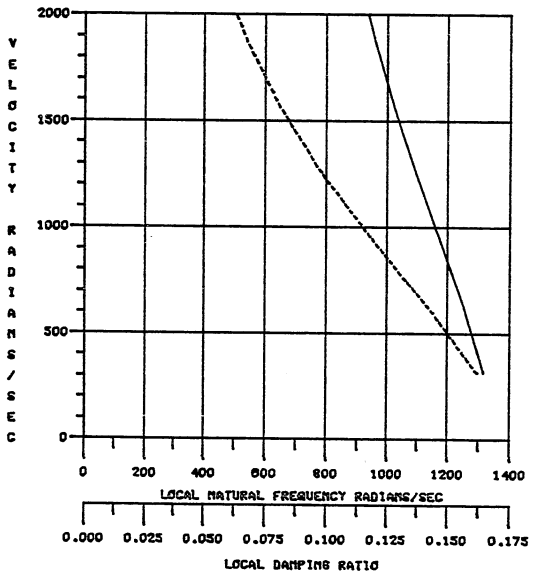

LOW SPEED NATURAL FREQUENCY AND DAMPING CURVES

FIGURE V-44

equals 1316 radians per second and the damping ratio equals .1625. If Equation V-17 is evaluated with these values and a detent torque of 5.5 oz-in, the amplitude of the error and error velocity response can be obtained.

At a 50 Hz drive frequency:

W_n = 1316 radians/sec

ζ = .1625

Therefore:

Ψ = .2185 radians

$\dot{\Psi}$ = 287.5 radians/sec

Likewise at a 200 Hz drive frequency:

W_n = 1093 radians/sec

ζ = .098

Therefore:

Ψ = .05 radians

$\dot{\Psi}$ = 65.8 radians/sec

These values correspond well with the amplitudes obtained from the limit cycles in Figures V-41 and V-43.

In addition to the detent torque, other inputs like impulses and steps behave according to linear system theory as long as they cause only "small" disturbances about the stable equilibrium point.

Multiple Drive Frequencies

All the dynamic characteristics discussed up to this point have involved a motor that is being driven at a single drive frequency. In many applications it may be necessary to operate a motor at more than one drive frequency. This method of operation can also be shown in the error plane. Figure V-45 shows the error plane of a motor that starts from rest with a drive frequency of 100 Hz. The motor's initial condition is Ψ = 0.0 rad and $\dot{\Psi}$ = -628.3 rad/sec. The motor goes through a transient and settles in on the stable equilibrium point located at Ψ =.64 rad and $\dot{\Psi}$ = 0. rad/sec. This response is similar to several that were shown earlier.

After .05 seconds the drive frequency is increased to 150 Hz. This appears as an instantaneous shift in the velocity error equal to minus the change in the drive frequency. See Figure V-45. The motor goes through a second transient and converges on the stable equilibrium point at a new location. The location of the stable equilibrium point changes because an entirely new error plane is obtained when the drive frequency is increased.

The drive frequency is increased to 200 Hz after an additional .05 seconds and the motor goes through a third dynamic transient converging toward a third equilibrium point. In this manner it is possible to use the error plane

JM= 3.25m TF= 1.01 ST= 0.00 B= 11.80m KT= 78.00
DTR= 0.00 DTRM= 4.00 KB= 448.60m VR= 5.40 IR= 1.50
RM= 3.60 LM= 20.00mPHZE= 4.00 STPR= 200.00

VS= 35.40 RS= 20.00 RF= 0.00 STS= 1.00 PHO= 2.00
EQTG=N FD=N FDL=N VRW=N DRTP=1
DVFG= 200.00

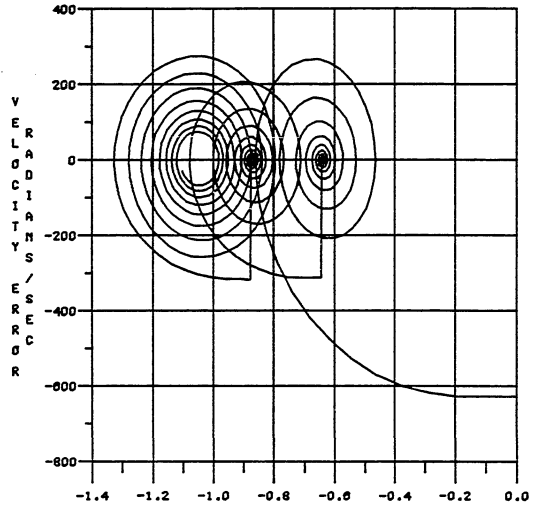

A MULTIPLE DRIVE FREQUENCY ERROR PLANE

FIGURE V-45

to demonstrate the dynamic characteristics of a motor being driven at several different frequencies.

Conclusion

The phase error plane can be used to represent the dynamic behavior of the synchronous motor in much the same manner as it was used with the stepping motor. While an understanding of the stepping motor phase error plane helps, it is by no means necessary to the understanding of the synchronous phase error plane. The synchronous phase error plane can be used to investigate many of the problems encountered by the user of the synchronous motor, as well as aid greatly in design applications.

In general the phase plane's strength lies in it ability to display a great deal of information in a compact yet informative manner.

CHAPTER VI

MID-FREQUENCY RESONANCE

Introduction

As the requirements of stepping motor applications have become more demanding, the application engineer has had to continually increase the level of performance of stepping motor and drive. One of the limitations often encountered is the phenomenon in which a motor behaves as though it is dynamically unstable. This is characterized by position and velocity oscillations that grow rather than decay, usually growing until they are large enough to cause the motor to lose synchronism with the drive commands. This phenomenon usually occurs at a drive frequency of about half the motor's maximum speed and is called mid-frequency resonance (MFR).

The drive frequency at which MFR occurs strongly depends upon the entire motor load and drive configuration. Changes in any of the system parameters, including inertia, damping, supply voltage and the drive configuration (constant voltage, constant current, number of phases energized, step size) will affect the frequency at which MFR occurs. It is possible to vary some of these parameters to "move" MFR to a different frequency so that it does not

interfere with a particular applications operation. Traditionally, it has been the drive that is most easily modified to vary the location of the MFR.

Mid-Frequency Resonance

Figure VI-1 shows the velocity profile of a stepping motor being ramped in quantized increments. The motor is started at 1000 steps/sec, and every 50 msec the drive frequency is increased by 400 steps/sec. Each time the drive frequency is incremented, the motor goes through an oscillatory transient. The oscillations damp out and the motor eventually settles in and runs at the drive frequency. As the drive frequency is increased, the period of the oscillation increases, and the rate at which the oscillation decays decreases. These effects are entirely consistent with the results shown in Chapter V, in which the small signal natural frequency and damping ratio were shown to be dependent upon the drive frequency.

The most interesting portion of Figure VI-1 is the point at which the drive frequency is increased past 3000 steps/sec. At this drive frequency the motor still goes through a transient when the drive frequency is changed. However, the oscillations no longer decay toward a steady state velocity. Instead, the velocity oscillations grow in amplitude. Even though the oscillations grow, the motor is still able to follow the step commands. And when the drive

Jm=	3.25m	To=	610.00m	Th=	1.00	St	0.00	Bv=	8.26m	Be=	5.00m
Kt	76.00	Dt=	4.00	Dm=	4.00	Kb=	448.00m	Vr=	5.40	Ir=	1.50
Rm=	3.60	Lm=	20.00m	PZ=	4.00	SR=	200.00	a2=	0.00	a1=	1.00
DT=U		Vs=	35.40	Re=	20.00	Rf=	0.00	SS=	1.00	PD=	2.00
ET=N		Fd=N		Fl=N		WR=N		DO=1			

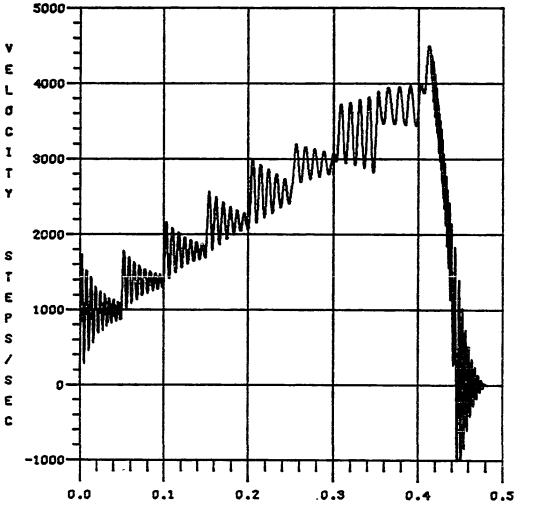

MID-FREQUENCY RESONANCE IN THE UNIPOLAR DRIVE SYSTEM

FIGURE VI-1

frequency is increased further, the motor runs at the increased speed. When the drive frequency exceeds 4000 steps/sec, the step commands are halted and the motor coasts to rest.

In Figure VI-2 the drive frequency is not increased once 3200 steps/sec is reached. Instead the motor is allowed to continue to run at that frequency. This plot shows that the oscillations increase until the amplitude reaches +/- 650 steps/sec. At this point the motor appears to have fallen out of synchronism with the input commands. This means that the rotor, because of the large oscillations, can no longer follow the flux vector as it moves from one step position to the next. Once the motor loses synchronism it coasts to zero velocity as the flux vector continues to rotate. The rotor has a small velocity oscillation about zero as it tries to respond to the flux vector that is still rotating. The final oscillation at the end of the sequence is the rotor moving to the final position of the flux vector after the step commands have stopped.

Figure VI-2 demonstrates the failure mode of MFR. The drive frequency is increased to some speed and the motor is expected to operate at that constant velocity for some period of time. Instead the oscillations grow and the motor eventually falls out of synch with the input commands, causing failure of the mechanism.

Jm=	3.25mTc=	610.00mTh=	1.00	St	0.00	Bv=	6.28mBe=	5.00m
Kt	78.00	Dt=	4.00	Dm=	4.00	Kb=	446.00mVr=	5.40	Ir=	1.50
Ra=	3.80	La=	20.00mPZ=	4.00	SR=	200.00	s2=	0.00	a1=	1.00
DT=U		Va=	35.40	Re=	20.00	Rf=	0.00	SS=	1.00	PO=	2.00
ET=N		Fd=N		Fl=N		WR=N		DO=1			

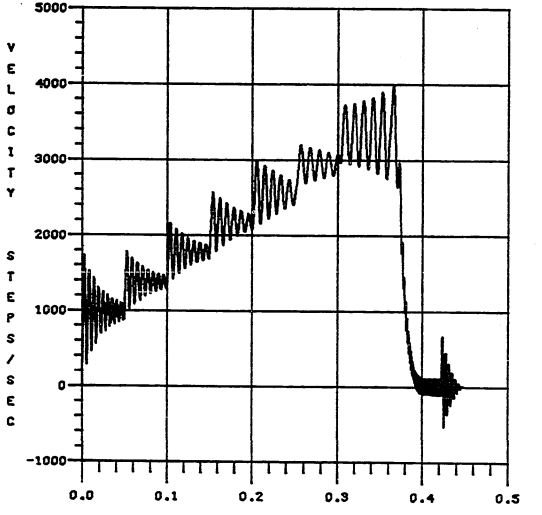

MID-FREQUENCY RESONANCE FAILURE

FIGURE VI-2

It should be noted that this simulation was run several times to determine that MFR just begins to develop at 3100 steps/sec. The experimental system used to verify the model in Chapter III begins to exhibit MFR characteristics at 3150 steps/sec. The difference between the onset of MFR in the model and this experimental system is less than two percent, indicating that the model can be used for accurate prediction of MFR in most applications.

An important point to recognize is that MFR failure occurs when the drive freqency remains constant for a period of time, thus allowing the amplitude of the oscillations to grow. It is possible to operate in regions of MFR for short periods of time, as well as to accelerate into and out of the MFR regions during sequences, without failure. This allows applications to be designed in which the motor can run into and through regions of instability without significant problems, as long as the drive frequency does not remain constant long enough to allow the oscillation amplitude to grow sufficiently to cause failure.

Comparison of Unipolar and Bipolar Drive Methods

It was mentioned earlier that the type of drive affects the drive frequency at which the MFR occurs. Figure VI-2 shows that with a unipolar, full step, two phase on L/R drive, MFR was a definite problem at 3200 step/sec. If all

the system parameters remain the same except the drive is changed to a bipolar drive, the velocity profile shown in Figure VI-3 is obtained. MFR now occurs at a drive frequency of 1200 steps/sec, significantly lower than the unipolar drive's frequency of 3200 step/sec.

This bipolar drive is not the most efficient one. With two phases energized the unipolar drive uses only half the stator winding copper at any one time. For consistency, the bipolar drive was configured so that it would use only half the copper also. It is possible to rewind the motor winding so that the voltage, resistance, current and power ratings remain the same. However, the bipolar drive then utilizes all the motor copper. This results in the bipolar drive-motor developing 1.414 times the ampere turns that the unipolar motor develops. The actual increase in torque developed by the motor will be less than 1.414 times greater due to magnetic saturation.

If this new bipolar drive-motor configuration is ramped up to the point at which MFR begins, Figure VI-4 is obtained. This figure shows that the MFR region starts at less than 1000 step/sec. This is an even lower drive frequency than predicted by the bipolar drive, using only half the copper. Initially, the results are opposite to what would be expected. The bipolar drive is usually considered to be the more efficient and higher performance drive of the two types. However, when MFR is considered, it appears that

Ja=	3.25m	To=	610.00m	Th=	1.00	St	0.00	Sv=	6.28m
Se=	5.00m	Kt	76.00	Dt=	4.00	Da=	4.00	Kb=	446.00m
Vr=	5.40	Ir=	1.50	Ra=	3.80	La=	20.00m	PZ=	2.00
SR=	200.00	a2=	0.00	a1=	1.00	DT=0		Ve=	35.40
Re=	20.00	Rf=	0.00	SS=	1.00	PD=	2.00	ET=M	
Fd=M		Fl=M		UR=M		DD=1			

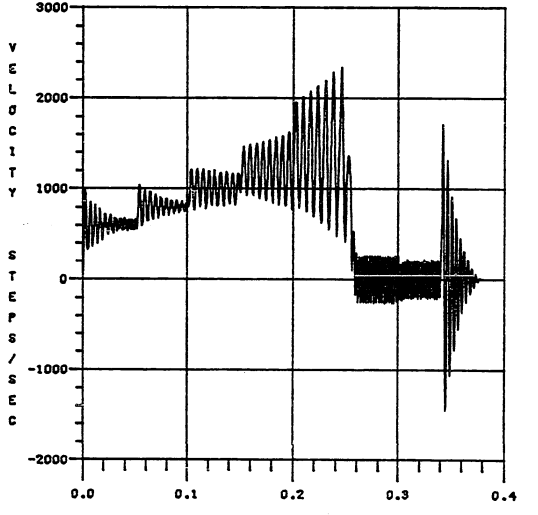

MID-FREQUENCY RESONANCE IN THE BIPOLAR DRIVE SYSTEM

FIGURE VI-3

Jm=	3.25mTo=	810.00mTh=	1.00	St	0.00	Bv=	6.26mBe=	5.00m
Kt	113.30 Dt=	4.00 Dm=	4.00	Kb=	651.00mVr=	5.40 Ir=	1.50
Rm=	3.60 Lm=	40.00mPZ=	2.00	SR=	200.00 a2=	0.00 a1=	1.00
DT=B	Ve=	35.40 Re=	20.00	Rf=	0.00 SS=	1.00 P0=	2.00
ET=N	Fd=N	Fl=N	WR=N	DO=1			

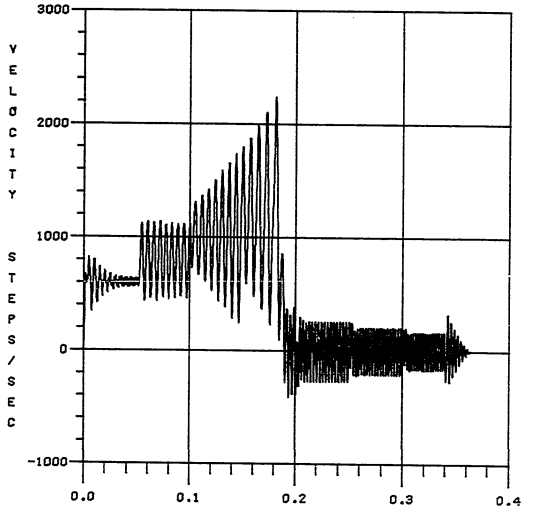

MID-FREQUENCY RESONANCE IN THE BIPOLAR DRIVE SYSTEM UTILIZING ALL THE COPPER

FIGURE VI-4

the unipolar drive operates in a stable mode over a much larger range of drive frequencies.

The reason for this vast difference in performance between the two drives can be explained when the current profiles for the drives are investigated. Figure VI-5 shows the current in each of the phases versus time for the unipolar drive. The corresponding plot for the bipolar drive is shown in Figure VI-6. Each time the bipolar drive is stepped, the current in the winding switches and it has an initial condition which is the negative of its final value. This means that a portion of the winding "on" time is spent trying to reverse the direction of the current flow before it can flow in the desired direction. This results in an overall decrease in the average current available to accelerate the motor over one step period.

The second bipolar configuration, because all its copper is utilized, has an inductive time constant twice that of the first, in which only half the copper is used. This increase causes it to take longer to reverse the direction of the current flow and, as a result, the average value of the current is even smaller.

The unipolar drive in Figure VI-5, does not have this problem because when a phase is energized, its initial condition is zero current. Therefore, the current is flowing in the proper direction for the entire phase on time and

Jm=	3.25mTo=	810.00mTh=	1.00	St	0.00	Bv=	6.26mBe=	5.00m	
Kt	76.00	Dt=	4.00	Dm=	4.00	Kb=	448.00mVr=	5.40	Ir= 1.50
Rm=	3.60	Lm=	20.00mPZ=	4.00	SR=	200.00	m2=	0.00	m1= 1.00
DT=U		Vs=	35.40	Re=	20.00	Rf=	0.00	SS=	1.00 PO= 2.00
ET=N		Fd=N		F1=N		WR=N		DO=1	

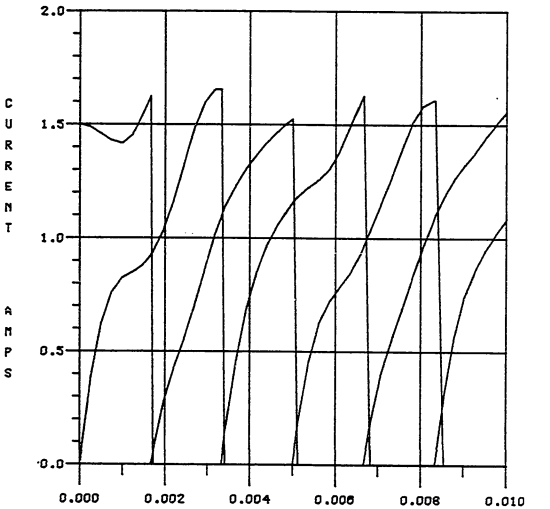

UNIPOLAR CURRENT PROFILE

FIGURE VI-5

Jm=	3.25mTo=	810.00mTh=	1.00 St	0.00 Bv=	6.28mBe=	5.00m
Kt	78.00 Dt=	4.00 Dm=	4.00 Kb=	448.00mVr=	5.40 Ir=	1.50
Rm=	3.60 Lm=	20.00mPZ=	2.00 SR=	200.00 a2=	0.00 a1=	1.00
DT=B	Ve=	35.40 Re=	20.00 Rf=	0.00 SS=	1.00 PO=	2.00
ET=M	Fd=M	Fl=M	WR=M	DO=1		

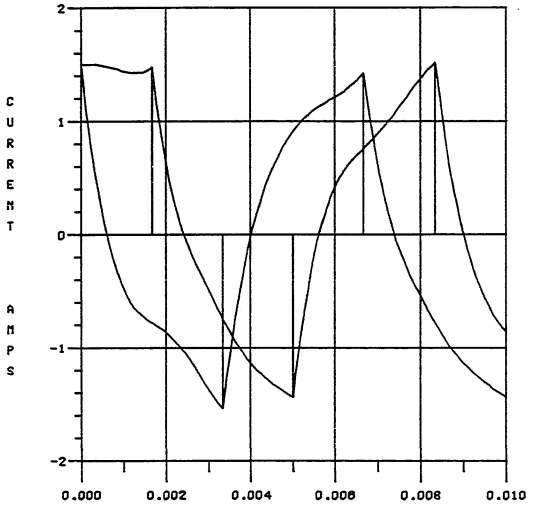

BIPOLAR CURRENT PROFILE

FIGURE VI-6

results in a higher average current. This assumes that the current in the phase just deenergized decays rapidly when compared to the inductive current rise time of the winding just energized.

The actual rate of current decay in the deenergized phase depends greatly on the type of diode suppression used in the drives. Different types of suppression cause the current decay time to vary. As the current decay time of the unipolar drive becomes larger, the differences between the unipolar and bipolar drive MFR characteristics become less noticeable.

The Synchronous Drive and Mid-Frequency Resonance

In Chapter V, the concept of, and the dynamic characteristics associated with, driving the hybrid motor as a synchronous device were discussed. While MFR is usually discussed in stepping motor applications where the motor is being stepped, MFR also occurs in synchronous applications.

In Figure VI-7, the velocity transient of a hybrid motor being driven synchronously is shown. The motor is started at a drive frequency of 150 Hz and every 200 msec the frequency is increased by 75 Hz. As with the velocity transients of the motor being stepped, each time the drive frequency is incremented, the motor goes through an oscillatory transient. The oscillations damp out and the

JM= 3.25m TF= 1.61 ST= 0.00 B= 11.80m KT= 78.00
DTR= 0.00 DTRM= 4.00 KB= 448.80m VR= 5.40 IR= 1.50
RM= 3.60 LM= 20.00mPHZE= 4.00 STPR= 200.00

VS= 35.40 RS= 20.00 RF= 0.00 STS= 1.00 PHO= 2.00
EQTQ=N FD=N FDL=N WRW=N DRTP=1
DVFQ= 300.00

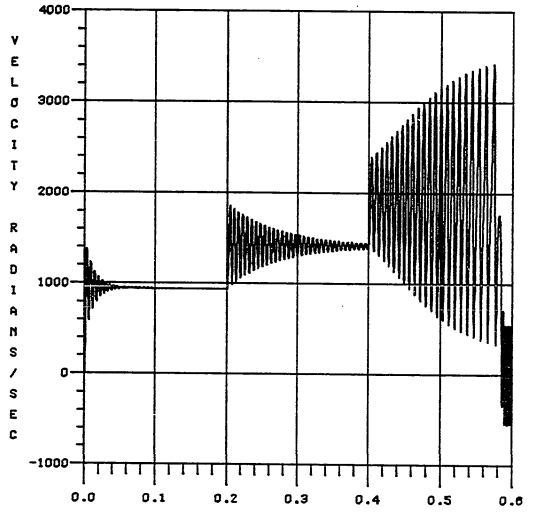

MID-FREQUENCY RESONANCE IN THE SYNCHRONOUS DRIVE SYSTEM

FIGURE VI-7

motor runs at the drive frequency.

Once the drive frequency is increased to 300 Hz, the oscillations no longer decay; rather they begin to grow in amplitude. Once the amplitude exceeds +/-1250 rad/sec, this motor also falls out of synchronism with the rotating flux vector. It should be noted that the motor loses synchronism at a drive frequency of 300 Hz. This equals a drive frequency of 1200 steps/sec, the same frequency at which the bipolar stepping drive becomes unstable. This is expected because driving a hybrid motor synchronously and a two phase on bipolar drive are very similar. This is because the synchronous drive wave form has the same waveform as the fundamental of the two phase on, bipolar square wave drive.

If the error plane of the synchronously driven motor is shown, the first of several interesting phenomena can been seen. See Figure VI-8. The motor starts at rest with a drive frequency of 150 Hz. It goes through a transient and pulls into synchronism with the rotating flux vector at a power angle of Ψ=-.85. This is identical to the response shown in Figure V-1a. When the drive frequency is increased 75 Hz, from 150 to 225 Hz, the motor goes through a second transient. The change in the drive frequency is seen as an instantaneous shift in the velocity error equal to the increase in the drive frequency. The motor then goes through a second transient and eventually pulls into synchronism at a new power angle of Ψ=-1.15.

JM= 3.25m TF= 1.81 ST= 0.00 B= 11.60m KT= 78.00
DTR= 0.00 DTRM= 4.00 KB= 448.80m VP= 5.40 IR= 1.50
RM= 3.60 LM= 20.00mPHZE= 4.00 STPR= 200.00

VS= 35.40 RS= 20.00 RF= 0.00 STS= 1.00 PHO= 2.00
EQTQ=N FD=N FDL=N WRV=N DRTP=1
DVFQ= 300.00

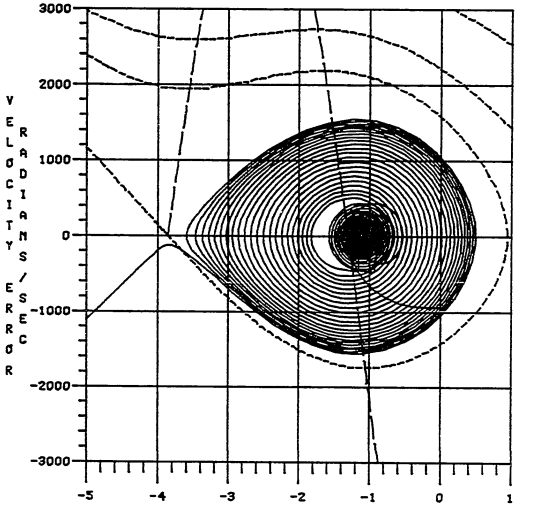

MID-FREQUENCY RESONANCE FAILURE IN THE SYNCHRONOUS ERROR PLANE

FIGURE VI-8

Each drive frequency that the motor operates at has a different error plane. This means that the trajectories, separatrix and zero slope isocline will be different for each drive frequency. The trajectories for the different drive frequencies are shown. However, the separatrix and zero slope isocline shown are for the final drive frequency at which the system is operated.

When the drive frequency is increased a second time, to 300 Hz, the motor goes through a third transient. However, this transient does not decay, hence the motor does not pull into synchronism with the flux vector. Instead the transient oscillations grow. The motor is still following the flux vector but oscillating about it as it does. This mode continues until the oscillations grow large enough to cause the trajectory to cross a separatrix. The moment that the trajectory crosses the separatrix, the motor has failed. It no longer is following the flux vector and it will coast to rest while the flux vector continues to rotate.

This is the mechanism of MFR failure. The oscillations grow until they become large enough to cross a separatrix. At that point the motor no longer operates within the stable region about the zero position error, zero velocity error equilibrium point.

Synchronous Limit Cycles

It has just been shown that the oscillations of a motor going through a dynamic transient will decay or grow depending upon the drive frequency. This might lead to the conclusion that at a particular drive frequency, the oscillations will not decay or grow. Rather, a stable limit cycle exists in the error plane where the motor will continue to follow the flux vector but have position and velocity error oscillations of constant amplitude. This rationale can be extended to the concept that there may be several drive frequencies that each cause a limit cycle in the error plane. Each different drive frequency will have a limit cycle of a different amplitude.

Figure VI-9a shows the existence of just such a limit cycle in the synchronous error plane. Three different trajectories are shown, each having a different initial condition. The motor is being driven at 260 Hz in each case. The inner trajectory is started at an initial condition of Ψ=-1.235 and $\dot{\Psi}$=0. This trajectory goes through a transient where the oscillations slowly grow with time. An expanded view of this trajectory is shown in Figure VI-9b. The outer trajectory is started at an initial condition of Ψ=-3.0 and $\dot{\Psi}$=0. This trajectory goes through a transient where the oscillations decay with time.

These two trajectories indicate that somewhere between them there exists a trajectory that will neither

JM= 3.25m TF= 1.61 ST= 0.00 B= 11.80m KT= 78.00
DTR= 0.00 DTRM= 4.00 KB= 448.80m VR= 5.40 IR= 1.50
RM= 3.60 LM= 20.00mPHZE= 4.00 STPR= 200.00

VS= 35.40 RS= 20.00 RF= 0.00 STS= 1.00 PHO= 2.00
EQTQ=N FD=N FDL=N WRW=N DRTP=1
DVFQ= 260.00

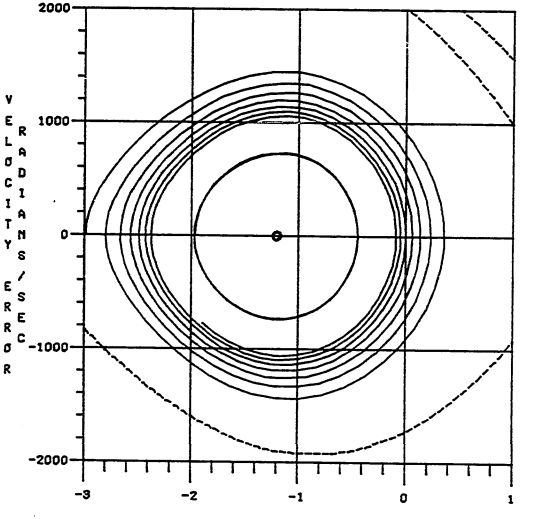

MID-FREQUENCY RESONANCE LIMIT CYCLING WITH
CONVERGING TRAJECTORIES IN THE SYNCHRONOUS ERROR PLANE

FIGURE VI-9a

JM= 3.25m TF= 1.61 ST= 0.00 B= 11.60m KT= 76.00
DTR= 0.00 DTRM= 4.00 KB= 448.60m VR= 5.40 IR= 1.50
RM= 3.60 LM= 20.00mPHZE= 4.00 STPR= 200.00

VS= 35.40 RS= 20.00 RF= 0.00 STS= 1.00 PHC= 2.00
EQTQ=N FD=N FDL=N WRW=N DRTP=1
DVFQ= 200.00

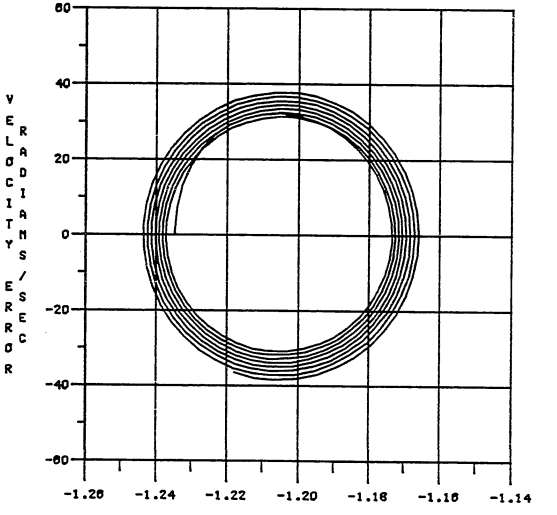

EXPANDED VIEW OF THE UNSTABLE TRAJECTORY

FIGURE VI-9b

grow nor decay. This trajectory continues to repeat over itself in the error plane, forming a limit cycle. A trial and error process of testing initial conditions between the initial conditions of the first two trajectories determined that a limit cycle does exist in the error plane. If a trajectory is started with the initial conditions ψ=-1.975 and $\dot{\psi}$=0, the amplitude of its oscillations neither grows nor decays. See Figure VI-9a. This limit cycle is stable because if the trajectory is disturbed a "small" distance off the limit cycle, either to the inside or the outside, the trajectory will return to the limit cycle.

If the phase currents are plotted one versus the other in the current plane while the motor is in the stable limit cycle, the currents no longer form the forced oscillation limit cycle that they did in Figure V-1b. See Figure VI-10. Rather the current trajectory appears to consist of sinusoidal terms.

In addition to finding the stable limit cycle, there are two other points of interest illustrated by Figure VI-9a. First, the second order model for the synchronous motor that was developed in Chapter V indicates that for every drive frequency there is a pair of equilibrium points. These points repeat every 2π in the error plane. One of the points is on the separatrix and therefore is a saddle point. The other point is the steady state operating point that the synchronous motor comes to after all dynamic transients have

JM= 3.25m TF= 1.61 ST= 0.00 B= 11.60m KT= 78.00
DTR= 0.00 DTRM= 4.00 KB= 448.80m VR= 5.40 IR= 1.50
RM= 3.60 LM= 20.00mPHZE= 4.00 STPR= 200.00

VS= 35.40 RS= 20.00 RF= 0.00 STS= 1.00 PHO= 2.00
EQTQ=N FD=N FDL=N WRW=N DRTP=1
DVFQ= 200.00

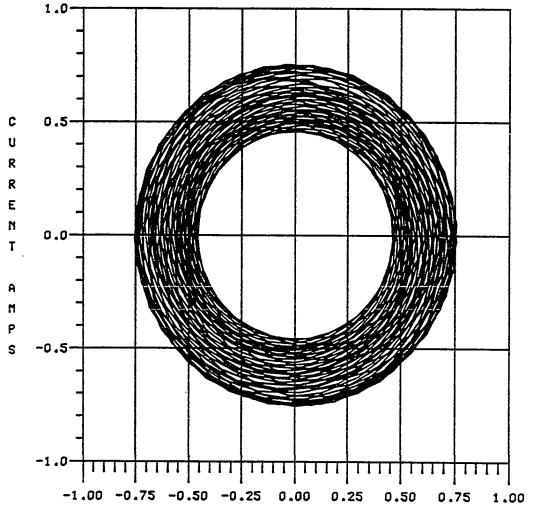

STABLE LIMIT CYCLE PHASE CURRENTS PLOTTED
IN THE CURRENT PLANE

FIGURE VI-10

died out. Because all the trajectories within a pair of separatrices converge upon this equilibrium point, it is considered stable. Obviously in Figure VI-9a, this stable equilibrium point does not exist if the trajectories are converging upon the limit cycle. Rather, the equilibrium points still exist, and the point on the separatrix is still a saddle point. However, the other point is no longer a stable equilibrium point. If it were possible to place a trajectory exactly on the equilibrium point it would remain there. If the slightest disturbance moved the trajectory off the equilibrium point it would then oscillate with increasing amplitude. Thus, by definition, the equilibrium point is unstable.

The second point of interest is the frequency of the oscillations. In Chapter V the second order synchronous model was linearized about the stable equilibrium point and it was possible to calculate a local damping ratio and local natural frequency. At a drive frequency of 260 Hz the local natural frequency is 1000 rad/sec. By looking at the velocity transients of each of the trajectories in Figure VI-9a, it is possible to measure their frequency of oscillation.

For: The linearized equilibrium point
the local W_n = 1000.0 rad/sec

The Ψ = 0.3 rad oscillation
the frequency of oscillation = 966.6 rad/sec

The Ψ = 0.8 rad oscillation
the frequency of oscillation = 942.5 rad/sec

The Ψ = 1.3 rad oscillation
the frequency of oscillation = 837.8 rad/sec

In a nonlinear system it is not unexpected that the frequency of the oscillations could depend upon the amplitude of the oscillation. And in this case the frequency of oscillation decreases as the amplitude of the oscillation increases. This must be kept in mind when trying to develop an analytical explanation for the limit cycle.

It was previously suggested that there may be more than one limit cycle. There may be several limit cycles, each one associated with a different drive frequency. Again using a trial and error process at different drive frequencies, it was determined that starting at a drive frequency of 247 Hz there exists a "family" of limit cycles. At 247 Hz a limit cycle is found with a position amplitude of .01 radians. As the drive frequency is increased, the amplitude of the limit cycle increases. This continues until a drive frequency of 294 Hz is reached. At this point the limit cycle just fits within the separatrix surface. A limit cycle of any larger amplitude can not fit within the separatrix and therefore can not exist.

Figure VI-11 shows the low frequency portion of the

synchronous motor zero work curve (ZWC). Plotted on the curve is the position error and velocity error amplitudes of three limit cycles. The horizontal line is the magnitude of the position error and the vertical line is the magnitude of the velocity error.

An Analytical Limit Cycle Model

In all the above analysis, higher order models were used to demonstrate the existence of MFR, whether the hybrid motor was being stepped or driven synchronously. If the inductance is ignored, resulting in a second order stepping motor model, the model does not predict the existence of MFR. In Chapter V a second order model was developed for the synchronously driven motor. In this model inductance was not ignored. However, it was assumed that the phase currents were sinusoidal and cosinusoidal. This model also does not predict the existence of MFR. Figure VI-12 shows an error plane trajectory for the second order synchronous model with an initial condition of ψ=-1.975 and $\dot{\psi}$=0.0. This is the initial condition of the limit cycle shown in Figure VI-9a. In Figure VI-12 there is no indication that a limit cycle exists. Rather, the trajectory converges to a stable equilibrium point. If other initial conditions are tried at other drive frequencies, there is still no indication of stable limit cycles.

The inability to find a stable limit cycle using the

JM= 3.25m TF= 1.61 ST= 0.00 B= 11.60m KT= 76.00
DTR= 0.00 DTRM= 4.00 KB= 448.60m VR= 5.40 IR= 1.50
RM= 3.60 LM= 20.00mPHZE= 4.00 STPR= 200.00

VS= 35.40 RS= 20.00 RF= 0.00 STS= 1.00 PHO= 2.00
EQTQ=N FD=N FDL=N WRW=N DRTP=1
DVFQ= 2.73k

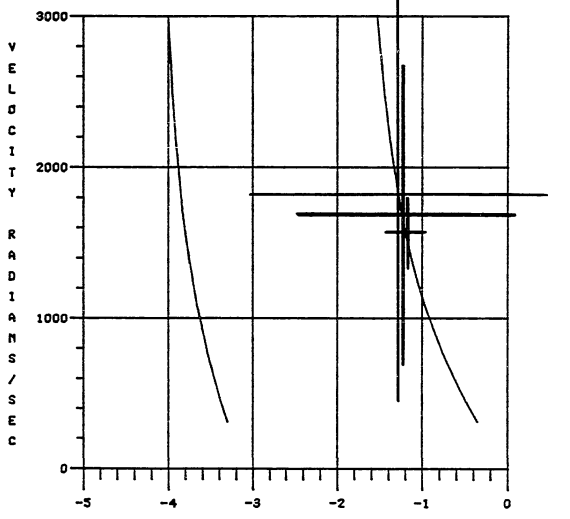

LIMIT CYCLE AMPLITUDES VERSUS DRIVE FREQUENCY

FIGURE VI-11

JM= 9.25m TF= 1.61 ST= 0.00 B= 11.80m KT= 76.00
DTR= 0.00 DTRM= 4.00 KB= 448.80m VR= 5.40 IR= 1.50
RM= 3.60 LM= 20.00mPHZE= 4.00 STPR= 200.00

VS= 35.40 RS= 20.00 RF= 0.00 STS= 1.00 PHO= 2.00
EQTQ=M FD=M FDL=M WRW=M DRTP=1
DVFQ= 260.00

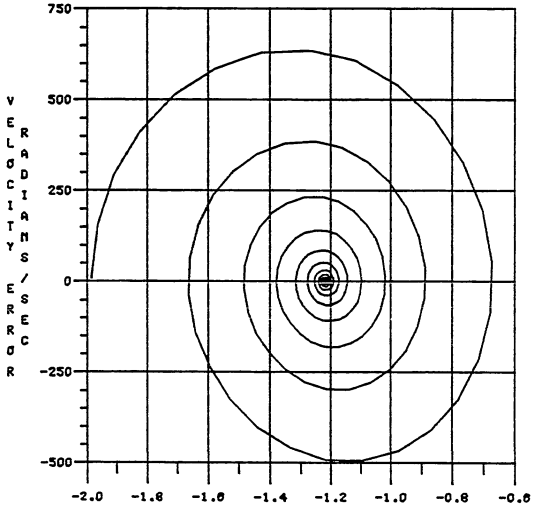

A STABLE, SECOND ORDER SYNCHRONOUS MODEL TRAJECTORY
AT A RESONANCE DRIVE FREQUENCY

FIGURE VI-12

second order synchronous model is not entirely unexpected. When the model was developed and the currents were assumed to be sinusoidal and cosinusoidal, it was also assumed that the current plane trajectory would always be similar to the one shown in Figure V-1b. Therefore no attempt was made to account for the additional current components shown in Figure VI-10.

In an attempt to simulate the limit cycle phenomenon in the second order synchronous model, an external disturbance was input to the system. This external disturbance took the form of a cosinusoidal torque input at a frequency of 942.5 rad/sec. This frequency corresponds to the frequency of the limit cycle in Figure VI-9a. The system is driven at the same 260 Hz drive frequency. Now the second order system no longer converges upon the stable equilibrium point. Rather it settles into a forced oscillation in the error plane. The amplitude of the forced oscillation depends upon the amplitude of the disturbance torque. If the disturbance torque amplitude is increased to 7.75 oz-in, the forced oscillation is almost identical to the limit cycle shown in Figure VI-9a. See Figure VI-13.

It should be noted that the initial condition selected for the forced oscillation case is critical. Unlike the limit cycle where any trajectory with an initial condition on the limit cycle will remain on the limit cycle, there is a critical phase angle between the input

JM= 3.25m TF= 1.61 ST= 0.00 B= 11.80m KT= 76.00
DTR= 0.00 DTRM= 4.00 KB= 446.80m VR= 5.40 IR= 1.50
RM= 3.60 LM= 20.00mPHZE= 4.00 STPR= 200.00

VS= 35.40 RS= 20.00 RF= 0.00 STS= 1.00 PHO= 2.00
EQTQ=N FD=N FDL=N WRW=N DRTP=1
DVFQ= 280.00

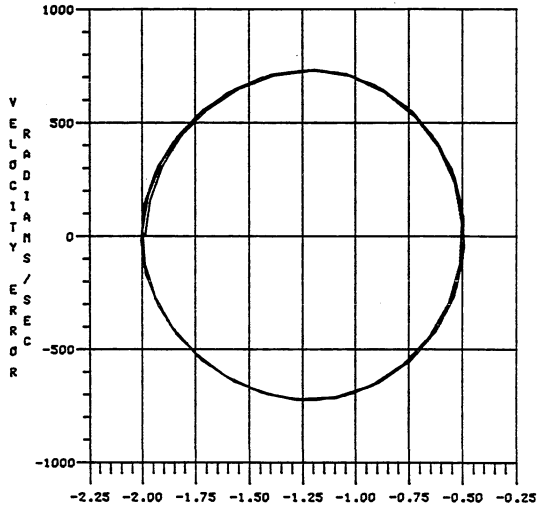

A SECOND ORDER SYNCHRONOUS MODEL TRAJECTORY LIMIT CYCLING DUE TO AN EXTERNAL DISTURBANCE

FIGURE VI-13

disturbance torque and the position or velocity error oscillations. Because the input disturbance is at the natural frequency of the system, there is a ~/2 radian phase shift between the input torque and the position error oscillation. Therefore, any other initial condition for the trajectory, besides the one selected, would have to go through a transient before settling in on the force oscillation.

The similarity between the true limit cycle in the higher order models and the forced oscillation in the second order synchronous model indicates that there might be some mechanism in the higher order model that generates a disturbance torque very similar to the external disturbance that was input to the second order model. In order to investigate this possibility, return to the synchronous motor electrical equations and the torque portion of the mechanical equation. See Equations VI-1a and 1b and VI-2.

$$V_s \text{CosA}\dot{\theta}_s t = I_1(R_s + R_m) + L_{ms}\frac{dI_1}{dt} - K_{bs}\dot{\theta}\ \text{SinA}\theta \quad \text{(VI-1a)}$$

$$V_s \text{SinA}\dot{\theta}_s t = I_2(R_s + R_m) + L_{ms}\frac{dI_2}{dt} + K_{bs}\dot{\theta}\ \text{CosA}\theta \quad \text{(VI-1a)}$$

$$T(\theta) = K_t S_f(I_1 \text{Sin A}\theta - I_2 \text{Cos A}\theta) \quad \text{(VI-2)}$$

When the system is in a limit cycle, it is possible to make the following substitutions for rotor angle θ and

velocity $\dot{\theta}$:

$$\theta = \dot{\theta}_s t + \frac{\dot{\theta}_1}{W_1} \text{Sin } W_1 t + \psi \qquad \text{(VI-3)}$$

$$\dot{\theta} = \dot{\theta}_s + \dot{\theta}_1 \text{Cos } W_1 t \qquad \text{(VI-4)}$$

Where: $\dot{\theta}_1$ = Limit cycle velocity ripple

W_1 = Limit cycle oscillation frequency

This assumes that the limit cycle is sinusoidal. Substituting for θ and $\dot{\theta}$ in Equations VI-1a and 1b yields:

$$V_s \text{Cos } A\dot{\theta}_s t + K_{bs}(\dot{\theta}_s + \dot{\theta}_1 \text{Cos } W_1 t) \text{ Sin } A(\dot{\theta}_s t + \frac{\dot{\theta}_1}{W_1} \text{Sin } W_1 t + \psi)$$

$$= I_1(R_s + R_m) + L_{ms} \frac{dI_1}{dt} \qquad \text{(VI-5a)}$$

$$V_s \text{Sin } A\dot{\theta}_s t - K_{bs}(\dot{\theta}_s + \dot{\theta}_1 \text{Sin } W_1 t) \text{ Cos } A(\dot{\theta}_s t + \frac{\dot{\theta}_1}{W_1} \text{Sin } W_1 t + \psi)$$

$$= I_2(R_s + R_m) + L_{ms} \frac{dI_2}{dt} \qquad \text{(VI-5b)}$$

Along with the torque equation:

$$T(\Theta) = K_t S_f (I_1 \text{Sin } A \left(\dot{\Theta}_s t + \frac{\dot{\Theta}_1}{W_1} \text{ Sin } W_1 t + \Psi \right) \quad \text{(VI-6)}$$

$$- I_2 \text{Cos } A \left(\dot{\Theta}_s t + \frac{\dot{\Theta}_1}{W_1} \text{ Sin } W_1 t + \Psi \right))$$

Inspection of Equations VI-5a and 5b and VI-6 yields a very interesting insight to possible causes of MFR. The first term of Equations VI-5a and VI-5b, the supply voltage, results in a sinusoidal voltage at the drive frequency. This is the normal excitation voltage that has always been assumed to exist. Table VI-1 lists the amplitude and frequency of the two phase drive voltages. Knowing the phase resistance and inductance, it is possible to calculate the phase current and phase shift between the voltage and the current. The letters 's' and 'c' preceeding the frequency term in the table are used to indicate whether the frequency terms are sinusoidal (s) or cosinusoidal (c). The first character applies to phase one and the second to phase two.

In Equation VI-5a the second term, the back EMF voltage, is more complex. The first portion of the back EMF term, the velocity term, consists of a constant velocity and a velocity ripple. The second portion of the back EMF term, the position term, consists of a sine of a sinusoid. In order to simplify understanding the significance of the different components of the back EMF terms, it is beneficial to look at the velocity ripple and position ripple effects

The Limit Cycle Parameters

Drive Frequency = 1634. rad/sec
Local (nl & l) Natural Frequency = 943. , 943. rad/sec
Local Damping Ratio = 0.0750
Limit Cycle Position Amplitude = 0.77 rad
Limit Cycle Velocity Amplitude = 730. rad/sec
Limit Cycle Equilibrium Point = -1.22 radians

The AC Drive Terms

Voltage	Frequency	Current	Phase
35.400	(c/s) 1633.600	0.878	-0.945

TABLE VI-1 SYNCHRONOUS DRIVE TERMS

separately before combining them. In Equation VI-7a the position ripple portion of Equation VI-5a has temporarily been set equal to zero.

$$K_{bs}(\dot{\theta}_s + \dot{\theta}_1 \text{Cos } W_1 t)(\text{Sin } A(\dot{\theta}_s t)) \qquad \text{(VI-7a)}$$

This leaves the constant velocity and the velocity ripple multiplied by the sinusoid of the position. Equation VI-7a is in the standard form of amplitude modulation (AM). See Equation VI-7b.

$$(A + B \text{ Cos } Ct) * \text{Sin } Dt \qquad \text{(VI-7b)}$$

Amplitude modulation results in a spectrum that contains a carrier and one upper and lower sideband.[5],[6] Equation VI-8a shows the general form of the expression that describes amplitude modulation.

$$\text{AM term} \quad \text{Sin } Dt + \frac{1}{2}\left[\frac{B}{A}(-\text{Sin}(C-D)t + \text{Sin}(C+D)t)\right] \qquad \text{(VI-8a)}$$

Where: $\frac{B}{A}$ = Amplitude modulation index

If Equation VI-7a is written in a similar format, Equation VI-8b is obtained. Equation VI-8b describes the amplitude modulation that is occurring in the back EMF portion of Equation VI-5a.

$$\text{Sin } \dot{\theta}_s t + \frac{1}{2} \frac{\dot{\theta}_1}{\dot{\theta}_s} (-\text{Sin}(\dot{\theta}_s - W_1)t + \text{Sin}(\dot{\theta}_s + W_1)t) \quad \text{(VI-8b)}$$

The actual amplitudes and frequencies of the modulation terms that occur due to the amplitude modulation can be calculated. Using the drive frequency, limit cycle amplitude and frequency of oscillation of the limit cycle shown in Figure VI-13 and listed in Table VI-1, it is possible to determine the actual AM spectrum that occurs in Equation VI-5a due to the limit cycle. Table VI-2a shows the magnitude and frequency term of the different components that make up the AM spectrum.

If the position ripple is returned to Equation VI-5a and the velocity ripple is temporarily set to zero, Equation VI-9a is obtained.

$$K_{bs}(\dot{\theta}_s) \text{ Sin } A(\dot{\theta}_s t + \frac{\dot{\theta}_1}{W_1} \text{ Sin } W_1 t + \psi) \quad \text{(VI-9a)}$$

Equation VI-9a contains the sine of a sinusoid. The sine of a sinusoid is one of the standard forms of frequency modulation (FM). See Equation VI-9b.

$$A \text{ Sin } (B + C \text{ Sin } Dt) \quad \text{(VI-9b)}$$

Frequency modulation results in a spectrum that contains a term at the fundamental plus a whole series of upper and lower sidebands.[5],[6] Equation VI-10a describes

The Velocity Ripple (AM) spectrum is:

Modulation Index =0.447

	Amplitude	Frequency
Fundamental:	(0) 1.0000	(c/c) 1633.6
Sidebands:	(-1) 0.2236	(c/c) 691.1
Sidebands:	(1) 0.2236	(c/c) 2576.1

TABLE VI-2a AMPLITUDE MODULATION TERMS

The Position Ripple (FM) spectrum is:

Modulation Index =0.775

	Amplitude	Frequency ($+\dot{\gamma}$)
Fundamental:	(0) 0.8554	(s/c) 1633.6
Sidebands:	(-1)-0.3591	(s/c) 691.1
Sidebands:	(1) 0.3591	(s/c) 2576.1
Sidebands:	(-2) 0.0714	(s/c) -251.4
Sidebands:	(2) 0.0714	(s/c) 3518.6
Sidebands:	(-3)-0.0093	(s/c)-1193.9
Sidebands:	(3) 0.0093	(s/c) 4461.1

TABLE VI-2b FREQUENCY MODULATION TERMS

the general form of frequency modulation spectra.

$$\text{FM Term} \quad A \sum_{n=-\infty}^{\infty} J_n \, C \, \text{Sin} \, (B - nD)t \qquad \text{(VI-10a)}$$

Where: J_n = Bessel function, term n

C = Frequency modulation index

If Equation VI-9a is written in a similar format, Equation VI-10b is obtained. Equation VI-10b describes the frequency modulation that occurs in Equation VI-5a.

$$\sum_{n=-\infty}^{\infty} J_n \, \frac{\dot{\theta}_1}{\bar{w}_1} \, \text{Sin} \, ((\dot{\theta}_s + nW_1)t + \Psi) \qquad \text{(VI-10b)}$$

$\frac{\dot{\theta}_1}{\bar{w}_1}$ = Frequency modulation index

The amplitudes of the different terms in the spectrum are calculated using the Bessel function. The actual amplitude depends upon the FM modulation index used in the Bessel function calculation.

Table VI-2b shows the resulting spectrum due to the frequency modulation calculation of the limit cycle shown in Figure VI-13.

Because the back EMF term in the winding equations

contains both amplitude and frequency modulation, the result is the product of the two modulations. The result of the combined modulation can be thought of as each term of the FM spectrum being amplitude modulated. The general form of the combined modulation is shown in Equation VI-11.[5],[6]

$$\sum_{n=-\infty}^{\infty} J_n \frac{\dot{\theta}_1}{W_1} \sin((\dot{\theta}_s + nW_1)t + \psi)$$

$$+ \frac{1}{2}\frac{\dot{\theta}_1}{\dot{\theta}_s} \sum_{n=-\infty}^{\infty} J_n \frac{\dot{\theta}_1}{W_1} \sin((\dot{\theta}_s + (n+1)W_1)t + \psi)$$

$$+ \frac{1}{2}\frac{\dot{\theta}_1}{\dot{\theta}_s} \sum_{n=-\infty}^{\infty} J_n \frac{\dot{\theta}_1}{W_1} \sin((\dot{\theta}_s + (n-1)W_1)t + \psi) \qquad \text{(VI-11)}$$

The total spectrum due to the limit cycle is shown in Table VI-3a. If the amplitudes in Table VI-3a are multiplied by $K_b \dot{\theta}_s$, the actual back EMF generated voltages are obtained. Knowing the back EMF voltage, frequency, phase inductance and resistance, it is also possible to calculate the back EMF generated currents and their respective phase angles. See Table VI-3b.

It can be seen that, rather than each phase generating a back EMF voltage at the drive frequency, back EMF voltages are generated at the drive frequency and at

The combined Back EMF (AM-FM) spectrum :

	Amplitude	Frequency (+ϕ)
Fundamental:	(0) 0.8554	(s/c) 1633.6
Sidebands:	(-1)-0.1519	(s/c) 691.1
Sidebands:	(1) 0.5663	(s/c) 2576.1
Sidebands:	(-2)-0.0110	(s/c) -251.4
Sidebands:	(2) 0.1538	(s/c) 3518.6
Sidebands:	(-3) 0.0068	(s/c)-1193.9
Sidebands:	(3) 0.0255	(s/c) 4461.1
Sidebands:	(-4)-0.0012	(s/c)-2136.4
Sidebands:	(4) 0.0030	(s/c) 5403.6

TABLE 3a THE COMBINED AM AND FM MODULATION TERMS

The combined Back EMF spectrum voltages and currents:

	Frequency	Voltage	Current	Phase (+ϕ)
Fundamental: (0)	(s/c) 1633.6	12.54	(+/-) 0.31	-0.945
Sidebands: (-1)	(s/c) 691.1	-2.23	(+/-)-0.08	-0.530
Sidebands: (1)	(s/c) 2576.1	8.30	(+/-) 0.15	-1.141
Sidebands: (-2)	(s/c) -251.4	-0.16	(+/-)-0.01	-0.210
Sidebands: (2)	(s/c) 3518.6	2.25	(+/-) 0.03	-1.247
Sidebands: (-3)	(s/c)-1193.9	0.10	(+/-) 0.00	-0.791
Sidebands: (3)	(s/c) 4461.1	0.37	(+/-) 0.00	-1.312
Sidebands: (-4)	(s/c)-2136.4	-0.02	(+/-) 0.00	-1.066
Sidebands: (4)	(s/c) 5403.6	0.04	(+/-) 0.00	-1.356

TABLE VI-3b THE COMBINED AM AND FM MODULATION VOLTAGES AND CURRENTS

each of the upper and lower sidebands. This results in each of the phase currents being made up of the sum of all the terms in Tables VI-1 and 3. Equation VI-12a shows the general form of the current in phase 1.

$$I_1 = I_{1ac} \cos(\dot{\theta}_s t + \Psi_{ac}) + \sum_{n=-\infty}^{\infty} I_{1n} \sin((\dot{\theta}_s + nW_1)t + \Psi_n + \Psi) \qquad \text{(VI-12a)}$$

And Equation VI-12b describes the current in phase 2.

$$I_2 = I_{2ac} \sin(\dot{\theta}_s t + \Psi_{ac}) + \sum_{n=-\infty}^{\infty} I_{2n} \cos((\dot{\theta}_s + nW_1)t + \Psi_n + \Psi) \qquad \text{(VI-12b)}$$

Where: I_{1ac} = Phase 1 component due to the AC drive

I_{2ac} = Phase 2 component due to the AC drive

Ψ_{ac} = The phase angle between the AC drive voltage and the current

I_{1n} = Phase 1, sideband n component due to the back EMF

I_{2n} = Phase 2, sideband n component due to the back EMF

Ψ_n = The phase angle between the back EMF voltage and the current

From Equations VI-12a and 12b it is seen that while the synchronous motor is operating in the stable limit cycle, the current in each of the phases consists of a sinusoidal term due to the AC drive and a series of sinusoidal terms at each of the modulation sideband frequencies. It should be noted that the AC drive term and the fundamental of the modulation terms occur at the same

frequency but at different phase angles. The sideband terms all occur at different frequencies and phase angles.

It is possible to verify the absolute magnitudes of these different terms. In Figure VI-10 the simulation phase currents corresponding to the stable limit cycle were plotted in the current plane. It was shown that they no longer form a forced oscillation limit cycle but rather a "donut" shaped envelope was obtained.

If each of the current and phase angle terms in Table VI-3b is summed for phases 1 and 2, it is possible to plot the resulting modulation analysis currents against one another in a format similar to that of Figure VI-10. See Figure VI-14. A comparison of Figures VI-14 and VI-10 indicates that there is an excellent correlation between the actual currents obtained from the simulation of the higher order model limit cycle, Figure VI-10, and the analytical sideband analysis, Figure VI-14.

It has just been shown that when the synchronously driven motor is in a stable limit cycle, the current in the stator phases is made up of a whole series of terms. In order to determine the torques that are generated by these different terms, it is necessary to return to Equation VI-6 and substitute I1 and I2 as defined by Equations VI-12a and 12b. See Equations VI-13, VI-14a and VI-14b.

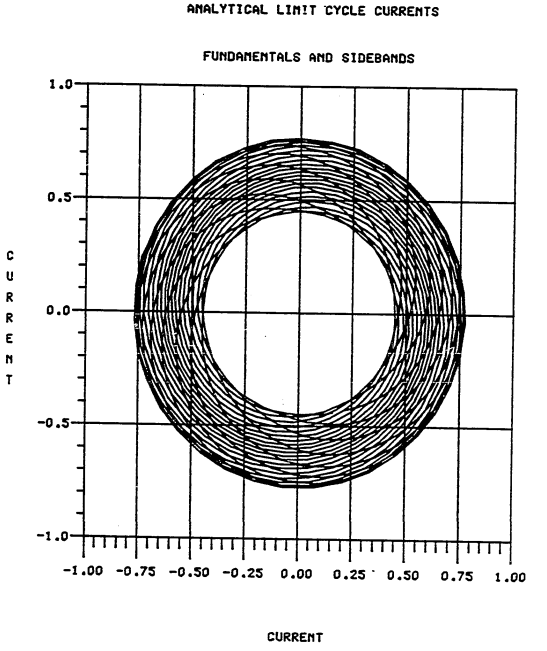

ANALYTICAL LIMIT CYCLE CURRENTS

FIGURE VI-14

$$T(\Theta) = K_t S_f (I_1 \sin A \left(\dot{\Theta}_s t + \frac{\dot{\Theta}_1}{W_1} \sin W_1 t + \Psi \right) \qquad \text{(VI-13)}$$

$$- I_2 \cos A \left(\dot{\Theta}_s t + \frac{\dot{\Theta}_1}{W_1} \sin W_1 t + \Psi \right))$$

Where:

$$I_1 = I_{1ac} \cos(\dot{\Theta}_s t + \Psi_{ac}) + \sum_{n=-\infty}^{\infty} I_{1n} \sin ((\dot{\Theta}_s + nW_1)t + \Psi_n + \Psi) \qquad \text{(VI-14a)}$$

$$I_2 = I_{2ac} \sin(\dot{\Theta}_s t + \Psi_{ac}) + \sum_{n=-\infty}^{\infty} I_{2n} \cos ((\dot{\Theta}_s + nW_1)t + \Psi_n + \Psi) \qquad \text{(VI-14b)}$$

Equation VI-13 contains the same form of frequency modulation in the position term as was present in Equations VI-5a and 5b. This results in both position terms in Equation VI-10 having spectra identical to the one in Table VI-2b.

When I1 and I2 are substituted into Equation VI-13 and all the current terms are multiplied by the position FM spectrum, the result is a whole series of sinusoids or cosinusoids multiplied by sinusoids or cosinusoids. Using trigometric identities, it is possible to reduce this to sinusoids or cosinusoids of the sums and differences of the angles.

These calculations can also be tabulated as the

modulation terms were. Table VI-4 shows the results of evaluating Equations VI-13, 11a and 11b. Table VI-4a contains the AC drive portions of Equations VI-14a and 14b multiplied by the FM position spectrum of Equation VI-13. The lefthand two columns contain the amplitude and frequency of the sum terms, while the middle two columns contain the amplitude and frequency of the difference terms. The righthand columns contain the phase angle associated with each difference term. This phase angle is due to the impedance of the windings and the location of the stable equilibrium point. Table VI-4b shows the corresponding back EMF current terms multiplied by the FM position spectrum, displayed in the same manner.

The result of evaluating Equations VI-13, VI-14a and VI-14b, Table VI-4, is a spectrum of torques that are generated in the motor due to the limit cycle oscillation. If the amplitude terms are multiplied by the torque constant, K_t, the torques will be in units of oz-in.

Investigation of the terms in Table VI-4 yields the cause of mid-frequency resonance. In both the AC drive and the back EMF terms, there are several components that occur at the limit cycle frequency, 942.5 radians/second. This limit cycle modulation analysis indicates that as a result of the modulation process in the torque equation, there are several torque terms that are generated at exactly the same frequency as the initial limit cycle that caused the

The AC Drive/Position Ripple Spectrum is:

Amplitude	Frequency	Amplitude	Frequency	Phase (-ϕ)
(AC Drv + Pos FM)		(AC Drv - Pos FM)		
0.3757	(s/-s) 3267.2	0.3757	(-s/-s) 0.0	-0.9452
-0.1577	(s/-s) 2324.7	-0.1577	(-s/-s) 942.5	-0.9452
0.1577	(s/-s) 4209.7	0.1577	(-s/-s) -942.5	-0.9452
0.0314	(s/-s) 1382.2	0.0314	(-s/-s) 1885.0	-0.9452
0.0314	(s/-s) 5152.2	0.0314	(-s/-s)-1885.0	-0.9452
-0.0041	(s/-s) 439.7	-0.0041	(-s/-s) 2827.5	-0.9452
0.0041	(s/-s) 6094.7	0.0041	(-s/-s)-2827.5	-0.9452

The Back EMF Current/Position Ripple Spectrum is:

Amplitude	Frequency	Amplitude	Frequency	Phase
(Back EMF + Pos FM)		(Back EMF - Pos FM)		
0.1331	(-c/c) 3267.2	0.1331	(c/c) 0.0	-0.9452
-0.0559	(-c/c) 2324.7	-0.0559	(c/c) 942.5	-0.9452
0.0559	(-c/c) 4209.7	0.0559	(c/c) -942.5	-0.9452
0.0111	(-c/c) 1382.2	0.0111	(c/c) 1885.0	-0.9452
0.0111	(-c/c) 5152.2	0.0111	(c/c)-1885.0	-0.9452
-0.0015	(-c/c) 439.7	-0.0015	(c/c) 2827.5	-0.9452
0.0015	(-c/c) 6094.7	0.0015	(c/c)-2827.5	-0.9452
-0.0348	(-c/c) 2324.7	-0.0348	(c/c) -942.5	-0.5298
0.0627	(-c/c) 4209.7	0.0627	(c/c) 942.5	-1.1413
0.0146	(-c/c) 1382.2	0.0146	(c/c) 0.0	-0.5298
-0.0146	(-c/c) 3267.2	-0.0146	(c/c)-1885.0	-0.5298
-0.0263	(-c/c) 3267.2	-0.0263	(c/c) 1885.0	-1.1413
0.0263	(-c/c) 5152.2	0.0263	(c/c) 0.0	-1.1413
-0.0029	(-c/c) 439.7	-0.0029	(c/c) 942.5	-0.5298
-0.0029	(-c/c) 4209.7	-0.0029	(c/c)-2827.5	-0.5298
0.0052	(-c/c) 2324.7	0.0052	(c/c) 2827.5	-1.1413
0.0052	(-c/c) 6094.7	0.0052	(c/c) -942.5	-1.1413
-0.0029	(-c/c) 1382.2	-0.0029	(c/c)-1885.0	-0.2099
0.0130	(-c/c) 5152.2	0.0130	(c/c) 1885.0	-1.2472
0.0012	(-c/c) 439.7	0.0012	(c/c) -942.5	-0.2099
-0.0012	(-c/c) 2324.7	-0.0012	(c/c)-2827.5	-0.2099
-0.0055	(-c/c) 4209.7	-0.0055	(c/c) 2827.5	-1.2472
0.0055	(-c/c) 6094.7	0.0055	(c/c) 942.5	-1.2472
0.0011	(-c/c) 3267.2	0.0011	(c/c) 3770.0	-1.2472
0.0011	(-c/c) 7037.2	0.0011	(c/c) 0.0	-1.2472
0.0013	(-c/c) 439.7	0.0013	(c/c)-2827.5	-0.7913
0.0017	(-c/c) 6094.7	0.0017	(c/c) 2827.5	-1.3122

TABLE VI-4 AC DRIVE AND BACK EMF MODULATED TORQUE SPECTRUM

modulation process.

If all the terms that occur at the limit cycle frequency are summed, a resulting amplitude and phase can be calculated. See Equation VI-15.

The Limit Cycle Torque Equals : 42.834 oz-in

(VI-15)

The Limit Cycle Phase Angle Equals : 0.053 radians

This indicates that if the motor is in a limit cycle it will produce a torque at the limit cycle frequency due to the sinusoidal modulation processes. If this generated torque is of the correct amplitude and phase it will maintain the limit cycle as a forced oscillation.

In order to determine if the limit cycle generated torque is of the proper magnitude, a simple forced oscillation analysis can be performed. By assuming that a torque consisting of a DC and an AC component at the limit cycle frequency is driving the mechanical portion of the system, Equation VI-16 is derived.

$$T_0 + T_1 \sin(W_o t + \Psi_o) = J_m \ddot{\theta} + B \dot{\theta} + T_f \frac{\dot{\theta}}{|\dot{\theta}|} \qquad \text{(VI-16)}$$

Assuming the system is in a forced oscillation:

$$\dot{\theta} = \dot{\theta}_d + \dot{\theta}_o \text{Cos } W_o t \qquad \text{(VI-17)}$$

$$\ddot{\theta} = - \dot{\theta}_o W_o \text{Sin } W_o t \qquad \text{(VI-18)}$$

Where: $\dot{\theta}_d$ = DC velocity

$\dot{\theta}_o$ = Forced oscillation velocity ripple

W_o = Forced oscillation frequency

Substituting Equations VI-17 and 18 into Equation VI-16 yields:

$$T_0 + T_1 \text{ Sin}(W_o t + \Psi_o) =$$

$$- J_m (\dot{\theta}_o W_o \text{Sin } W_o t) + B (\dot{\theta}_d + \dot{\theta}_o \text{Cos } W_o t) + T_f \frac{\dot{\theta}}{|\dot{\theta}|} \qquad \text{(VI-20)}$$

The constant terms of Equation VI-20 must be equal.

$$T_0 = B \dot{\theta}_d + T_f \frac{\dot{\theta}}{|\dot{\theta}|} \qquad \text{(VI-21)}$$

And the time dependent terms must also be equal.

$$T_1 \text{ Sin}(W_o t + \Psi_o) = - J_m(\dot{\theta}_o W_o \text{Sin } W_o t) + B (\dot{\theta}_o \text{Cos } W_o t) \qquad \text{(VI-22)}$$

The constant torque terms contribute the DC component of the motor velocity and are not of interest at this point. The time dependent or AC torque terms in

Equation VI-22 are the torques that generate the forced oscillation. The torque T_1 causes the system to have a forced velocity oscillation of amplitude $\dot{\theta}_o$ and a phase ψ_o.

By rearranging Equation VI-22, it is possible to solve for T_1 and ψ_o assuming a known forced oscillation velocity amplitude and frequency. See Equation VI-23.

$$T_1 = \sqrt{(J_m \dot{\theta}_o W_o)^2 + (B \dot{\theta}_o)^2} \qquad \text{(VI-23)}$$

And:

$$\psi_o = - \text{Tan}^{-1}\left(\frac{B}{J_m W_o} \right) \qquad \text{(VI-24)}$$

The torque and phase angle that can be determined from Equations VI-23 and VI-24 are the actual torque and phase margin necessary for the assumed known limit cycle to exist. If the actual system is driven by a torque larger than T_1, then the actual system will have a forced oscillation amplitude larger than the one assumed in the evaluation of Equation VI-23 and VI-24. Likewise, if the actual system is driven by a torque smaller than T_1, then the actual system will have a forced oscillation smaller than the one assumed.

Returning to Figure VI-9a and the sideband limit cycle analysis, it is possible to calculate a torque generated due to the modulation process. See Equation VI-15. If the same limit cycle amplitude and frequency are used in

Equations VI-23 and 24, it is possible to solve for the torque required to maintain a forced oscillation of the same amplitude. See Table VI-1 and Equation VI-25.

The Forced Oscillation Torque Equals : 44.762 oz-in

(VI-25)

The Forced Oscillation Phase Angle Equals : -0.024 radians

Comparing Equations VI-15 and VI-25 indicates that the torque produced as a result of the limit cycle modulation process in the electrical and mechanical equations closely matches the torque required to maintain the limit cycle as a forced oscillation. The amplitudes compare within 4.3 percent and the phase angles compare within 1.2 percent.

To further verify the process two other points can be considered. Assume that instead of the limit cycle shown in Figure VI-9a, a much smaller limit cycle exists at the same drive frequency. The sideband modulation analysis can be performed on this smaller limit cycle and the resulting torques can be determined. From Equations VI-23 and VI-24 it is possible to determine the torque and phase margin necessary for the smaller limit cycle to exist.

The process can be repeated for an assumed limit cycle larger than the actual limit. Table VI-5 contains a list of the torques that were calculated for the actual

The Assumed Limit Cycle Parameters

The drive frequency is 1634. rad/sec
The local damping ratio is 0.0750
The limit cycle equilibrium point is -1.22 radians

Assumed limit cycle	Actual limit cycle	Assumed limit cycle	
0.07	0.78	1.78	Oscillation amplitude (radians)
966.6	942.5	837.0	Oscillation frequency (rad/sec)
4.198	42.57	65.31	Sideband torque analysis (oz-in)
4.252	44.76	81.09	Forced oscillation analysis (oz-in)
98.7%	95.1%	80.5%	Ratio of torques
5.15%	5.15%	5.15%	Additional torque % due to other terms
103.6%	100.0%	84.9%	Final ratio of toques

TABLE VI-5 SIDEBAND AND FORCED OSCILLATION ANALYSIS
TORQUE ANALYSIS

limit cycles and the two assumed limit cycles. Because none of the sideband generated torques in Table VI-5 exceeds the torque necessary to maintain a corresponding limit cycle, it can assumed that the modulation process does not cause sufficient torque to be generated to explain the limit cycle phenomenon.

However, in the initial development of the sideband analysis it was assumed that the limit cycle was sinusoidal. This assumption was not strictly correct, as the limit cycle is not a pure sinusoid. The actual limit cycle varies from a pure sinusoid in amplitude by approximately five percent. To more accurately model the limit cycle it would be necessary to use a Fourier series. It can be shown that including the additional terms in the series results in additional torque components at the oscillation frequency. If it is assumed that the additional terms in the series would contribute approximataly 5.15 percent more torque to the sideband analysis, then there would be the torque necessary to maintain the known limit cycle. See Table VI-5.

In addition, the assumed limit cycle that is smaller than the actual limit cycle is now shown to generate more torque than necessary to maintain itself and therefore is not stable and will grow in amplitude. Likewise, the assumed limit cycle that was larger than the known limit cycle still does not generate sufficient torque to maintain itself and will still decay in amplitude.

Conclusion

This analysis indicates that MFR is due to the sideband modulation process that occurs within the stepping motor. As the motor undergoes a sinusoidal oscillation about the equilibrium point several phenomena occur.

First, amplitude and frequency modulation occur in the stator phases. The currents in the phases therefore consist of a series of terms. This series consists of a fundamental at the drive frequency and an infinite number of upper and lower sidebands.

And second, when this series of currents is evaluated in the torque equation, a second modulation process occurs and an infinite series of torque terms is obtained. One of the torque terms will always occur at the frequency of the initial oscillation.

This torque that is generated at the frequency of oscillation will cause one of three affects to occur in the system.

1) If the torque generated equals the torque required to maintain the forced oscillation at that amplitude and frequency, the oscillation will form a stable limit cycle.
2) If the torque generated due to the oscillation

exceeds the torque necessary to maintain a forced oscillation of that amplitude and frequency, the oscillation will be unstable. This oscillation will grow in amplitude until the conditions for a stable limit cycle are met or until the oscillations no longer fit within the separatrix and the motor loses synchronism.

3) Likewise, if the torque generated due to the oscillation is less than the torque necessary to maintain a forced oscillation of that amplitude and frequency, the oscillation will also be unstable. Now however, the oscillation will decay in amplitude until the conditions for a stable limit cycle are met or the oscillations converge upon the stable equilibrium point.

This is the basic phenomena of mid-frequency resonance. When the motor undergoes an oscillation, a torque is generated at the oscillation frequency. The magnitude of the generated torque determines whether the oscillation amplitude decays, remains the same or grows.

CHAPTER VII

SUMMARY AND FUTURE WORK

In Chapter II the effects of inductance in the stepping motor model were discussed. It was shown that these effects could be included in the model without altering the techniques for solving the equations or displaying the results. Motor performance was still discussed in terms of the phase plane or velocity-position error plane. However, the results of the simulation are a projection back into the phase plane from a higher order state space, rather than being totally contained within the phase plane. While the vast majority of the phenomona observed using the second order model remained basically the same, there were some new concepts and ideas that that one must keep in mind when interpreting the results of a higher order simulation.

Including the inductance and understanding its effect in the phase plane opens the stepping motor model up to being used in a much wider range of applications. In addition to including the inductance in the model, it was necessary to include other magnetic effects when the model was used to describe stepping motors such as the hybrid motor with its more efficient magnetic structures. In particular the magnetic saturation of the stator iron, as

well as hysteresis and eddy current losses in the stator, had to be included in the model. These additions to the model does not increase the dynamic complexity of the model as did the inductance. Rather they increase the algebraic complexity of the model. These additions to the model also made the representatin of the experimental measurement results more precise. It was not necessary to design new measurement systems to make the measurements, though additional characteristics had to be considered when conducting the test.

Having included inductance in the model as well as magnetic saturation, hysteresis and eddy current losses, it would now be beneficial to extend the model to describe the variable reluctance and canstack stepping motors. Models for both of these designs will be affected by these properties. The inductance and saturation will be of particular importance to the VR motor. Eddy currents will strongly influence the behavior of the canstack motor.

The dynamic performance of the hybrid motor was also investigated when it was being driven as a synchronous device. The same model was used, yet the results were displayed in a rather different format. In addition to displaying the results in terms of the position error, a velocity error was also developed. Like the stepping phase plane, the synchronous phase plane has the advantage of being a compact and extremely insightful way to look at the

motor's performance. The startup and failure mechanisms were only two of several dynamic characteristics that were investigated; however, they demonstrated that considerable insight into the performance of an AC synchronous device that can be gained from this form of representation.

The synchronous error plane investigation can be extended in several directions. The same basic model and techniques can be used with any permanent magnet AC device. The error plane should yield a method to determine how a synchronous motor might be ramped to frequencies above which it can start from a dead start. In addition it might be possible to devise a technique that would ramp the motor directly into the desired frequency and eliminate the oscillations normally associated with accelerating a synchronous device. It would also be possible to modify the AC drive model to include the resistor-capacitor network that is usually added to one of the phases so the motor can be run off a single AC source. This would not be necessary for a system that would be run off normal two and three phase electrical circuits.

In addition, because the synchronous drive is similar to the stepping drive at high step rates, the synchronous concepts could be used to investigate the high speed performance of stepping motors.

The concept of an error plane could also be extended

to a range of other nonlinear dynamic systems where the system is tracking some input.

Using the higher order model concepts and the synchronous error plane, the phenomenon of mid-frequency resonance was investigated. Mid-frequency resonance was shown to be caused by amplitude and frequency modulation in the stepping motor. The results developed could also be used to test the stability of the equilibrium point. If a small oscillation is assumed to exist about each equilibrium point, that oscillation could be tested for its stability. The stability of the small limit cycle would indicate the stability of the equilibrium point.

In addition, it should be possible to make a significant contribution to the design of stepping motor drives that attempt to eliminate or change the resonance characteristics. For the first time the cause and effect of mid-frequency resonance has been clearly explained.

REFERENCES

1. Gauthier, R.G., "Analysis and Simulation of Stepping Motor Systems using the Phase Plane Approach", Ph.D. Thesis, University of New Hampshire, 1979

2. Dietz, P.S., "Analysis, Simulation and Design of Stepping Motor Drive Systems", Masters Thesis, University of New Hampshire, 1981

3. Dahl, P.R., "Measurement of Solid Friction Parameters of Ball Bearings", Proceedings of the 6th Symposium on Incremental Motion Control Systems and Devices, May 1977

4. Gauthier, R.G., Harned, T.J. and Taft, C.K., "Stepping and Brushless Motor System Design and Analysis", Workshop Text, University of New Hampshire, 1985

5. Hund, A., "Frequency Modulation", McGraw Hill Book Co., 1942

6. Cuccia, B.L., "Harmonics, Sidebands and Transients in Communication Engineering", McGraw Hill Book Co, 1952

7. Pollack, S.H., "An Analysis and Prediction of the Mid-Frequency Resonance Phenomenon in Permanent Magnet Step Motors", Proceedings of the 8th Symposium on Incremental Motion Control Systems and Devices, 1979

8. Pickup, I.E.D. and Russell, A.P., "Parametric Instability in Stepping Motors, Part One: Fundemental Principles", Proceedings of the 8th Symposium on Incremental Motion Control Systems and Devices, 1979

APPENDIX A
TORQUE ANGLE CURVE MEASUREMENTS

Introduction

Measuring the torque angle curves of a small angle stepping motor is often a complex problem. All torque measurement systems are designed around a spring that deflects under an applied load. The amount the spring deflects depends on its spring constant. By measuring the amount of deflection and knowing the spring constant, the load or the torque can be calculated.

The measurement system must be designed so that the spring constant of the torque transducer is greater than the effective spring constant or stiffness of the stepping motor under test. However, the torque transducer can not be so stiff that resolution is lost and it becomes difficult to obtain an accurate measurement.

On first consideration this might not seem a difficult problem, as most stepping motors produce 200 ounce-inches of torque or less. There are several torque transducers available in this range. However, as stated earlier, it is necessary to also consider the stiffness of the device. Around the equilibrium points, a stepping motor can be thought of as a linear spring. A 1.8' stepping motor that produces 200 oz-in of torque has a stiffness of almost

10,000 oz-in per radian. A typical 90' permanent magnet motor has a spring constant of only 0.50 oz-in per radian.

In addition to the torque transducer, the high torque output of the stepping motor may cause measurement errors in the motor itself. These errors are due to the torsional deflection of the rotor.

Torque Angle Measurement Systems

To gain further insight into the effect of the torque transducer on the measurement system, a simple model can be constructed based on the system in Figure A-1.

$$K_{tt}(\theta_t - \theta) = K_t I \sin(A\theta) + D_t \sin(D_m A\theta) + T_f \frac{\dot{\theta}}{|\dot{\theta}|} + B\dot{\theta} + J\ddot{\theta} \quad \text{(A-1)}$$

Where: θ = Motor position

$\dot{\theta}$ = Motor velocity

$\ddot{\theta}$ = Motor acceleration

θ_t = Torque transducer position

J = Inertia

B = Damping

T_f = Friction

K_t = Torque constant

K_{tt} = Torque transducer spring constant

I = Stator current

Because the gearhead turns at a slow, constant rate and the

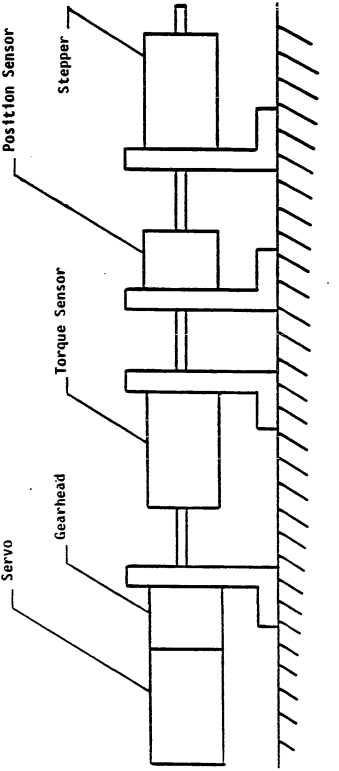

TORQUE ANGLE MEASUREMENT SYSTEM

FIGURE A-1

damping and friction are usually small, the following assumptions can be made:

$$\ddot{\theta} = 0$$
$$B = 0$$
$$T_f = 0$$

Equation A-1 then reduces to:

$$K_{tt}(\theta_t - \theta) = K_t I \sin(A\theta) + D_t \sin(D_m A\theta) \qquad (A-2)$$

The gearhead (θ_t) rotates at a constant velocity, thus:

$$\theta_t = \dot{\theta}_t t \qquad (A-3)$$

Substitution yields Equation A-4.

$$K_{tt}\dot{\theta}_t t = K_{tt}\theta + K_t I \sin(A\theta) + D_t \sin(D_m A\theta) \qquad (A-4)$$

There are two curves of interest that can be developed from Equation A-4. The first is time versus the position of the motor under test. The second is the torque versus position or torque angle curve as measured by the torque transducer.

Figures A-2 and A-3 show two typical curves for a 1.8' motor with two phases energized and a torque constant of 78.0 oz-in per ampere. The stator current level is 1.0 ampere. The torque transducer is rated at 200 oz-in and has a stiffness of 6500 oz-in per radian.

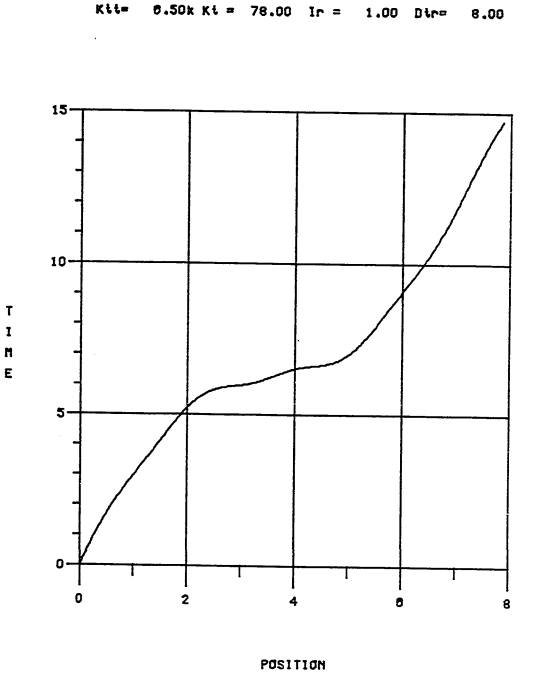

TIME VERSUS POSITION FOR THE MUT WITH I_r = 1.0 amps

FIGURE A-2

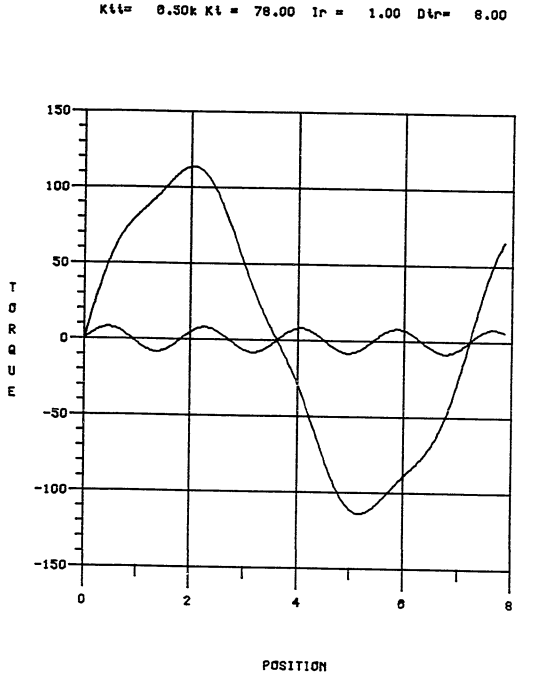

TORQUE VERSUS POSITION FOR THE MUT WITH I_r = 1.0 amps

FIGURE A-3

Figure A-2 illustrates that even though the gearhead turns at a constant velocity, the motor under test does not move at a constant rate due to the winding and unwinding of the torque transducer. However, the torque measurement is still valid as long the motor position can be measured. Figure A-3 is a plot of the torque versus motor position for this system.

If the current is raised to 1.5 amperes, which is rated current for this motor, Figures A-4 and A-5 are obtained. Figure A-4 shows that the motor under test is rotated to 2.6 electrical radians and then "jumps" to 5.4 electrical radians. The corresponding torque angle curve in Figure A-5 shows that the torque is measured from the stable equilibrium point, up over the peak onto the back side of the torque angle curve. On the back side of this curve the slope has changed sign. When the slope of the torque angle curve becomes equal but opposite in sign to the stiffness of the torque transducer, the system becomes unstable and jumps to the next point where the slope of the torque angle curve is again less than the stiffness of the torque transducer.

While the above discussion concerns only the torque transducer, it applies to all the components of the torque angle measurement system. Each part of the torque angle system must have torsional spring constants greater than the stepping motor. This includes any shafts, couplings and the

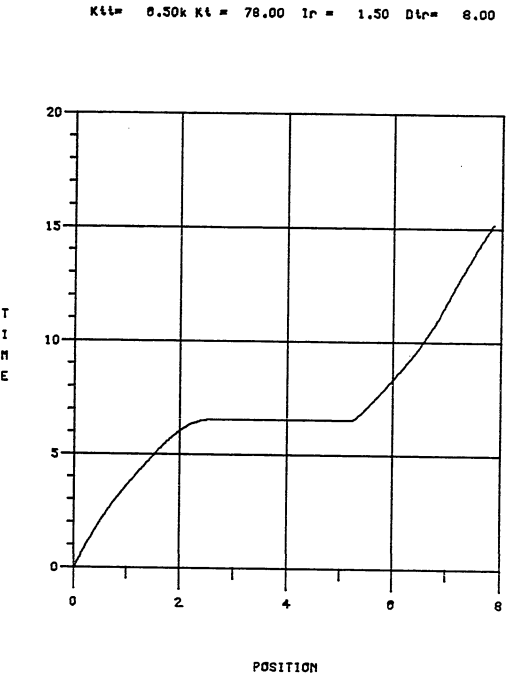

TIME VERSUS POSITION FOR THE MUT WITH I_r = 1.5 amps

FIGURE A-4

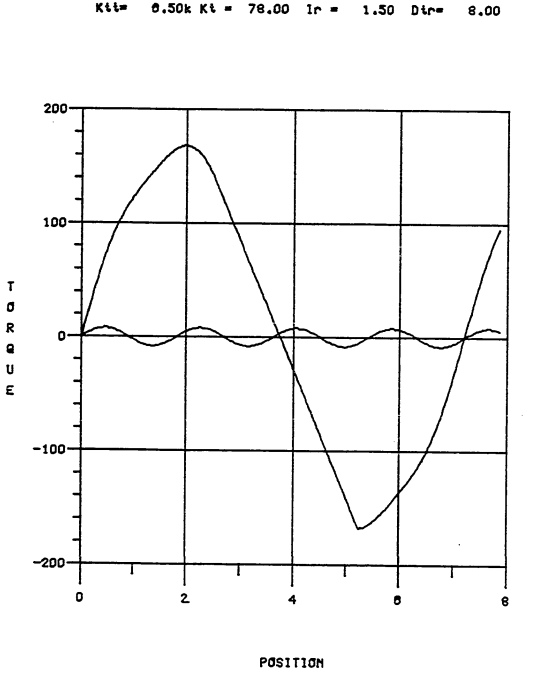

TORQUE VERSUS POSITION FOR THE MUT WITH I_r = 1.5 amps

FIGURE A-5

position encoder.

Stepping Motor Windup

In addition to being concerned about the stiffness of the torque angle measurement system, it is also necessary to account for the torsional stiffness in the motor itself. Figure A-6 is a plot of the torque angle curve for the stepping motor used to verify the model in Chapter 3. The data was measured with two phases energized. The detent torque contribution to the measured curves was subtracted out so the torque in Figure A-6 is due solely to the stator winding. Looking at Figure A-6, the peak of the torque angle curves should be at approximately 90′ electrical or 1.8′ mechanical degrees. This is Line AB in Figure A-6 and it is measured relative to the first zero crossing of the torque angle curve.

However, Figure A-6 indicates that the peaks of the curves are to the right of 90 electrical degrees. First it could be assumed that the torque curve is not as sinusoidal as expected and that Figure A-6 is the true shape of the torque angle curves. However, looking at the back EMF waveform proves this assumption incorrect. The actual cause of this shift is the windup in the shaft of the motor. Calculating the torsional stiffness of the motor shaft, it can be determined that a 0.25 inch diameter shaft will

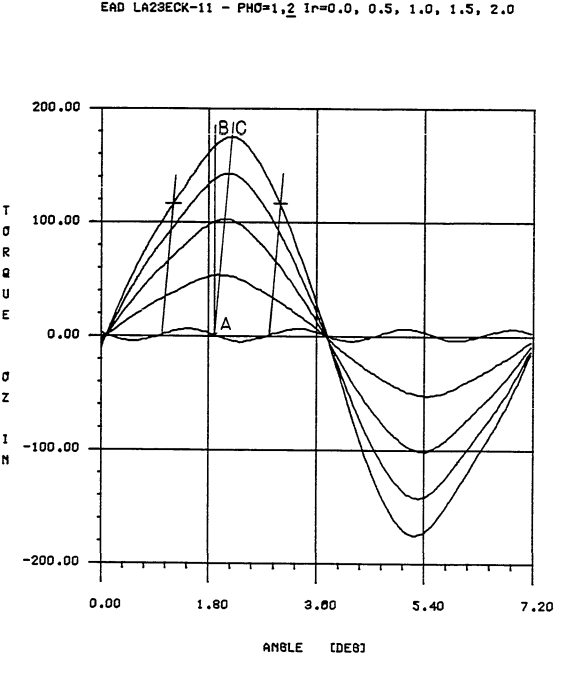

ROTOR WINDUP DURING TORQUE ANGLE CURVE MEASUREMENT

FIGURE A-6

deflect 0.225 mechanical degrees per inch per one hundred oz-in of torque applied.

In order to determine the effect of the windup in the measurements it is necessary to determine the length of the shaft affected. This can be a problem because is not easy to establish what portion of the shaft inside the laminations is affected by the torque. For a size 23, 2.5" hybrid motor, experience indicates that one inch of the shaft will deflect.

Having determined the length of shaft that will be affected, it is possible to calculate a correction factor. Line AC in Figure A-6 shows the true 90 electrical degree point as the current is varied. Further verification of this correction can be obtained by looking at the 90 +/- 45 degree points on the torque angle curve. At these two points the torque should be equal if the torque angle curve is sinusoidal.

APPENDIX B

EXPERIMENTAL PHASE PLANE GENERATION

Introduction

In order to verify the model developed in Chapter III, a measurement device must be developed so that the actual motor reponse can be compared to those predicted by the model. It is also desired that the measurement device produce the velocity versus position error plots. There are several approaches to obtaining a velocity signal. However, because of the discontinuous process used to represent stepping in the velocity-error plane, experimental verification using velocity-error methods has always been difficult.

Gauthier used a one turn, continuous analog potentiometer and developed a position signal that recycled every 360 degrees. The disadvantages of this system include the inability to look at experimental error-velocity planes and poor resolution for small angle steppers.

In order to solve these problems, an alternative method was developed using an optical incremental encoder. The encoder allows much greater resolution for measuring small angle steppers. In addition, because the encoder is a digital device, it is possible to develop the position error signal using digital logic.

Position

The encoder chosen for this application was a Disc Series 990 incremental encoder. The disk was mounted on the motor shaft and the sensor was mounted on the motor case. There is no contact between the encoder disk and the sensors. The benefit of this type of encoder is that it reduces the added inertia to the system and does not introduce any friction or damping. This minimizes the change in the stepper system due to the measurement system. An incremental encoder of this type has two square wave outputs, A and B, which are usually +/-90' out of phase with respect to one another. The direction of rotation determines whether B leads or lags A. This has two advantages. First it allows one to quadruple the number of output pulses per revolution of the encoder. And, second, it allows one to decode the direction of rotation from the phase angle between channels A and B.

Figure B-1 shows the two output signals from the encoder, channels A and B, as the encoder is rotated at a constant speed. By conventional logic means, one can invert channels A and B of the encoder output to create $\bar{A}$ and $\bar{B}$ output signals. One shots are used to detect the rising edges of A, $\bar{A}$, B and $\bar{B}$. By decoding these eight output signals, one may decode the direction of rotation of the

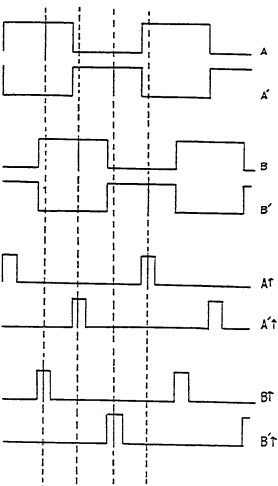

CLOCKWISE ROTATION

FOR COUNTER CLOCKWISE ROTATION B=B+180°

INCREMENTAL OPTICAL ENCODER OUTPUTS

FIGURE B-1

motor and encoder. Equation B-1 shows the logical output states for positive, clockwise rotation. Equation B-2 shows the logical output states required for counterclockwise rotation:

Clockwise Rotation =

$$(\hat{A|}*\bar{B})+(A*\hat{B|})+(\hat{\bar{A}|}*B)+(\bar{A}*\hat{\bar{B}|}) \qquad \text{(B-1)}$$

Counterclockwise Rotation =

$$(\hat{A|}*B)+(A*\hat{\bar{B}|})+(\hat{\bar{A}|}*\bar{B})+(\bar{A}*\hat{B|}) \qquad \text{(B-2)}$$

Where: $*$ = a Logical AND

$+$ = a Logical OR

A = Output of channel A

$\bar{A}$ = Inverse of channel A

$\hat{A|}$ = Rising edge of channel A

$\hat{\bar{A}|}$ = Falling edge of channel A

B = Output of channel B

$\bar{B}$ = Inverse of channel B

$\hat{B|}$ = Rising edge of channel B

$\hat{\bar{B}|}$ = Falling edge of channel B

Once these two directions are established and the number of pulses coming out of the encoder are detected, one can count them using an up-down counter. This count is the relative output position. The clockwise pulses are fed into one count up input of the counter, the counterclockwise pulses are fed into the count down input. At this point in the measurement system, one may take the position given by

the up-down counter and use a digital-to-analog converter to obtain an analog voltage proportional to the position.

Typically this type of encoder yields a resolution of one part in 10,000 per mechanical revolution or a resolution of .0036', more than adequate for even the smallest angle stepping motor, 0.75'.

For this application, it is desirable to be able to "instantaneously" shift the output of the position system to represent the stepping process in the velocity-error plane. In order to do this, one must devise a method to subtract the number of encoder pulses equal to one step, each time an input step command to the motor is received by the controlling driver logic. This was implemented in the position system by an arithmetic logic unit (ALU).

The ALU was configured to operate in the subtraction mode. One input of the ALU was connected to the output of the counter which was the current motor position. The other input to the ALU was the number of pulses equal to one step, based on the encoder's resolution. The output of the ALU, therefore, contains the current position of the motor minus one step. At the instant the stepping motor's drive circuit is pulsed to make another step, the position circuit is also pulsed. The output of the ALU is loaded into the counter. This in effect causes the counter's contents, representing position, to be shifted backward an amount equal to one

step. The output of the counter is used with a DAC to generate an analog voltage that is now proportional to the position error. Figure B-2 is a block diagram of the encoder circuit. The ability to preset the counter before the first step was also implemented.

There are two potential problems that must be dealt with in this system. First, the up-down counters that contain the position signal can not be incremented or decremented by the encoder and be preset from the ALU at the same time. Therefore, upon receiving a step command, the system must wait until after the next encoder pulse to reload the counters. Knowing the top speed of the stepping motor system and the encoder resolution, it is possible to calculate the minimum period between two successive pulses from the encoder. It is during this window that the encoder must be reset.

The second problem is that a buffer must be placed between the output of the counter and the input of the ALU. This buffer will pass information except when the counter is being reloaded. This prohibits a subtraction race condition from existing around the counter and ALU loop.

Selection of the optical encoder is also critical. To ensure adequate resolution, a sufficient number of pulses should be generated for each step of the motor. The step size must also be equal to an integer number of pulses, or

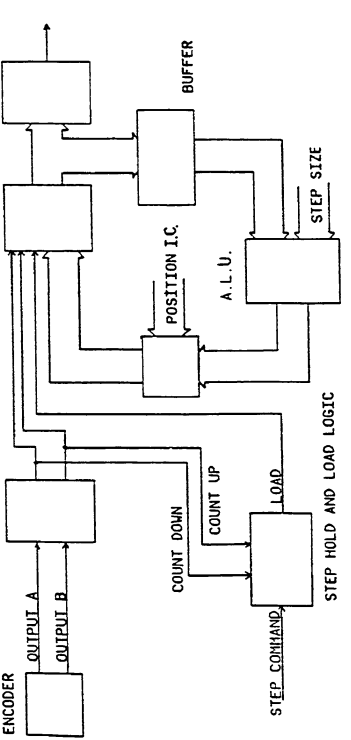

ANGULAR ERROR LOGIC CIRCUIT

FIGURE B-2

the binary subtraction cannot be performed in the ALU.

If a switch were placed in the counter load line, it would be possible to prohibit the stepping back. Then the encoder circuit could also be used to generate a continuous position signal when desired.

Velocity

The simplest method to obtain a velocity signal is to use a DC tachometer. A tachometer works well at low speeds where brush noise and bounce are not a problem. For the experimental verification of the model in Chapter III, a tachometer was used in conjunction with the encoder position device.

During stepping there can be significant torsional resonance between the motor and tach even when a solid coupling is used. This appears as a high frequency oscillation about the signal of interest. See Figure B-3. As long as there is at least one decade between the natural frequency of the motor and the resonant frequency, it is possible to filter out most of the resonant oscillation.

A second order active filter was used to filter the tach output. This resulted in a velocity signal of much higher quality. See Figure B-4. The filter introduces a phase shift in the output signal. This is seen as a slight

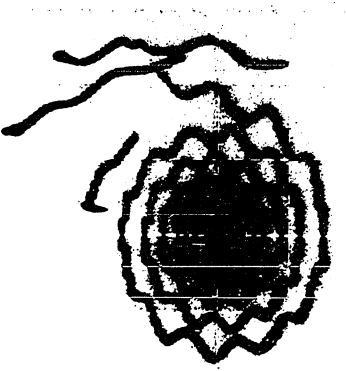

VELOCITY STEPS/SEC 666/DIVISION

.5 / DIVISION

POSITION STEPS

UNFILTERED DC TACHOMETER OUTPUT

FIGURE B-3

VELOCITY STEPS/SEC

666/DIVISION

.5 / DIVISION

POSITION STEPS

FILTERED DC TACHOMETER OUTPUT

FIGURE B-4

skew of the spiral portion of the trajectory. In addition, there may be a slight distortion of the tach output just as the motor is stepped. This results from the discontinuous nature of the velocity signal at the moment the motor is stepped.

In high speed applications, the tachometer brush bounce and wear become a problem. In this case the following concept can be used to develop the velocity signal. It utilizes the same optical encoder used for generating the position and position-error signals.

To develop a velocity signal, two aspects must be considered. First the magnitude of the signal must be developed, then the sign, indicating positive or negative velocity, must be determined.

The magnitude of the velocity signal can be generated using a lookup table in a PROM. A fixed frequency clock is input to a counter causing the counter to count up. The count-up and count-down pulses from the encoder logic are OR'ed together. Whenever a pulse is generated, either up or down, the contents of the counter is latched into a buffer. The counter is also reset to zero and allowed to count up again. The output of the buffer that the counter was latched into serves as the address of the PROM. Because each pulse from the encoder represents a fixed change in displacement, the contents of the counter is also inversely

proportional to the velocity. It is this inverse function that is programmed into the PROM. The address word of the PROM is the time between changes in displacement and the output of the PROM is the velocity that corresponds to that time interval.

The output of the PROM feeds into a digital-to-analog converter. This provides an analog signal proportional to the magnitude of the stepper velocity. This analog signal is then fed into the circuit that determines the velocity sign. See Figure B-5 for the block diagram of the velocity magnitude circuit.

Considerable care must be taken in selecting the contents of the PROM lookup table. For low speed motor operation, the counters may overflow between the pulses from the encoder. However, the frequency of the clock can not be reduced too far because resolution at higher motor speeds would be lost. It should be noted that at maximum stepper speed, velocity resolution will be very coarse unless a sufficient number of counts are allowed to accumulate between encoder pulses.

There are two ways to solve this problem. First, the PROM's dimensions (Address x Output) can be increased to a sufficient dimension so that both low speed and high speed can be monitored. Second, the decision can be made that there will never be a need to look at high and low speeds at

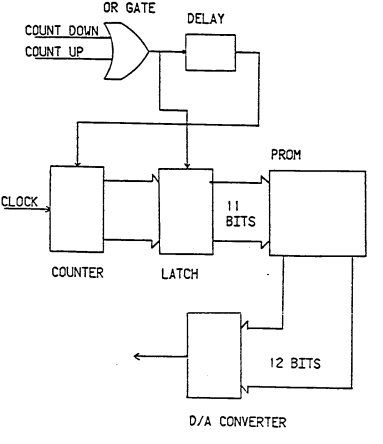

ANGULAR VELOCITY MAGNITUDE LOGIC CIRCUIT

FIGURE B-5

the same time. If this assumption is made then a PROM of smaller dimensions can be used and the frequency of the clock can be changed depending upon the velocity range of interest. For this application, two 2716 PROMs were used in parallel. This generated an eleven bit address with a sixteen bit output.

A hybrid circuit is used to determine the sign of the velocity signal. A J-K flip-flop "remembers" whether the last pulse from the encoder circuit indicated clockwise or counterclockwise rotation. Depending upon the output of the flip-flop, the velocity signal is fed through either one or two inverting op-amps. In this manner the sign of the velocity signal can be determined. Figure B-6 is a schematic of this circuit.

The major drawback of this method of velocity detection is that the encoder will have some jitter between outputs A and B, Normally an encoder is specified at A = B + 90' +/- 45'. This jitter causes the displacement between successive pulses to vary. While this is not a significant problem for the position, it will cause error in the velocity. For this reason the analog tachometer remains the best overall velocity transducer for a wide range of applications.

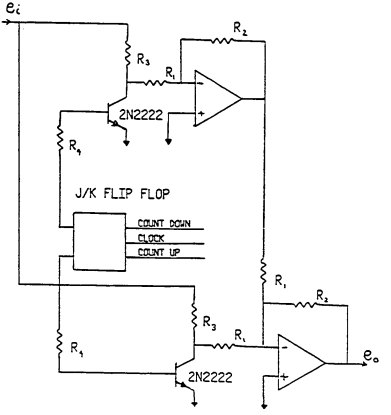

ANGULAR VELOCITY DIRECTION LOGIC CIRCUIT

FIGURE B-6